The Role of
Paleoviral Sequences in Immune Tolerance
to Ebola Virus Infections

Dissertation

Submitted by

Christoph Henkel

for the attainment of the degree Doctor rerum naturalium

from the Faculty of Mathematics, Informatics, and Natural Sciences

Department of Biology

University of Hamburg

Hamburg

2024

The present work was performed under the guidance of Prof. Dr. César Muñoz-Fontela and Dr. Beatriz Escudero-Pérez at the Bernhard Nocht Institute for Tropical Medicine (BNITM) in Hamburg.

1st Reviewer: Prof. Dr. Tim-Wolf Gilberger
                     Bernhard Nocht Institute for Tropical Medicine
                     Cellular Parasitology
                     Bernhard-Nocht-Straße 74, 20359 Hamburg

2nd Reviewer: Prof. Dr. César Muñoz-Fontela
                     Bernhard Nocht Institute for Tropical Medicine
                     Virus Immunology
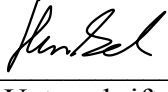   Bernhard-Nocht-Straße 74, 20359 Hamburg

Oral defense: 21.02.2025

Eidesstattliche Erklärung - Affidavit

Hiermit versichere ich an Eides statt, die vorliegende Dissertationsschrift selbst verfasst und keine anderen als die angegebenen Hilfsmittel und Quellen benutzt zu haben. Sofern im Zuge der Erstellung der vorliegenden Dissertationsschrift generative Künstliche Intelligenz (KI) basierte elektronische Hilfsmittel verwendet wurden, versichere ich, dass meine eigene Leistung im Vordergrund stand und dass eine vollständige Dokumentation aller verwendeten Hilfsmittel gemäß der Guten wissenschaftlichen Praxis vorliegt. Ich trage die Verantwortung für eventuell durch die generative KI generierte fehlerhafte oder verzerrte Inhalte, fehlerhafte Referenzen, Verstöße gegen das Datenschutz- und Urheberrecht oder Plagiate.

I hereby declare and affirm that this doctoral dissertation is my own work and that I have not used any aids and sources other than those indicated. If electronic resources based on generative artificial intelligence (AI) were used in the course of writing this dissertation, I confirm that my own work was the main and value-adding contribution, and that complete documentation of all resources used is available in accordance with good scientific practice. I am responsible for any erroneous or distorted content, incorrect references, violations of data protection and copyright law or plagiarism that may have been generated by the generative AI.

Hamburg, 22. 11. 2024
_____
Ort, Datum

Christoph Henkel, _____
Vorname und Nachname, Unterschrift

Acknowledgements

I would like to express my deepest gratitude to everyone who has provided continuous support and guidance throughout my research and motivated me during my studies and the preparation of this thesis.

First and foremost, I would like to thank Prof. Dr. César Muñoz-Fontela for introducing me to this fascinating research topic at the beginning of my journey. His expertise and invaluable feedback provided essential guidance throughout the process, culminating in his thorough review of this thesis. Special thanks go to my co-supervisor, Dr. Beatriz Escudero-Pérez, for providing foundational training in the BSL-4 laboratory and assistance with animal experiments. Your steadfast support and thoughtful advice have been fundamental to my development throughout this journey. I am deeply grateful for your guidance and even more so for the friendship I could always count on. I would also like to thank Prof. Dr. Tim-Wolf Gilberger for reviewing this thesis and for introducing me to the Flp-In System.

A heartfelt thank you goes to the entire Virus Immunology research group at BNITM for countless hours of stimulating discussions, troubleshooting, and experimental support. Special thanks to Michelle Heung and Julia Nave for their assistance with animal experiments in the BSL-4 laboratory, and Dr. Linda Niemetz, Dr. Lina Widerspick, and Molly Vickers for their support during troubleshootings, and Stephanie Wurr for her help with the Flp-In cell lines. I also extend my gratitude to all collaborators, both within BNITM and externally, without whom this project would not have been possible, including the BSL-4 staff and technicians, the animal facility at BNITM, the FACS facilities at BNITM and LIV and Dr. Susanne Krasemann (Institute for Neuropathology, University Medical Center Hamburg-Eppendorf) for performing the immunohistochemistry staining.

On a personal note, I would like to thank my family and friends for their love, encouragement, and continuous belief in me, which have been a constant source of strength.

Finally, my sincere thanks go to Wong Yat Ho for your linguistic expertise and unwavering support. Your patience, understanding and encouragement through every high and low have meant the world to me. Thank you for *eeeeverything*!

Table of Contents

XII

List of Figures

List of Supplementary Figures

List of Tables

List of Abbreviations

AFBs	Angolan free-tailed bats	CXCL	Chemokine (C-X-C motif) ligand
AI	Artificial intelligence	DC	Dendritic cells
AIRE	Autoimmune regulator	DC-SIGN	DC Specific Intercellular adhesion molecule-3-Grabbing Non-integrin
Amp	Ampicillin		
ampR	Ampicillin resistance	ddH2O	Double-distilled water
ANOVA	Analysis of variance	DIC	Disseminated intravascular coagulation
APC	Antigen-presenting cell		
APECED	Autoimmune poly-endocrinopathy candidiasis ectodermal dystrophy	DMEM	Dulbecco's Modified Eagle's Medium
		DMSO	Dimethyl sulfoxide
approx.	Approximately	DNA	Deoxyribonucleic acid
AST	Aspartate aminotransferase	dpi	Days post infections
ATP	Adenosine triphosphate	DRC	Democratic Republic of Congo
BDBV	Bundibugyo virus	DREG	Depletion of regulatory T cell
BDV	Borna Disease Virus	dsDNA	Double strand DNA
BLAST	Basic Local Alignment Search Tool	DSMO	Dimethyl sulfoxide
		dsRNA	Double-stranded RNA
BLAT	BLAST-like alignment tool	DT	Diphtheria toxin
BNITM	Bernhard-Nocht-Institute for Tropical Medicine	E	Expect value
		E. coli	*Escherichia coli*
BOMV	Bombali virus	EBLN	EBL nucleoprotein
bp	Base pair	EBLs	Endogenous bornavirus-like elements
BSA	Bovine serum albumin		
BSL	Biosafety level	EBOV	Ebola virus
cAMP	cyclic adenosine monophosphate	EDI	EVE-derived immunity
		EDTA	Ethylenediaminetetraacetic acid
Cas	CRISPR associated protein	EFL	Endogenous filovirus-like element
CCL	Chemokine (C-C motif) ligand	EFLs	endogenous filovirus-like elements
CD	Central domain		
cDCs	Classical DCs	eGFP	Enhanced GFP
cDNA	Complementary DNA	ELISpot	Enzyme-Linked Immune absorbent Spot
CFA	Complete Freund's adjuvant		
CFRs	Case fatality rates	EMA	European Medicines Agency
CHIKV	Chikungunya virus	EpCAM	Epithelial cellular adhesion molecule
CO2	Carbon dioxide		
cP	Centipoise	ERBs	Egyptian rousette bats
CRISPR	Clustered regularly interspaced short palindromic repeats	ERV	Endogenous retrovirus
		EST	Expressed sequence tag
		et al.	*Et alii*
cTEC	Cortical thymic epithelial cell	EtOH	Ethanol
CTLA-4	Cytotoxic T-lymphocyte-associated protein 4	EVD	EBOV disease
		EVEs	endogenous viral elements
CTRL	Control	FACS	Fluorescence-activated cell sorting
		FCS	Fetal calf serum

Abbreviation	Definition
FDA	Food and Drug Administration
FELASA	Federation of European Laboratory Animal Science Associations
FEZF2	forebrain embryonic zinc finger-like protein 2
FFU	Focus forming unit
FIWIV	Fiwi virus
FOXP3+	Forkhead box p3 positive
FSC	Forward scatter
fw	Forward
g	Gram
GAPDH	Glyceraldehyde 3-phosphate dehydrogenase
GFP	Green fluorescent protein
GM-CSF	Granulocyte-macrophage colony-stimulating factor
GOI	Gene of interest
GP	Glycoprotein
h	Hour
HEK	Human Embryonic
hpi	Hours post-infection
hpt	Hours post-transfection
HRP	Horseradish peroxidase
HSC	Hematopoietic stem cell
HSCs	Hematopoietic stem cells
HSP	Heat shock protein
HUJV	Huángjiāo virus
i.n.	Intranasal
IB	Inclusion body
IBA1	Ionized calcium-binding adaptor molecule 1
IDO	immunosuppressive enzyme indoleamine 2,3-dioxygenase
IEDB	Immune Epitope Database
IFN	Interferon
IFN-1	Type 1 interferon
IFNAR	Interferon-α/β receptor
IFN-γ	Interferon gamma
IgG	Immunoglobulin
IL	Interleukin
Inc.	Incorporation
IP-10	IFNγ-inducible protein 10
iRNA	Interfering RNAs
IPEX	Immunodysregulation polyendocrinopathy enteropathy X-linked syndrome
IVC	Individually ventilated cage
JAX	The Jackson Laboratory
kb	Kilo bases
kDa	Kilodalton
KNDV	Kander virus
KO	Knockout
KoRV	Koala retrovirus
L	Polymerase (viral protein)
LAG3	Lymphocyte activation gene 3
LB	Lysogeny broth
LINEs	Long interspersed nuclear genome elements
LLOV	Lloviu virus
LN	Lymph node
LTBV	Lötschberg virus
LTR	Long terminal repeats
luc2	Firefly luciferase
M	Marker
maEBOV	Mouse-adapted EBOV
MARV	Marburg virus
MCP1	Monocyte chemoattractant protein 1
MCS	Multiple cloning site
MDA-5	Melanoma differentiation-associated protein 5
mg	Minigenome
MGE	Mobile genetic element
MHC	Major histocompatibility complex
MIP	Macrophage inflammatory proteins
μg	Microgram
μl	Microliter
ml	Milliliter
MLAV	Měnglà virus
moDCs	Monocyte-derived DCs
MOI	Multiplicity of infection
mRNA	Messenger RNA
mTEC	Medullary thymic epithelial cell
MVA	Modified Vaccinia Ankara virus
n.s.	Non-significant
NCBI	National Center for Biotechnology Information
NCRs	Non-coding regions

NF-κB	Nuclear factor kappa B	RESTV	Reston virus
ng	Nanogram	rev	Reverse
NHPs	Non-human primates	RIG-I	Retinoic acid inducible gene I
NIKI	NP-NIRV KO	RNA	Ribonucleic acid
NIRV	Non-retroviral integrated RNA virus element	RNA+ve	Positive-sense, single-stranded RNA
NIRVS	Nonretroviral integrated RNA virus sequences	RNAi	RNA-Interference
		RNP	Ribonucleoprotein
NK	Natural killer	RNA-ve	Negative-sense, single-stranded RNA
nluc	Nanoluciferase		
nm	Nanometer	rpm	Rounds per minute
NO	Nitric oxide	RPMI	Roswell Park Memorial Institute medium
NP	Nucleoprotein		
NPBP	NP binding peptide	rVSV	Recombinant vesicular stomatitis virus
NPC1	Niemann-Pick C1 receptor		
nr	Non-redundant	s.c.	Subcutaneous
nrEVEs	Non-retroviral EVEs	SCID	Severe combined immunodeficiency
NXF1	Nuclear RNA export factor 1		
OBLV	Oberland virus	SEM	Standard error of the mean
OD	Optical density	sGP	Soluble glycoprotein
ORF	Open reading frame	siRNA	Small interfering RNA
P/S	Penicillin und Streptomycin	SSC	Side Scatter
p0	Producer cells	ssDNA	Single-stranded DNA
p1	Target cells passage 1	ssGP	Small soluble glycoprotein
PALM	Pamoja Tulinde Maisha	SUDV	Sudan virus
PBS	Phosphate buffered saline	TACE	Tumor necrosis factor-α-converting enzyme
PCR	Polymerase chain reaction		
PD-1	Programmed death 1 receptor	TAE	Tris-acetate-EDTA
PFA	Paraformaldehyde	TAFV	Taï Forest virus
PHA	Phytohemagglutinin	Tann	Annealing temperature
piRNA	PIWI-interacting RNA	TAPV	Tapajós virus
PIWI	P-element Induced Wimpy testis	TCR	T cell receptor
		TE	Transposable element
pmol	Picomole	TECs	Thymic epithelial cells
pos.	Positive	TEs	Transposable elements
PP2A	Protein phosphatase 2A	Tfh	T follicular helper
PRRs	Pattern recognition receptors	TGF-β	Tumor growth factor beta
pTregs	Peripheral Tregs	Th1	T helper 1
RANTES	Regulated on activation, normal T-cell expressed and secreted	TIM	T cell immunoglobulin mucin receptor
		TLR	Toll-like receptor
RAVV	Ravn virus	Tm	Melting temperature
RBC	Red blood cell	TMB	3,3′,5,5′-Tetramethylbenzidine
rep	Reporter gene	TNF-α	Tumor necrosis factor alpha

TRA	Tissue-restricted antigens
Tregs	Regulatory T cells
trVLP	Transcription- and replication-competent virus-like particle
TSA	Tissue specific antigens
tTregs	Thymic Tregs
UEA I	Ulex europaeus agglutinin I
UK	United Kingdom
univ	Universal
USA	United States of America
UV	Ultraviolet
V(D)J	Variable–diversity–joining rearrangement
v/v	Volume per volume
VLP	Virus-like particles
VP	Viral protein
vRNA	Viral RNA
w/v	Weight per volume
WHO	World Health Organization
WT	Wild type
WP	Well plate
x g	Times gravity
XILV	Xīlǎng virus

Zusammenfassung

Filoviren, wie das Ebola-Virus (EBOV), verursachen bei Menschen und nicht-menschlichen Primaten schwerwiegende Erkrankungen mit einer Sterblichkeitsrate von bis zu 90 %. Das Ebolafieber ist durch eine ausgeprägte Entzündungsreaktion gekennzeichnet, die in schweren Fällen zu Multiorganversagen führt. Im Gegensatz dazu scheint EBOV für andere Säugetierarten, wie Fledermäuse und Nagetiere, nicht pathogen zu sein. Die Ursachen für diesen markanten Unterschied in der Pathogenese sind bislang nicht vollständig geklärt.

Ein gemeinsames Merkmal bestimmter Fledermaus-, Nager- und Beuteltierarten ist das Vorhandensein Filovirus-ähnlicher Sequenzen in ihrem Genom. Während bislang vor allem retrovirale Sequenzen bekannt waren, die in Wirtsgenome integriert sind, wurde kürzlich nachgewiesen, dass auch nicht-retrovirale Ribonukleinsäure (RNA)-Viruselemente in Säugetiergenomen vorkommen. Diese Überreste früherer Virusinfektionen, bekannt als *non-retroviral integrated RNA virus elements* (NIRVs), verdeutlichen die dynamischen Interaktionen zwischen Viren und ihren Wirten im Verlauf der Evolution. Viele dieser paläoviralen Sequenzen enthalten intakte offene Leserahmen, und einige zeigen nachweisbare Expressionsprodukte. Trotz ihrer Entdeckung bleiben sowohl ihre genaue Funktion als auch ihr Entstehungsmechanismus weitgehend unklar. Es gibt jedoch Hinweise darauf, dass diese Sequenzen die Anfälligkeit für Viren sowie die Resistenz gegenüber viralen Erkrankungen beeinflussen könnten.

In dieser Studie konzentrierten wir uns auf die Charakterisierung eines spezifischen NIRVs, das vom Nukleoprotein (NP) von EBOV (NP-NIRV) abgeleitet ist und in Mäusen (*Mus musculus*) vorkommt. Wir fanden heraus, dass NP-NIRV als *messenger*-RNA (mRNA) in der Milz, der Niere und dem Thymus exprimiert wird. Interessanterweise war die Expression insbesondere in medullären thymischen Epithelzellen (mTECs), die während der T-Zell-Entwicklung eine zentrale Rolle spielen, auffallend.

Unsere Ergebnisse zeigen, dass NP-NIRV unter der Kontrolle des Autoimmunregulators (AIRE) exprimiert wird und von Mäusen eher als körpereigenes Peptid statt als fremdes, immunogenes Peptid erkannt wird. Dies deutet stark darauf hin, dass NP-NIRV bei Mäusen eine Immuntoleranz gegenüber EBOV-Infektionen fördert. Die Deletion von NP-NIRV bei Mäusen führte weder zu Veränderungen in der Pathogenese noch zu ausgeprägten Entzündungsreaktionen nach einer EBOV-Infektion. Dagegen führte die Depletion aller regulatorischen T-Zellen (Tregs) zu einer verstärkten Pathogenese, was auf die Existenz weiterer NIRVs hinweist, die möglicherweise ähnliche Funktionen erfüllen.

Schließlich zeigten unsere *In-silico*-Analysen, dass mehrere weitere Peptide, die vermutlich von Filoviren und anderen Viren der Ordnung *Mononegavirales* abgeleitet sind, im Thymus von Mäusen, jedoch nicht von Menschen, exprimiert werden. Dies deutet auf eine evolutionäre Strategie hin, die darauf abzielt, Infektionen durch bestimmte Virusfamilien zu tolerieren.

Abstract

Filoviruses such as Ebola virus (EBOV) cause severe disease in human and non-human primates (NHP) with fatality rates of up to 90%. EBOV disease (EVD) is characterized by exacerbated inflammatory response leading to multiorgan failure in severe cases. Conversely, EBOV seems to be non-pathogenic for other mammalian species such as bats and rodents. The reasons for this outstanding difference in pathogenesis have still not been elucidated.

A common characteristic of some species of bats, rodents, and marsupials is that they all possess filovirus-like sequences inserted in their genomes. Until recently, only retroviral sequences had been found integrated into host genomes. However, it has been discovered that non-retroviral ribonucleic acid (RNA) virus elements are also present in mammalian genomes. These remnants of ancient viral infections, known as non-retroviral integrated RNA virus elements (NIRVs), further underscore the dynamic interactions between viruses and their hosts throughout the course of evolution. These paleoviral sequences often retain intact open reading frames (ORFs) and for some of them, messenger RNA (mRNA) can be detected. Despite their prominence, their exact role and origin mechanism remain largely unknown. However, studies suggest that these sequences might influence susceptibility and resistance to viruses and the diseases they cause.

In this study, we focused on the characterization of a specific NIRV derived from the nucleoprotein (NP) of EBOV (NP-NIRV) present in mice (*Mus musculus*). We found that NP-NIRV was expressed as mRNA in the spleen, kidney, and thymus. Intriguingly, we observed that its expression was particularly unique to medullary thymic epithelial cells (mTECs), which is known to play an important role during T cell development.

Our findings demonstrate that NP-NIRV was expressed under the control of autoimmune regulator (AIRE) and recognized as a self-peptide rather than a foreign immunogenic peptide in mice. This strongly suggests that NP-NIRV induced immune tolerance against EBOV infection in mice. Depletion of NP-NIRV in mice did not result in changes in either pathogenesis or inflammatory responses after EBOV infection, but depletion of all regulatory T cells (Tregs) resulted in enhanced pathogenesis suggesting the presence of additional NIRVs.

Finally, through *in-silico* analysis, we demonstrated that several other peptides putatively derived from filoviruses and other viruses of the order *Mononegavirales* exist in the thymus of mice but not humans, suggesting an evolutionary strategy to tolerate infection with specific virus families.

1 Introduction

Examining the evolutionary remnants of ancient viral sequences within host genomes offers a glimpse into virus-host co-evolution. This thesis explores how Ebola virus (EBOV) paleoviral sequences might influence the host immune system, potentially contributing to resistance against EBOV disease. The following section will introduce the scientific concepts essential for understanding this study.

1.1 Paleovirology

Viruses have evolved to exploit a wide range of hosts, and few organisms, if any, are completely free from viral threats. During infections, it can occur that viral sequences or the entire viral genome are integrated into the host's genome. It is because of these integrations that although viruses are not part of the tree of life, it is suggested that they have had a significant impact on the evolution of nearly all its members.[1] Paleovirology studies these integrations of ancient viruses (paleoviruses), making a distinction between two branches: direct and indirect paleovirology.[2,3] The direct approach primarily involves studying viral remnants in host genomes, known as endogenous viral elements (EVEs), which result from germline infections leading to heritable genome integration. Indirect paleovirology, on the other hand, examines the evolutionary impact of paleoviruses on their hosts. Such investigations illustrate that the sources of genetic inheritance are more diverse than previously appreciated.[4]

1.2 Retroviral EVEs

Throughout the co-evolution of viruses and their hosts, integrations of viral sequences have accumulated to a substantial proportion of the genomes of modern organisms. For instance, around 8 % of the human genome is made up of viral sequences from retroviruses.[5] To put this into perspective, the total amount of coding DNA in humans is only around 1-2%.[6] Thus, it is suggested that viruses have had a substantial impact on all living organisms as the conservation of paleoviral sequences in host genomes over millions of years must have a reason. Several cases have been documented in the literature, and they vary widely in terms of how viral integrations benefit the host, as well as the mechanism in which this is achieved.[7] This is backed up by research findings in placental biology.[8] Most research in this area has focused on genes derived from transposable elements (TEs). Also known as "jumping genes", these DNA sequences can change their position within a genome and are thought to have originated from ancient viruses.[9] This includes retrotransposons encoding for endogenous retrovirus (ERV)-derived proteins, which have been co-opted by the host to promote cell-cell fusion and immune modulation in the placenta, ensuring physical protection of the fetus and providing immune protection throughout gestation.[10–12] As live birthing is a key feature of placental mammals, it has been suggested that there would be no mammals without retroviruses.[13,14]

Retroviruses are by far the most common origin of EVEs due to their necessary genome integration step. This special characteristic of retroviruses is called retrotransposition. In this stage of their life cycle, the ribonucleic acid (RNA)-based viral genome is reverse transcribed into complementary deoxyribonucleic acid (cDNA) and inserted into the host cell's genome via the retrovirus' own reverse transcriptase and integrase. From there, the integrated virus (provirus) initiates the production of viral proteins to complete its life cycle.[15]

When egg or sperm cells are infected, integrations have the potential to become ERVs that are inherited by the offspring. These integrations into the germline can lead to entire populations being infected with a provirus. One example is the koala retrovirus (KoRV) in which an active endogenization process can still be observed.[16] Notably, once a virus is integrated, its mutation rate becomes the rate of the host. Over time, naturally occurring mutations in the host's genome can lead to alterations of the provirus, resulting in the impairment of the virus' functionality to replicate.[17] This leads to EVEs found in today's genetic pools. Paleovirologists utilize these viral sequences to estimate the time of integration and thus the minimal age of the virus.[2,18]

1.3   Non-retroviral EVEs

For many years, the feature of genome integration has been attributed exclusively to retroviruses and certain DNA tumor viruses. However, recent research has shown that non-retroviruses can also integrate into their host's genome.[4] Unlike retroviruses, most RNA viruses lack the necessary enzymes to produce cDNA or integrate their genetic material into the host genome, as it is not needed for their life cycle. Despite this, EVEs from all major virus genome types have been identified, suggesting that genome integration is more widespread and complex than previously thought.[19] In fact, besides retrotransposons, the human genome contains numerous other TEs, constituting a substantial proportion of the genome.[20] For other mammalians, such as rodents and bats, the TE proportion is even greater compared to their genome size.[21] It is proposed that some of these TEs might have originated from non-retroviral integrations and have accumulated over time.[22] Besides EVEs from other DNA virus' families such as *Circoviridae* and *Parvoviridae*, EVEs from RNA viruses have been under intense investigation e.g., *Bornaviridae*, *Filoviridae* and *Flaviviridae*.[4,23] These paleoviral sequences have been named non-retroviral integrated RNA virus elements (NIRVs) [(1)]. This study is focused on NIRVs but will also use the term EVEs in the context of general assumptions for paleoviral sequences.

[(1)] also referred to as non-retroviral EVEs (nrEVEs) or nonretroviral integrated RNA virus sequences (NIRVS)

1.4 Integration and Maintenance of NIRVs

It is assumed that the integration of NIRVs follow the same principle as it is for retroviruses: an ancient viral infection led to the integration of the viral genome (or parts of it) into the germline of the host which was then inherited until today.[2,7]

Despite their varied replication strategies, viruses rely on infecting a host cell to exploit its molecular machinery for their own purposes. Although a virus does not need a germline-specific tropism, for a heritable integration, the virus must invade the germline. In addition to either of the two gametes, there are other possible targets e.g., germline precursor cells, the zygote or an early-stage embryo. Once the virus has entered the cell, the process leading to integration varies depending on the type of viral genome. While double strand DNA (dsDNA) viruses can readily integrate into host genomes, single-stranded DNA (ssDNA) viruses must first synthesize a complementary strand. For RNA viruses, reverse transcription is the sole way to generate complementary dsDNA genomes (Figure 1).[7]

The mechanisms involved in the integration of viral dsDNA into the host's genome are not fully understood. Currently, two genomic integration strategies are proposed. First, it has been suggested that the host cell's double-strand-break repair machinery captures nearby viral DNA sequences and insert them in unstable regions of the genome through non-homologous recombination.[24,25] This type of genetic recombination involves the exchange of genetic material between DNA molecules without the need for sequence similarity between the regions involved. Second, it is possible that NIRVs integration takes place through the interactions between the viral DNA and host retroelements, e.g. long interspersed nuclear elements (LINEs).[2,26,27] The incidental recombination with retrotransposons could also explain the preceding presence of a viral DNA intermediate that is required for host genome insertion.[28]

Once a viral element becomes endogenous, it has the potential to become fixed within the population. However, through mutations and other events involving mobile genetic elements, EVEs can either be modified and thus lose previously functioning open reading frames (ORFs), alter to an extent where they become unrecognizable, or be completely wiped out of the genome.[29] Yet, the maintenance of NIRVs over millions of years suggests that they provide an evolutionary advantage to the host. Although research findings suggest a wide range of possible benefits, the function for many NIRVs has yet to be elucidated.[30] Paleovirologists have documented several cases of such advantages over the past decades. The following sections summarize the past research on NIRVs and highlight some of these examples.
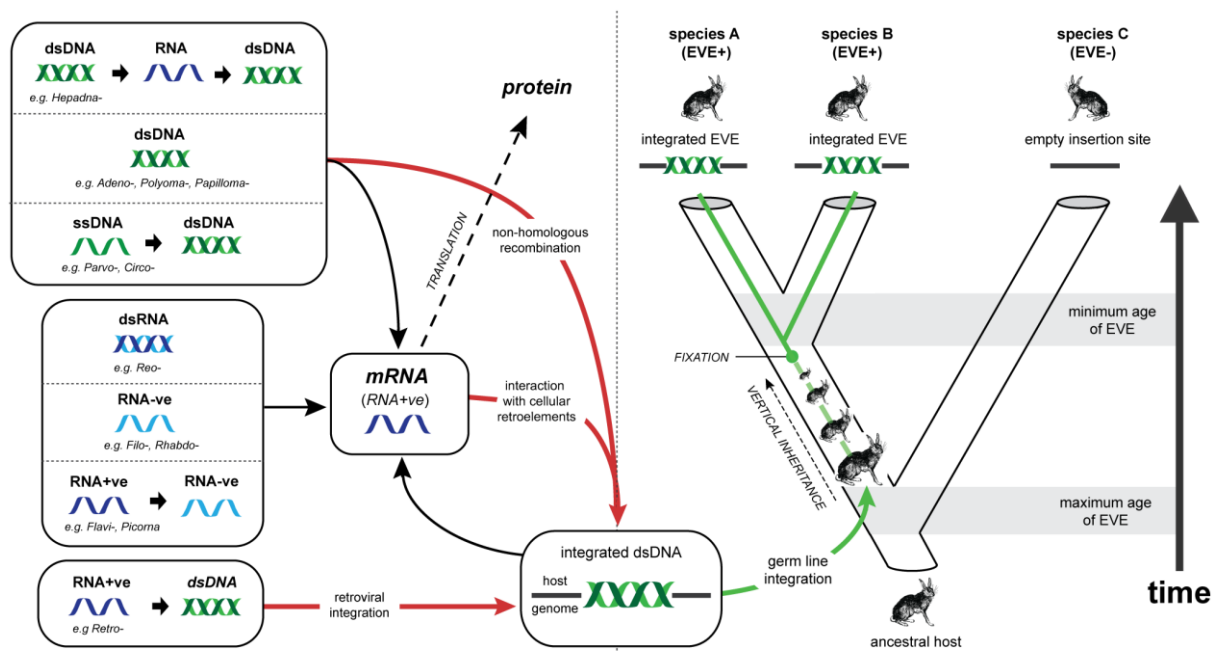
Figure 1: Genomic Integration Strategies Suggested for Different Viral Families

Left half: Animal viruses have diverse genome types and replication strategies, but all must produce mRNA to express proteins. The figure illustrates these strategies, with representative families listed. Arrows depict replication steps, and red lines highlight pathways leading to the integration of viral genetic material into the host genome. Retroviruses uniquely require integration for replication, while other viruses integrate infrequently, often via cellular retroelements such as LINEs or through non-homologous recombination. **Right half:** Integration into germline cells can result in EVEs. Green lines trace the evolutionary history of an EVE, which, if fixed in a population, is inherited by all descendants. Related EVEs at the same genomic locus in species A and B indicate insertion before their divergence, allowing a minimum age estimate, while the absence of the insertion in species C provides a maximum age. Abbreviations: dsDNA (double-stranded DNA), ssDNA (single-stranded DNA), dsRNA (double-stranded RNA), RNA-ve (negative-sense, single-stranded RNA), RNA+ve (positive-sense, single-stranded RNA). (Adapted from Katzourakis *et al.*, 2010)

1.5 Arbovirus (Arthropod-borne) Virus NIRVs

To date, the majority of NIRVs found in insect genomes have been described in mosquitos from the *Aedes* genus including virus families of positive and negative single stranded viruses e.g., *Flaviviridae* and *Rhabdoviridae,* respectively.[31,32] As indicated by the term arthropod-borne virus (arbovirus), mosquitoes, as well as other insects, such as ticks, play a major role in the life cycle of many viruses. This relationship, along with the presence of many arboviral NIRVs in these insects, suggests a tight co-evolution. One primary hypothesis for the function of NIRVs in arthropods is their role in antiviral immunity.[23,33] While the small interfering RNA (siRNA) pathway is the primary and most direct antiviral mechanism, the PIWI-interacting RNA (piRNA) pathway adds an additional layer of defense, particularly in the long-term regulation and potential suppression of arboviruses in mosquitoes.[34,35] Viral sequences tend to integrate into piRNA clusters within the mosquito genome, facilitating the production of NIRV-derived viral piRNAs similar to TE-targeting piRNAs from these clusters.[36,37] These RNAs could target and degrade viral RNA, thereby limiting the replication of active viruses.[33] Another possibility is the involvement of NIRVs in the regulation of gene expression. Integrated viral sequences can influence the expression of nearby host genes, either by providing regulatory elements or by altering chromatin structure. This can impact various physiological processes within the mosquito, potentially including those related to immunity and vector competence.[38] This is supported by a recent study on Chikungunya virus (CHIKV) persistence in *Aedes albopictus*, which suggests that NIRV-derived viral piRNAs have diverse functions, including targeting viral sequences directly and regulating mosquito transcript expression.[39]

1.6 NIRVs in Mammalian Genomes

Since the early 2000s, when integrated viral sequences in insects were first discovered, advancements in sequencing technologies have led to a surge in the identification of NIRVs in mammalian genomes, which were first described in 2010.[23,40,41] Bioinformatical studies point towards a majority of integrations from one particular order: *Mononegavirales.*[4,7] Notably, this order contains several pathogenic and highly transmissible viruses for humans and other mammals including Measles, Mumps, Rabies, Bornavirus as well as Filoviruses such as EBOV and Marburg virus (MARV).

1.6.1 Bornaviruses NIRVs

To date, paleoviral sequences from Borna Disease Virus (BDV) are the most thoroughly characterized mammalian NIRVs. These sequences, known as endogenous bornavirus-like elements (EBLs), have been identified in a variety of species, including humans, elephants, marsupials, bats, and squirrels.[7,42,43] The proximity of these integrations to LINEs in the genome suggests that these TEs may play a role in the integration process.[41] Notably, bornaviruses are unique among RNA viruses in that they replicate within the host cell's nucleus. This, combined

with their ability to establish persistent infections, may increase the likelihood of viral genomic integrations.[44] A well-studied example is an EBL nucleoprotein (EBLN) element in the genome of the thirteen-lined ground squirrel (*Ictidomys tridecemlineatus*). Using a BDV mini-replicon system, it was demonstrated that the EBLN element reduces viral replication, likely by interfering with the BDV polymerase as a dominant-negative version of the original BDV nucleoprotein. Additionally, it was demonstrated that the expression of the EBLN blocks BDV infection.[45] BDV NIRVs have also been identified in the human genome.[4,41] A non-coding bornavirus-like element in humans has been found to suppress the expression of an adjacent gene, possibly influencing pathogen defense mechanisms.[46] Other human BVD NIRVs are expressed as proteins and possess cellular functions such as cycle transit, microtubule organization, genome stability or interact with mitochondrial proteins and affect cell viability.[47,48]

1.6.2 Filovirus NIRVs

Simultaneously with the discovery of EBLs, endogenous filovirus-like elements (EFLs) were detected in mammals (Figure 2).[4,7] The majority of EFLs found to date originate from EBOV and MARV. Similar to bornaviruses, filoviruses do not possess a reverse transcriptase. In contrast to bornaviruses, which replicate in the nucleus, filoviruses replicate exclusively in the cytoplasm, reducing the likelihood of integration into the host genome. Despite these circumstances, several filovirus-like sequences have been identified in the genomes of bats, rodents, shrews, tenrecs and marsupials.[7,18] Since transcription site duplications were observed close to EFLs, it is suggested that their integration is associated with retrotransposons e.g., LINEs.[7] Phylogenetic analysis of these paleoviral sequences indicates that filoviruses have been present for at least tens of millions of years. Common EFLs are derived from the nucleoprotein (NP), viral protein 35 (VP35) and the polymerase (L). Interestingly, most genomic integrations in mammals are limited to one or very few copies of a NIRV per species, suggesting that after the initial germline integration, subsequent integrations either did not succeed or conferred minimal benefit to the host.[18,49]
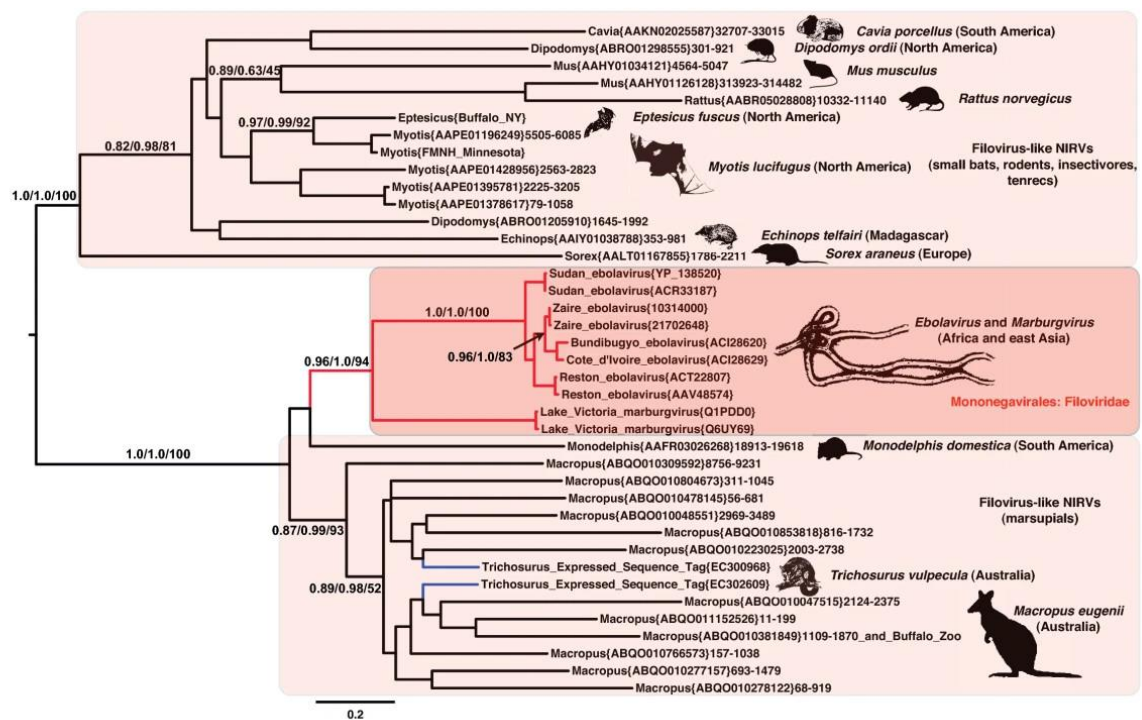
Figure 2: Phylogram of NP Amino Acid Sequences from Filoviruses and Related Mammalian Sequences

The figure shows a midpoint-rooted maximum likelihood phylogenetic tree of filoviruses and related mammalian genomic and expressed sequence tag (EST) sequences, illustrating mammalian paraphyly. Strongly supported branches (≥90 bootstrap or ≥95 Bayesian posterior probability) display support values (in the order of approximate likelihood ratio tests, Bayesian Posterior Probabilities, and non-parametric bootstrap values). Parentheses contain GenBank accession numbers and nucleotide ranges. Red branches represent viral clades (*Mononegavirales*), black branches denote mammalian sequences, and blue lines indicate ESTs. Geographic origins appear in parentheses next to species names, with shaded images outlining species included in the analysis (Adapted from Taylor *et al.*, 2010)

9

1.7 EVE-derived Immunity

The conservation of large ORFs in several instances suggest a biological advantage for the host. This is further supported by an observed correlation between the presence of paleoviral sequences and a species' resistance to related viral diseases.[4] The co-option of viral genes which are used against the virus after their integration is called EVE-derived immunity (EDI).[50] Currently, three possible functions for EVEs are being proposed: (1) protein coding EVEs, (2) EVEs that produce interfering RNAs (iRNA) and (3) EVEs that affect transcriptional regulation in the genome by introducing promoters and alternative splice sites.[7,30,41] These three roles align with the theory of EVE-derived immunity and could explain the preservation of these elements in genomes. This study, however, explores a fourth potential function that is also in line with this theory: the involvement of EVEs in immune tolerance. When a paleoviral sequence is integrated into the host's genome, its immune system could access this blueprint of a viral protein (or viral peptide) and educate its T cells to recognize it as 'self'.[51–53] Consequently, the immune system might either ignore the pathogen or mount a diminished response against it. This mechanism parallels molecular mimicry, employed by viruses and other pathogens to evade the host's immune system, and could thus explain reservoir competence.[54] The following section will explain the immunological concepts on which this theory is based.

1.8   Immune Tolerance

Immune tolerance refers to a state of indifference or non-reactivity towards an antigen.[55] It has also been described as an immunological process wherein the immune system fails to mount a response against an antigen. This feature is essential for maintaining normal physiology and immune homeostasis.[56] In the context of the immune system, homeostasis is the state of equilibrium in which it effectively balances immune responses to protect the body from pathogens while preventing excessive inflammation or autoimmunity. It involves two primary mechanisms: (i) central tolerance and (ii) peripheral tolerance. Central tolerance enables the immune system to differentiate between self and non-self-antigens, thereby recognizing benign self-antigens as non-threatening while remaining responsive to harmful pathogens. However, central tolerance alone is insufficient. To address this, peripheral tolerance acts as an additional mechanism, regulating potentially harmful immune responses to self-antigens, epithelial microbiomes, and environmental antigens, such as food-derived antigens. While immune tolerance mechanisms are crucial for preventing autoimmunity and allergies, they can also enable pathogens and cancerous cells to evade detection and remain rather undisturbed by the host's immune system.[57,58]

Although all types of immune cells are involved in immune tolerance and both B and T cells undergo the educational process of central tolerance, T cells are particularly crucial in this process. Therefore, this study focuses on T cell tolerance.

1.9   Central Tolerance

B and T cells are lymphocytes, a type of white blood cell that develop from hematopoietic stem cells (HSCs) in the bone marrow. While B cells mature in the bone marrow, T cells migrate to the thymus for maturation. The thymus, located under the sternum and above the heart, is a primary lymphoid organ of the immune system (Figure 3). T cell progenitors continue their development in the cortex of the thymus with the variable–diversity–joining rearrangement (V(D)J) of their T cell receptor (TCR) genes. This somatic recombination of TCR genes produces a remarkably diverse repertoire of cell surface receptors, crucial for T cells to recognize antigens. However, the rearrangement process also results in non-functional or self-reactive TCRs. To eliminate cells with undesirable TCRs, T cell progenitors undergo two additional steps to become functional mature T cells.[57,59,60]

1.9.1   Positive Selection

In the first step, immature T cells are tested for their ability to recognize self-major histocompatibility complex (MHC) molecules presented by cortical thymic epithelial cells (cTECs).[61] In general, antigens are presented in the context of these complexes, making it essential for T cells to interact with the body's own MHC molecules for functionality. There are

two primary classes: MHC-I and II. While MHC-I is found on all nucleated cell surfaces, MHC-II is found on cells that play an important role in initiating an antigen-specific immune response (e.g., DCs, mononuclear phagocytes, and B cells).[57,62] T cell progenitors expressing non-functional TCRs that fail to bind to self-MHC molecules die by neglect, while cells with functional TCRs receive survival signals for further maturation. This process is called positive selection, as only reactive TCRs are selected. Additionally, the TCR's affinity to bind to either of the two classes of MHC molecules, class I or II, determines the fate of T cell progenitors to become CD8 or CD4 T cells, respectively[57,59,60]

1.9.2   Negative Selection

After positive selection, T cell progenitors migrate to the medulla of the thymus, where they undergo the final maturation step known as negative selection (Figure 3). In this process, only T cells with non-reactive TCRs receive survival signal.[57,63] In the medulla, T cell progenitors encounter self-antigens presented primarily by medullary thymic epithelial cells (mTECs) and also by thymic DCs. mTECs can express self-antigens from all over the body, known as tissue-restricted antigens (TRAs)[(2)], such as insulin.[64,65] The expression of these antigens is mainly facilitated through the action of the autoimmune regulator (AIRE) and forebrain embryonic zinc finger-like protein 2 (FEZF2). However, it is likely that more TRA transcription factors are involved in this process.[66,67] Although rare, mutations in the human *Aire* gene can lead to a life-threatening autoimmune disease called autoimmune poly-endocrinopathy candidiasis ectodermal dystrophy (APECED)[(3)]. This condition attacks multiple organs starting from early childhood.[68]

The fate of T cell progenitors is determined by the affinity of their TCR to bind to self-antigens. High affinity results in the elimination of the cell through a process called clonal deletion, facilitated by apoptosis. However, T cell progenitors can evade death by either converting into forkhead box p3 positive (FOXP3+) regulatory T cells (Tregs) or undergoing a second gene rearrangement of their TCR. Although receptor editing has been reported, most cells either undergo clonal deletion or clonal diversion into Tregs. The differentiation is influenced by the strength and duration of the TCR signaling as well as the presence of specific cytokines such as interleukin 2 (IL-2) and IL-15.[69,70] An intermediate affinity for self-antigens induces differentiation into Tregs rather than deletion. A study on polyclonal CD4 T cells has also shown that tolerance in CD4 T cells is shaped by the location and presentation pattern of self-peptides.[71]

[(2)] Also called tissue specific antigens (TSAs)
[(3)] Also known as autoimmune polyglandular syndrome type I, APS I

Approximately 90 % of T cell progenitors die during development in the thymus, failing either positive or negative selection. The remaining 10 % leave the thymus as mature naïve T cells, including CD8, CD4, and regulatory T cells, each possessing a distinct antigen-specific TCR variant.[72]
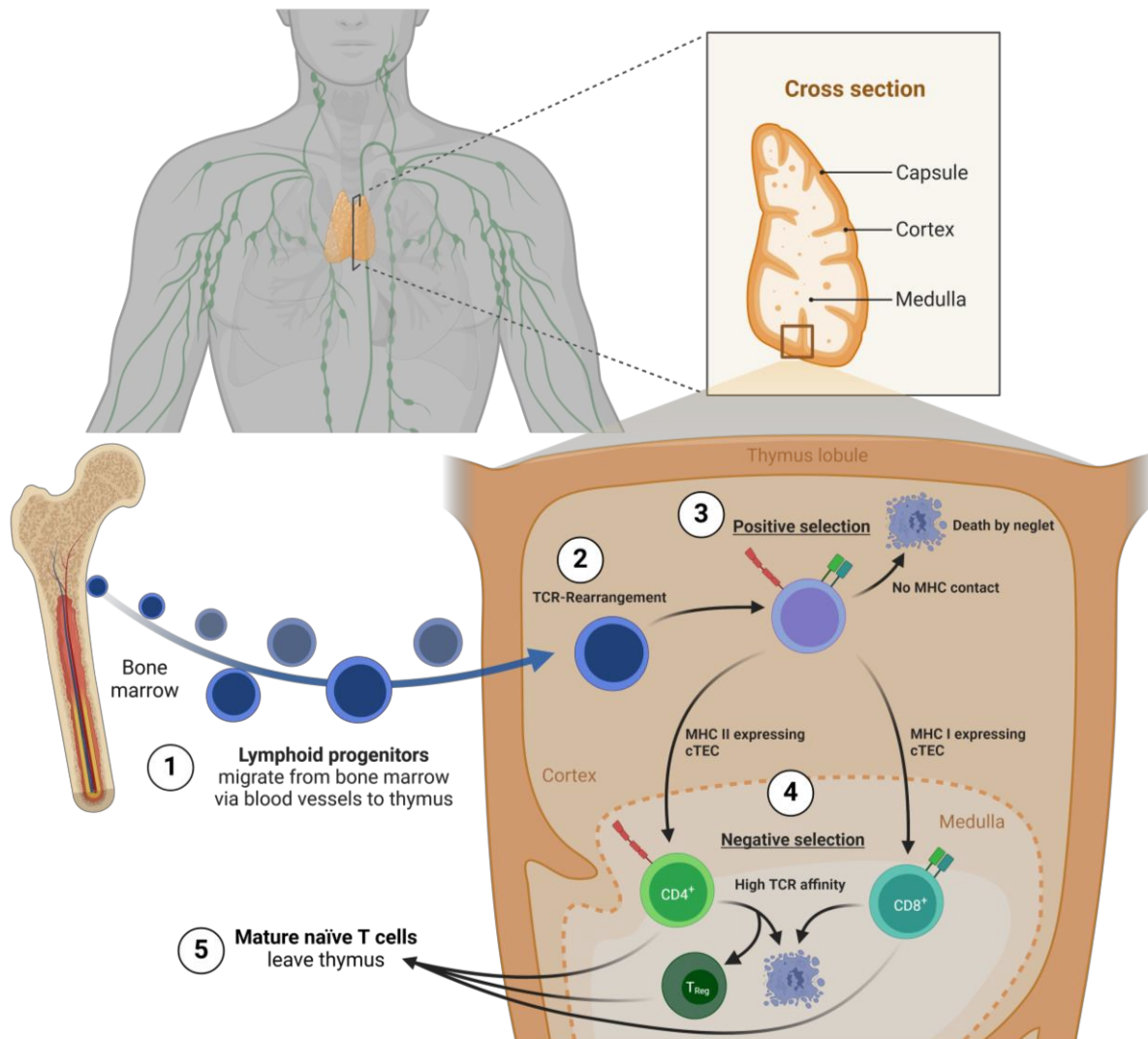
Figure 3: Simplified T cell Development; Anatomic Location and Cross Section of the Thymus

The thymus, a primary lymphoid organ located beneath the sternum and above the heart, is where T cell maturation occurs. **1: Lymphoid progenitors** originate in the bone marrow and migrate to the thymus via blood vessels. **2:** Upon entering the cortex, **TCR rearrangement** takes place. **3: Positive selection** ensures T cells recognize self-MHC-I or II molecules via their TCRs, guiding development into CD8 or CD4 T cells, respectively. Failure to recognize MHC leads to apoptosis. **4:** T cells migrate to the medulla, where **negative selection** eliminates those with high-affinity TCRs for self-antigens, preventing autoimmunity. Some CD4 T cells are converted into Tregs. **5: Mature naive T cells** exit the thymus to participate in the immune response. (Figure created with BioRender)

1.10 Peripheral Tolerance

Despite strict and multilayered mechanisms, some self-reactive T cells can escape central tolerance, especially those with low-affinity binding TCRs. In the periphery, T cells might encounter antigens that are not presented to them during their maturation in the thymus. These antigens include some TRAs, as well as environmental agents such as allergens and gut microbiota. Peripheral tolerance acts on these mature circulating T cells and regulates their activity through mechanisms such as anergy, apoptosis, and suppression by Tregs.[57,70]

Before activation, T cells are considered naïve as they have yet to encounter their specific cognate antigen recognized by their TCR. However, full activation of a T cell also requires additional co-stimulatory signals that involve cytokines and the interaction of the T cell's CD28 receptor with CD80 and CD86 ligands on antigen presenting cells (APCs) (Figure 4).[57,73] APCs, particularly DCs, are responsible for capturing antigens, processing them into fragments, and presenting them as peptides (epitopes) [(4)] on MHC molecules to T cells.[74] If a TCR recognizes an antigen in the absence of the co-stimulatory signal, the T cell enters a state of unresponsiveness known as anergy. APCs can upregulate their expression of co-stimulatory ligands on their surface e.g., during infections.[75] This two-signal mechanism ensures that T cells are only activated in appropriate scenarios. In the absence of inflammation, APCs may present self-antigens without upregulation of CD80 and CD86 (primarily tolerogenic DCs). The lack of adequate co-stimulation results in an active repression of self-reactive TCRs, increasing the number of anergic T cells and thereby enhancing self-tolerance.[70] Furthermore, this mechanism regulates the intensity and duration of the immune response and is helpful in final phases of infections during convalescence where the immune system returns to its normal state (homeostasis). Additionally, co-stimulatory pathways can also send negative signals which is the case of the programmed death 1 (PD-1) receptor. Interactions of TCR and PD-1 can inhibit T cell effector functions in an antigen-specific manner and leads to apoptosis or conversion of naïve T cells to Tregs.[76,77] Although there are significant similarities in the gene expression profiles during peripheral deletion and anergy induction in T cells, the exact mechanisms remain to be elucidated.[70,78]

Lymph nodes (LNs) also play a crucial role in self-tolerance beyond their primary functions of filtration and pathogen response. Strategically distributed throughout the body, they serve as check points for passing T cells. Potential autoreactive T cells are tested by stromal cells that present self-antigens in a non-inflammatory context.[79]

[(4)] For simplification, peptides presented on MHC are called antigens in this study.
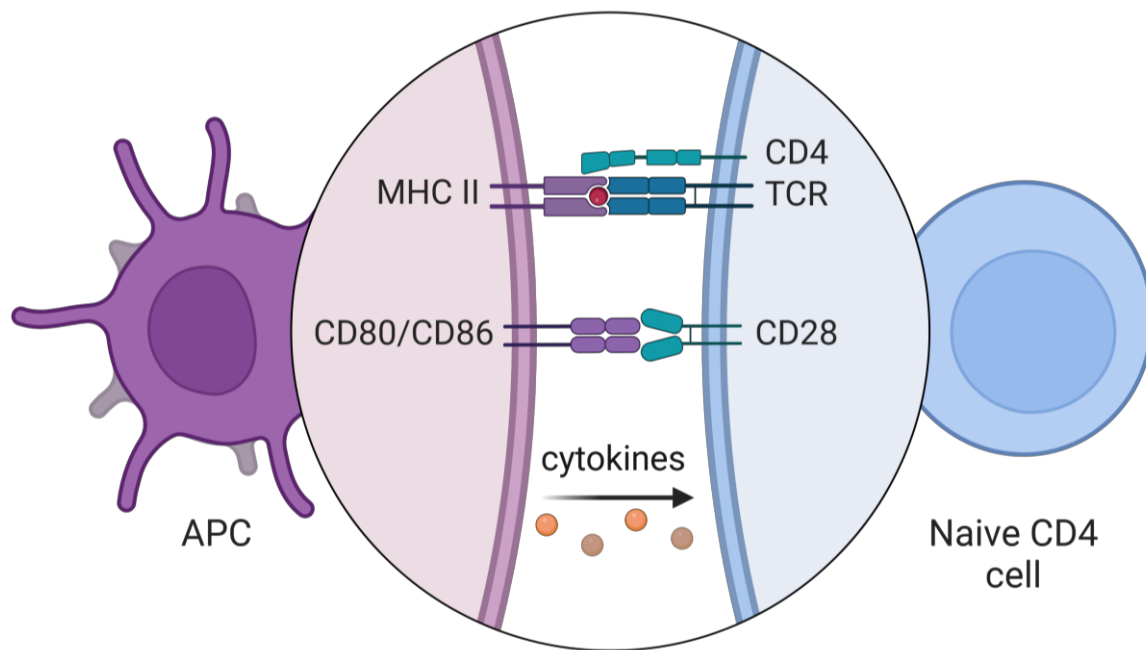
Figure 4: CD4 T cell Activation (simplified)
T-cell activation requires, the interaction between the TCR and the peptide-MHC-II complex on the APC, the binding of the T-cell co-receptor CD28 to CD80/CD86 on the APC and involves cytokines binding to their specific receptors on the T cell surface. The combination of these cytokines determines T cell differentiation into various subtypes. (Adapted from Lazaratos *et al.*, created with BioRender)

1.10.1 Regulatory T cells

Tregs are essential for peripheral tolerance and in maintaining homeostasis.[80] The defining feature of these cells is their expression of the transcription factor FOXP3, which is critical for their development and regulatory functions.[81]

Through clonal diversion, self-reactive T cells are re-programmed to develop a suppressive or regulatory phenotype, influencing the behavior of a wide spectrum of cell types, including CD4 Th cells, cytotoxic CD8 T cells, B cells and dendritic cells.[82–84] Besides Tregs that originate from the thymus (tTregs), Th cells (CD4) can convert to Tregs in the periphery (pTregs) provided the presence of tumor growth factor beta (TGF-β) and IL-2 when their TCR recognizes its antigen.[85,86] tTregs are primarily reactive to self-peptides, whereas pTregs establish tolerance to environmental antigens from food and commensal bacteria (non-self-antigens), particularly at mucosal surfaces such as the digestive and respiratory tract.[80,87,88] Although CD8 regulatory T cells are possibly complementing CD4 Tregs in the periphery, the latest research assumes that CD4 Tregs play a much bigger role in immune tolerance.[89,90]

Despite their different origin, tTregs and pTregs employ a variety of suppressive and regulatory mechanisms, including inhibitory cytokines, metabolic disruption, induction of cytolysis and modulation of DCs (Figure 5). The activation of Tregs depends on the interaction with other immune cells and the microenvironment.[82] Once activated, Tregs can release anti-inflammatory cytokines such as IL-10, TGF-β and IL-35, changing the immediate environment around the cell which affects the behavior of other immune cells such as effector T cells or differentiation of other CD4 T cells.[91] Tregs can also secret granzymes, leading to perforin-dependent cytolysis in natural killer (NK) cells and CD8 T cells.[92] Moreover, Tregs can affect the metabolism of other cells through various mechanisms, such as CD25-dependent IL-2 depletion from the surrounding milieu, leading to apoptosis of IL-2-dependent effector T cells. IL-2 also induces a negative feedback loop, wherein IL-2 produced by activated T cells enhances the suppressive functions of Tregs.[93,94] Furthermore, Tregs can perform their regulatory role via cell-cell contact.[82] Cytotoxic T-lymphocyte-associated protein 4 (CTLA-4) on their surface competes with CD28 on T cells for binding to CD80 and CD86 on APCs, thereby inhibiting T cell activation and inducing anergy.[70,95] Additionally, lymphocyte activation gene 3 (LAG3), a CD4 homologue, can also bind MHC-II molecules, thus inhibiting DC maturation.[96] It has also been shown that Tregs not just inhibit T cell activation by binding to their cognate antigen presented on DCs but that they can remove the entire peptide-MHC-II molecule from the DC's surface, resulting in a reduction of overall ability to present antigens.[97]

While the regulatory functions of Tregs are indispensable for preventing autoimmunity and homeostasis by regulating potential immunopathogenic immune responses, they can also suppress anti-tumor immunity and pathogen-specific effector responses, potentially aiding in immune evasion.[98,99] However, Tregs are also associated with enhanced adaptive immune responses by limiting the early, innate inflammatory phase during viral infections.[100,101] Mutations in the human *Foxp3* gene can lead to a lack of Tregs, resulting in severely impaired immune regulation and conditions such as poly-endocrinopathy and enteropathy, collectively known as immunodysregulation polyendocrinopathy enteropathy X-linked (IPEX) syndrome.[102] Despite significant advancements in our understanding of Tregs over the past decades, much of the research has been conducted *in vitro*, which limits our ability to fully grasp their functions *in vivo*.
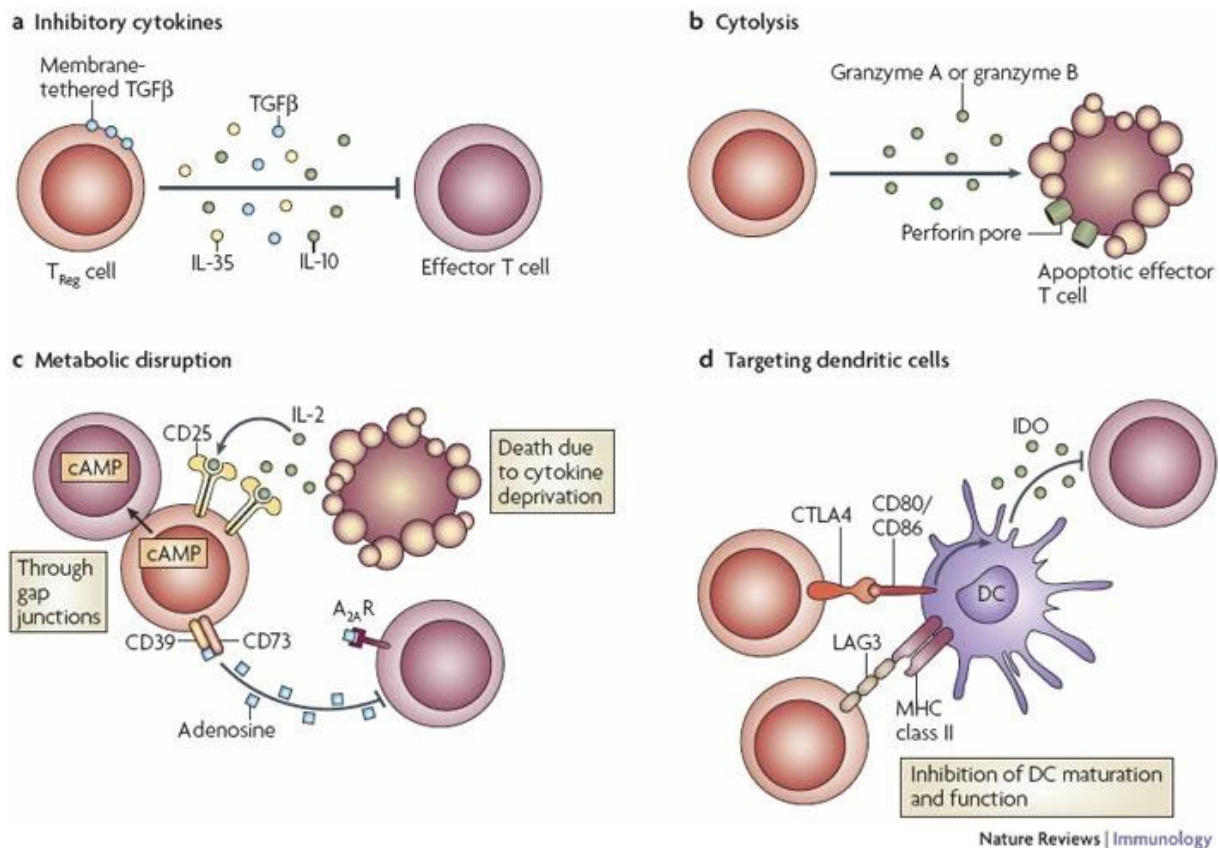
Figure 5: Basic Mechanisms Used by Tregs

This figure illustrates four core mechanisms of action employed by Tregs cells to mediate immune regulation, allowing them to maintain immune homeostasis and prevent autoimmunity. **a) Inhibitory Cytokines**: Tregs produce cytokines such as interleukin-10 (IL-10), IL-35, and transforming growth factor-β (TGFβ) to suppress immune responses. **b) Cytolysis**: Tregs can induce cell death through granzyme-A- or granzyme-B-dependent pathways and perforin-mediated mechanisms. **c) Metabolic Disruption**: Mechanisms include cytokine deprivation via high-affinity CD25 (IL-2 receptor α), cyclic adenosine monophosphate (cAMP) -mediated inhibition, and adenosine-mediated immunosuppression through CD39/CD73-generated adenosine binding to A2A receptors. **d) Targeting Dendritic Cells (DCs)**: Tregs modulate DC function and maturation through pathways such as LAG3 (CD223) binding to MHC class II to suppress DC maturation, and CTLA4 interaction with CD80/CD86 to induce production of the immunosuppressive enzyme indoleamine 2,3-dioxygenase (IDO) in DCs. (Adapted from Vignali *et al.*, 2008)

1.11 CD4 T cells

CD4 T cells, also known as Th cells, are a crucial component of the adaptive immune system. Unlike cytotoxic T cells (CD8), which directly eliminate infected cells, CD4 T cells do not attack pathogens.[103] Instead, they play a pivotal role in orchestrating the immune response by assisting other immune cells in mounting an effective defense. They activate other cells, including phagocytes of the innate immune system, B-lymphocytes, CD8 T cells, and even non-immune cells. Upon activation, the cytokine milieu around the cell determines the T cell's fate.[57]

In addition to converting into pTregs, CD4 T cells can differentiate into various subtypes under specific conditions. These subtypes play distinct roles and are adapted to respond to different threats.[104] Th2 cells are central to the humoral immune response, particularly in defending against extracellular parasites such as helminths.[105] Th17 cells are involved in the immune response against extracellular bacteria and fungi. They also contribute to inflammation and are associated with the pathogenesis of various autoimmune diseases, including multiple sclerosis and rheumatoid arthritis.[106,107] Th17 cells are closely interconnected with Tregs, highlighting the plasticity of T cell subsets. Even after differentiation, Th cells can be reprogrammed into another subset.[108]

However, while pTregs can lose their suppressive function (Foxp3 expression), tTregs typically keep their role imprinted by the thymus.[109] T follicular helper (Tfh) cells specialize in assisting B cells,[110] whereas Th9 cells are involved in mucosal immunity, contributing to allergic responses and anti-tumor immunity.[111,112] Finally, Th1 cells differentiate in response to the cytokine IL-12, produced by antigen-presenting cells, and IFN-γ.[113] The transcription factor T-bet is crucial for their differentiation.[114,115] Th1 cells are primarily involved in cellular immunity, particularly in defending against intracellular pathogens such as viruses and certain bacteria.[57] They secrete cytokines such as IFN-γ, TNF-α, and IL-2, which activate macrophages, enhance antigen presentation, and promote the cytotoxic functions of CD8 T cells and NK cells. Th1 cells also play a role in the activation and proliferation of B cells, especially in the production of certain subclasses of immunoglobulin (IgG) antibodies.[116,117]

The diverse subsets of CD4 T cells add dynamic complexity to the immune system, allowing for tailored responses to various threats. The interplay between Th1 and Tregs during viral infections is particularly noteworthy, as these two subsets must balance to ensure viral clearance and limit immunopathogenic effects.[118–120] However, the specifics of this balance particularly during filovirus infections remain to be elucidated. Studying the interactions between EBOV and its host can provide valuable insights into this dynamic. The following section will review the latest research on EBOV.

1.12 Taxonomy of Filoviruses

In 1982, the virologic taxon *Filoviridae* was defined[121]. The name 'Filoviruses' has its origin in the filamentous form of the viral particles (Figure 6a). Since the discovery of MARV in 1967,[122] followed by EBOV in Zaire in 1976,[123] many other members of the family *Filoviridae* have been discovered. Recently, the taxon was refined, resulting in changes to the genus names *Ebolavirus* and *Marburgvirus* to *Orthoebolavirus* and *Orthomarburgvirus*, respectively (Table 1).[124]

Table 1: Taxonomy of *Filoviridae* family

Genus name	Species name	Virus name (abbreviation)
Cuevavirus	*Cuevavirus lloviuense*	Lloviu virus (LLOV)
Dianlovirus	*Dianlovirus menglaense*	Měnglà virus (MLAV)
Loebvirus	*Loebvirus percae*	Lötschberg virus (LTBV)
Oblavirus	*Oblavirus percae*	Oberland virus (OBLV)
Orthoebolavirus	*Orthoebolavirus bombaliense*	Bombali virus (BOMV)
	Orthoebolavirus bundibugyoense	Bundibugyo virus (BDBV)
	Orthoebolavirus restonense	Reston virus (RESTV)
	Orthoebolavirus sudanense	Sudan virus (SUDV)
	Orthoebolavirus taiense	Taï Forest virus (TAFV)
	Orthoebolavirus zairense	Ebola virus (EBOV)
Orthomarburgvirus	*Orthomarburgvirus marburgense*	Marburg virus (MARV)
		Ravn virus (RAVV)
Striavirus	*Striavirus antennarii*	Xīlǎng virus (XILV)
Tapjovirus	*Tapjovirus bothropis*	Tapajós virus (TAPV)
Thamnovirus	*Thamnovirus kanderense*	Kander virus (KNDV)
	Thamnovirus percae	Fiwi virus (FIWIV)
	Thamnovirus thamnaconi	Huángjiāo virus (HUJV)

1.13 Ebola Virus

The term EBOV refers to the species *Orthoebolavirus zairense* and exists alongside five other species in the genus *Orthoebolavirus* (Table 1). In this study, the Mayinga variant of *Orthoebolavirus zairense* was investigated (annotated genome: AF086833.2). This variant is named after a nurse, Mayinga N'Seka, who contracted and eventually succumbed to the disease during the 1976 Ebola outbreak in Zaire (now the Democratic Republic of the Congo (DRC)).[123]

1.13.1 Virologic Features

Filoviruses such as EBOV belong to the order *Mononegavirales*, meaning their genome is linear, non-segmented, single-stranded, negative sensed RNA.[125] The EBOV genome length is approximately 19 kilobases (kb) and encodes for seven structural proteins: the nucleoprotein (NP), the glycoprotein (GP), the polymerase (L), the viral protein (VP)35, VP24, VP30 and

VP40 (Figure 6b).[126–128] Notably, the surface GP, which form trimers, is generated by transcriptional editing and is composed of two subunits: the receptor-binding subunit GP1 and the fusion subunit GP2.[129] Part of the surface glycoprotein is cleaved by the cellular tumor necrosis factor-α-converting enzyme (TACE) and is then released in a soluble form-called shed GP.[130] Additionally, the primary transcript of the *GP* gene results in synthesis of another soluble protein: secreted glycoprotein (sGP), which is then cleaved by the cellular enzyme furin into sGP and Δ-peptide.[131,132] Moreover, through transcriptional editing by the viral polymerase L, one additional mRNA species is generated encoding the small soluble glycoprotein (ssGP).[133–135]
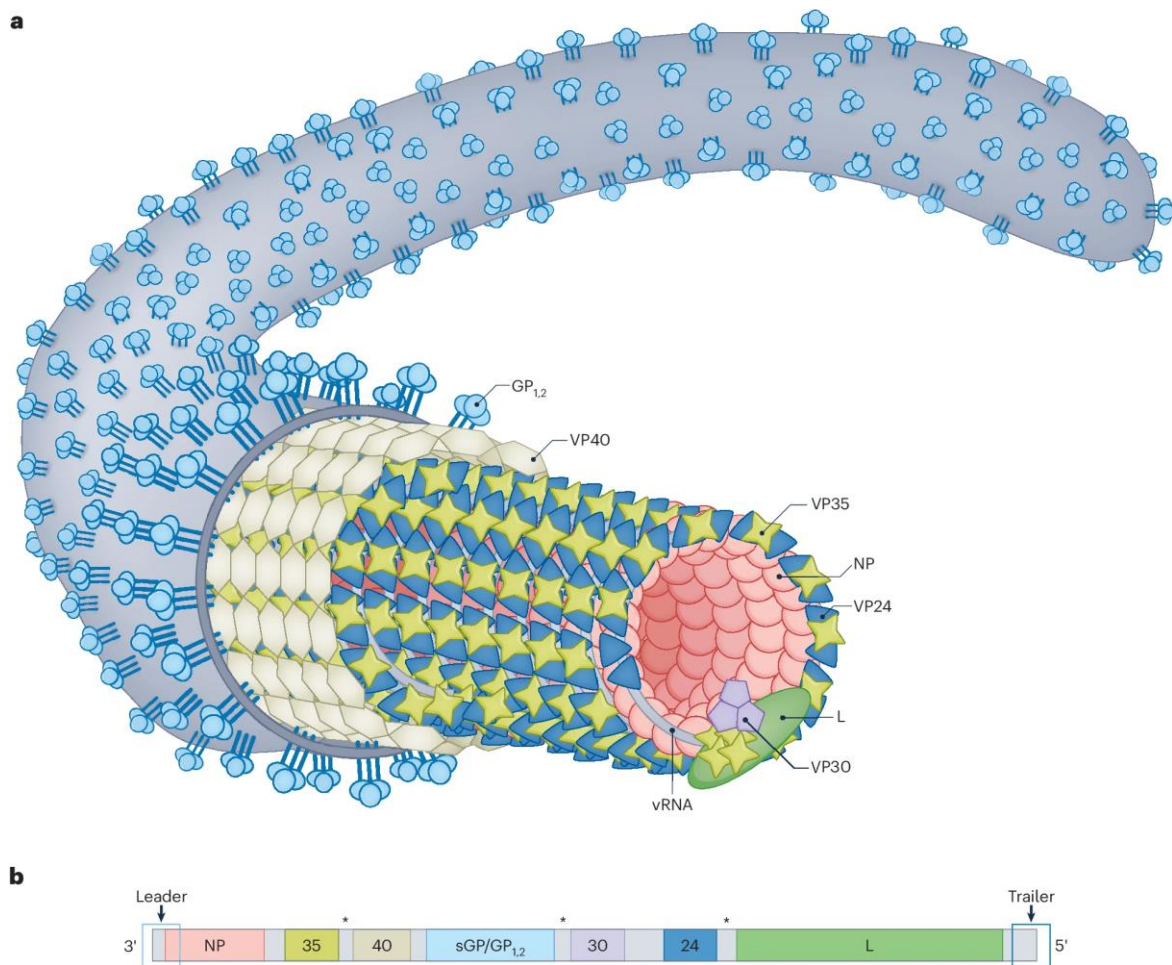
Figure 6: Viral particle of EBOV

a. Particle Structure: The viral genome (vRNA, light grey) is encapsidated by the nucleoprotein (NP, red) and associated with viral proteins VP35 (light green), VP30 (purple), and the polymerase (L, green), forming the nucleocapsid. VP24 (dark blue) is also linked to the nucleocapsid. Beneath the viral membrane (dark grey), the matrix layer consists of VP40 (tan). The viral glycoprotein (GP1,2, light blue) is embedded as trimers in the membrane. **b. Genome Organization**: Orthoebolaviruses possess a single-stranded RNA genome of negative polarity, encoding seven genes with protein-coding regions (colored) flanked by untranslated regions (grey). The genome ends, known as the leader and trailer (grey), contain replication promoters (3′ end: light blue box, trailer: dark blue box). Asterisks denote overlapping genes in orthoebolaviruses, except for Reston virus. (Adapted from Bodmer *et al.*, 2024)

1.14 EBOV Life Cycle

The life cycle of EBOV occurs entirely in the cytoplasm and resembles that of other *Mononegavirales* viruses (Figure 7).[126] The infection of cells by EBOV begins with the attachment of the viral particle to the host cell surface, primarily facilitated by GP. The spike protein, embedded in the virus envelope, binds to various cell surface molecules, including C-type lectins such as DC-SIGN and L-SIGN, and sialoadhesins such as Siglec-1.[127] Additionally, EBOV can bind to T cell immunoglobulin mucin receptors (such as TIM-1 and TIM-4) via phosphatidylserines in the viral membrane. This process, known as apoptotic mimicry, enhances uptake of viral particles by phagocytes and their subsequent infection.[136,137] Although *in-vitro* studies have shown antibody-dependent attachment mechanisms, their significance in disease progression for naïve individuals remains uncertain.[138,139] Following attachment, EBOV is internalized into endosomes, primarily through macropinocytosis, a process involving the uptake of extracellular fluid via vesicles.[140] In the acidic environment of late endosomes, host proteases such as cathepsin B and L alter the conformation of GP1, enabling it to bind with the Niemann-Pick C1 (NPC1) receptor. This interaction facilitates the GP2-mediated fusion of the viral and endosomal membranes, resulting in the release of the viral ribonucleoprotein (RNP) complex into the cytoplasm, where EBOV replication and transcription occur.[128,141,142]

The RNP complex is composed of the NP, polymerase L, polymerase cofactor VP35, and transcription activator VP30. The viral RNA-dependent RNA polymerase (L protein) transcribes the viral RNA, producing mRNA for viral protein synthesis and replicating the genome via an antigenomic intermediate. Initial transcription results in viral mRNA that is translated into viral proteins by the host cell machinery.[143] These new proteins support subsequent waves of viral mRNA transcription and genome replication, facilitated within viral factories known as inclusion bodies (IBs).[144] Within these membrane-less liquid organelles formed by liquid–liquid phase separation, driven primarily by NP oligomerization, new RNA genomes are encapsidated by NP (nucleocapsids) with VP35 acting as a chaperone for NP.[145,146] Interestingly, various host proteins, such as heat shock proteins, seem to support viral processes.[143,147] The transition between transcription and replication is regulated by VP30. Its non-phosphorylated form is necessary for transcription, whereas phosphorylation shifts the balance towards replication.[148,149] NP-encapsidated viral genomes can leave IBs and move to budding sites. Viral mRNAs exit IBs via nuclear RNA export factor 1 (NXF1) recruited by NP.[150] Once in the cytoplasm, most mRNAs are translated on free ribosomes, with the GP mRNA being translated at the endoplasmic reticulum.[143] EBOV produces various forms of GP, including membrane-bound GP1,2 and several soluble forms (sGP, Δ-peptide, shed GP, ssGP), through transcriptional and enzymatic processes.[135] Some viral proteins have properties that affect the host's immune system, contributing to completing EBOV's life cycle. sGP is secreted

by infected cells. It can act as decoy and has anti-inflammatory functions.[151,152] VP35 is involved in blocking innate intracellular immune responses and VP24 inhibits type I interferon (IFN-I) responses.[153,154] VP24 is also involved in nucleocapsid formation and assembly by condensing the ribonucleoprotein complexes into a packaging-competent form.[155,156] The ribonucleoprotein complexes are transported to the cell surface via actin filaments, along with VP40, which plays a key role in virion assembly and budding.[157–159] GP follows the secretory pathway and is transported to VP40-rich regions at the plasma membrane. VP40 then facilitates viral egress, leading to the budding of newly formed virions from the host cell, completing the EBOV life cycle.[143]
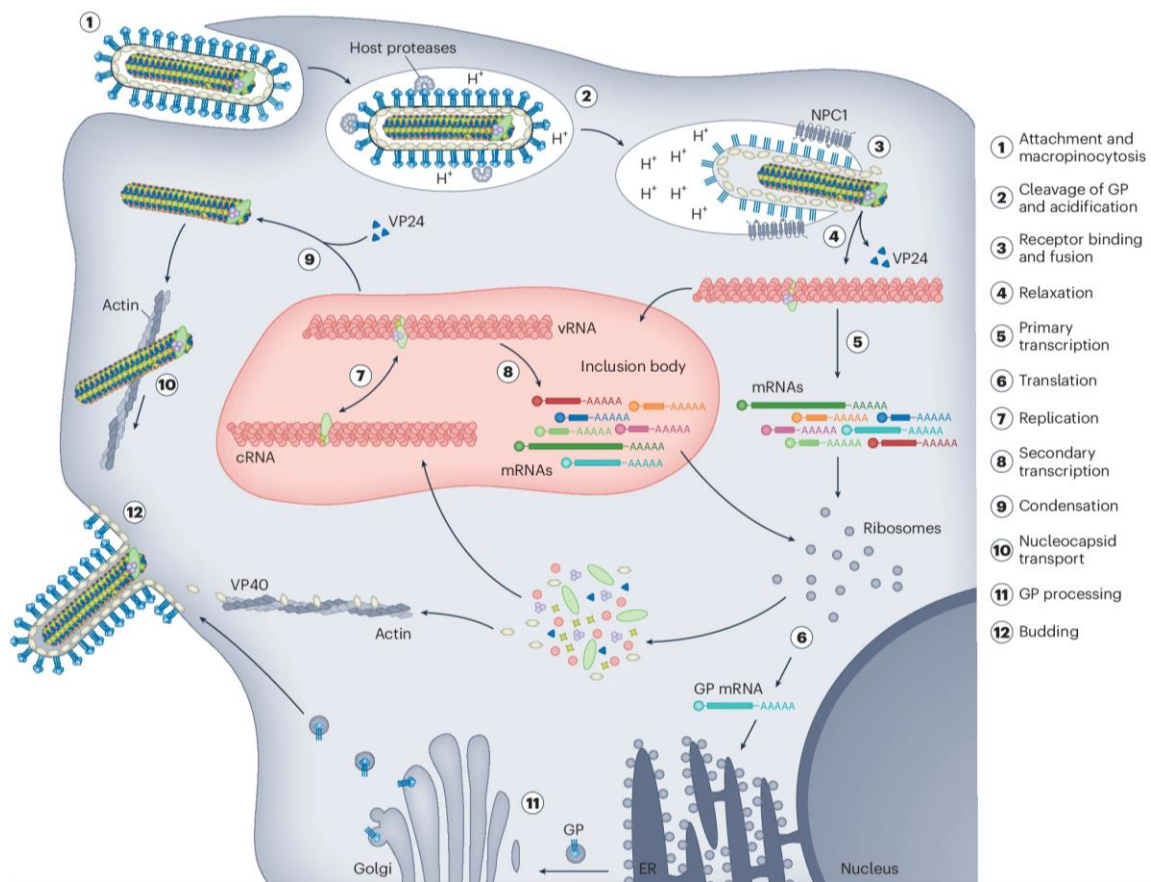
Figure 7: *Orthoebolavirus* life cycle

The virus attaches to cell-surface receptors, triggering uptake via macropinocytosis **(1)**. Endosomal acidification activates host proteases, such as cathepsins, to cleave GP1,2 **(2)**, enabling binding to the intracellular receptor NPC1 and fusion of the viral and endolysosomal membranes **(3)**. This releases the nucleocapsid into the cytoplasm, where VP24 displacement relaxes the nucleocapsid structure **(4)**, facilitating primary transcription in the cytoplasm **(5)**. Viral mRNAs (except GP mRNA) are translated at free ribosomes **(6)**, with the resulting proteins driving genome replication **(7)** and secondary transcription **(8)** within viral inclusion bodies. RNP complexes are condensed into nucleocapsids by VP24 **(9)** and transported, along with VP40, to the plasma membrane via actin filaments **(10)**. GP mRNA is translated at ER-bound ribosomes, and the glycoprotein is processed and glycosylated in the ER/Golgi network before being transported to the plasma membrane via the secretory pathway **(11)**. Viral budding, mediated by VP40, involves the ESCRT complex and membrane lipids **(12)**. Viral and host components are color-coded as in figure 6, with host elements shown in grey. (Adapted from Bodmer *et al.*, 2024)

1.15 EBOV Tropism and Systemic Spread in Human Hosts

EBOV typically enters the human body via mucous surfaces or micro lesions in the skin.[127] Dendritic cells (DCs) and macrophages are EBOV primary targets (Figure 8).[160,161] Additionally, it has been shown that EBOV attaches to activated monocytes and subsequently enters the cell with a delay upon their differentiation into macrophages or DCs.[162] These initial target cells are suspected to contribute to virus dissemination due to their migratory characteristics.[163] With progression of the infection, the virus is released into the circulation and becomes systemic, showing a broad tissue and cell tropism including epithelial and endothelial cells, fibroblasts, hepatocytes, and adrenal cortical cells.[164] Studies also suggest that EBOV can persist in the body, most likely in immune privileged sites e.g., the brain, testes, gonads and the eye, enabling the chances for a relapse.[165]

1.16 Immune Response to EBOV Infections in Humans

The immune system identifies foreign agents and typically initiates a response tailored to eliminate them. Infection with EBOV prompts an immune reaction that includes both innate and adaptive mechanisms. The innate immune system responds immediately as the first line of defense, with macrophages releasing cytokines and chemokines to combat the infection. The adaptive immune response, while highly specific, takes longer to develop and involves the activation of B cells and T cells, which are essential for the clearance of the virus.[166–168]

Despite the immune system's sophisticated mechanisms to combat pathogens, it can occasionally overreact, causing more harm than benefit to the host.[169] It is important that the immune responses are precisely coordinated and tightly regulated. Conversely, viruses employ various strategies to evade these immune responses.

1.16.1 Innate Immune Response

Once EBOV breaches the skin, it infects dendritic cells (DCs) and macrophages.[160] This infection activates macrophages, which in turn exacerbates the inflammatory response. This response is marked by the release of cytokines such as IL-1β and tumor necrosis factor (TNF)-α, as well as chemokines like macrophage inflammatory proteins (MIP)-1α and nitric oxide (NO). This induces the additional migration of macrophages, as well as other immune cells, such as monocytes and neutrophiles, to the site of infection.[166,170,171]

A key cytokine for the early antiviral response is IFN-I, produced by all types of infected cells, with DCs and macrophages releasing it in relatively high concentrations. IFN-I production is triggered by the recognition of viral RNA by pattern recognition receptors (PRRs), mainly retinoic acid inducible gene I (RIG-I) and melanoma differentiation-associated protein 5 (MDA-5). Secreted IFN-I from infected cells is detected by IFN-I cell surface receptors, inducing an antiviral state that blocks viral replication.[57,172] However, EBOV counteracts IFN-

I responses through the actions of VP35 and VP24. VP35 inhibits IFN-I production, disrupting both autocrine signaling (where cells respond to their own IFN) and paracrine signaling (where neighboring cells respond to IFN). Meanwhile, VP24 prevents bystander cells from responding to IFN-I.[153,154,173] These mechanisms are crucial for controlling viral replication in the early stages of EBOV infection, though an excessive IFN-I response can lead to immunopathology.[174]

DCs play a crucial role during EBOV infections as mediators between innate and adaptive immune system.[175,176] It has been shown that EBOV can infect DCs, contributing to the virus' spread.[177] Recent studies have revealed that not all DC subsets are equally susceptible to EBOV infection.[178] Specifically, while monocyte-derived DCs (moDCs) are more susceptible, classical DCs (cDCs) exhibit only minimal infection. This limited infection of cDCs leads to their activation rather than inhibition, resulting in heightened CD8 T-cell activation.[179]

1.16.2 Adaptive Immunity

Adaptive immunity involves cellular and humoral responses, which are essential for eliminating infected cells and producing antibodies, respectively. In the cellular response, infected cells display cytosolic viral antigens on their surface using MHC-I molecules. The TCR on CD8 T cells recognizes these antigens, leading the CD8 T cells to release granzyme B and perforin, which induce apoptosis in the infected cells.[57] Additionally, extracellular antigens can be presented by DCs via MHC-I in a process called cross-presentation, which is suggested to drive T cell proliferation during EBOV infection.[180]

CD4 T cells are crucial regulators of the immune response. Their activation relies on professional APCs such as DCs and macrophages. Viral peptides derived from extracellular proteins bind to MHC-II molecules and are then presented on the cell surface of APCs. Naïve CD4 T cells that recognize the antigen via their TCRs may differentiate into Th1 effector cells, aiding CD8 T cells in lysing infected cells, or into Tfh cells, which assist B cells in antibody production. CD4 T cells also recruit innate immune cells, such as macrophages and NK cells, to infection sites.[57,181] Although Tregs are important for a balanced immune system and influence disease outcomes, their role during EBOV infection has yet to be elucidated.

Clinical studies have shown that EBOV-infected patients generate robust adaptive immune responses, with high numbers of activated, EBOV-specific CD8 and CD4 T cells found in both survivors and fatal cases.[167] However, T cells in patients with fatal outcomes displayed lower TCR diversity and higher expression of inhibitory molecules, such as CTLA-4 and PD-1, indicating a dysregulated T-cell response.[168,182] Severe lymphopenia is often observed during EBOV infection. It is proposed that exposure of T cells to EBOV results in an abortive infection, likely contributing to increased T-lymphocyte depletion.[183] Additionally, *in-vitro* studies suggest that bystander T cells die due to high levels of TNFα released from T cells that come

into contact with EBOV particles. Despite extensive research, much remains unclear concerning the immune response to EBOV infections.[184,185]

The humoral response involves the production of antibodies by activated B cells. Antibodies have various functions, including direct neutralization of viruses by blocking viral entry receptors, activation of the complement system, facilitation of cellular cytotoxicity, and aiding phagocytosis.[186] Studies on EBOV have linked a strong antibody response to viral clearance and disease survival. Conversely, patients with fatal outcomes often do not mount virus-specific antibody responses.[187] However, there have been cases where fatal outcomes occurred despite high antibody levels, and some survivors had undetectable EBOV-specific antibodies for weeks post-recovery.[188–190] Thus, the role of humoral immune responses against EBOV infections remains poorly understood.
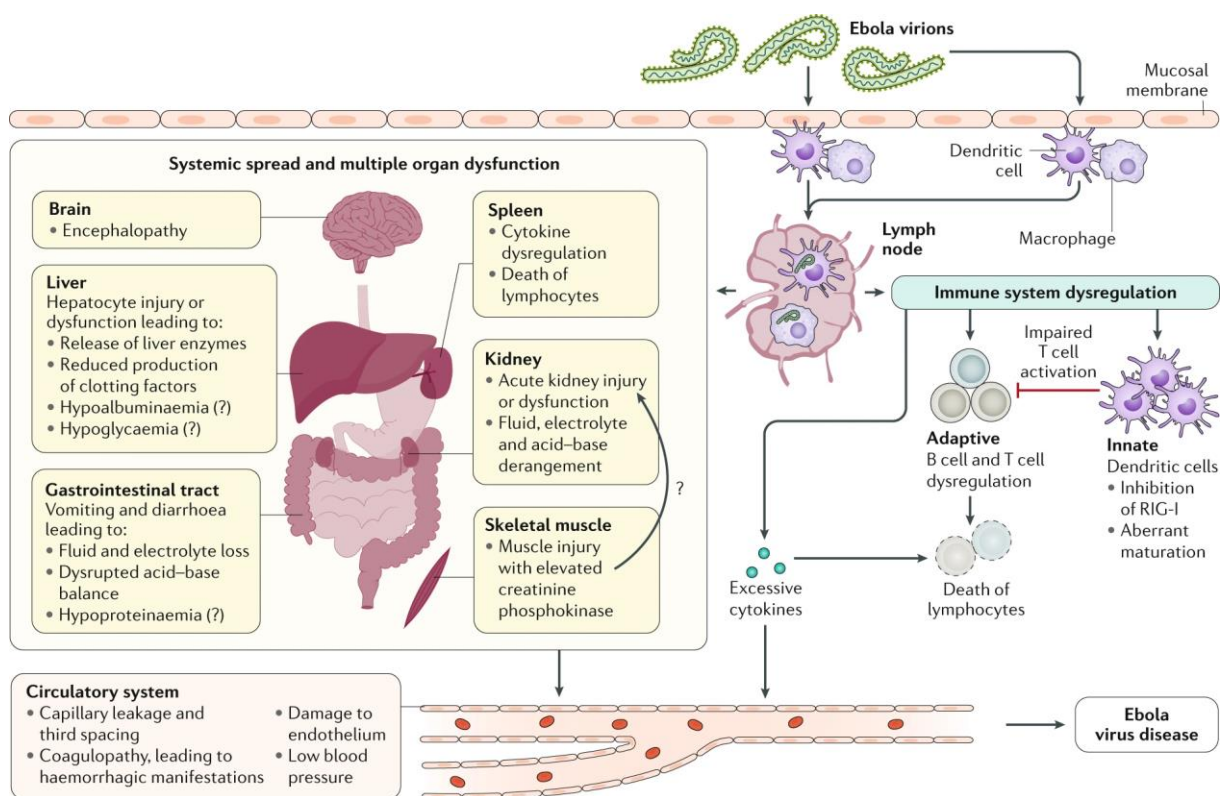
Figure 8: Ebola Virus Pathogenesis and Ebola Virus Disease
Ebola virus enters the body through dermal wounds (either microscopic or macroscopic) or direct contact with mucosal membranes. The primary cells targeted are macrophages and dendritic cells, which migrate to regional lymph nodes contributing to viral spread. By suppressing intrinsic, innate, and adaptive immune responses, the virus achieves systemic distribution, infecting secondary target cells across other organs. Critical organ-specific interactions occur in the gastrointestinal tract, liver, and spleen, leading to markers of organ damage or dysfunction that align with disease outcomes in humans. Question marks (?) indicate speculative effects. (Adapted from Jacob *et al.*, 2020)

1.17 Clinical Manifestations

EBOV and other filoviruses cause severe disease in humans and non-human primates, with fatality rates in humans ranging from 25 to 90 %.[191,192] This depends highly on disease progression before the start of treatment. On top of the direct damage to the host due to viral replication, with viremia levels at hospitalization correlating with disease outcome, disease severity is strongly associated with the host immune response. The symptoms are collectively referred to as Ebola virus disease (EVD).[193–195]

The incubation period ranges from two to 21 days, with most individuals exhibiting symptoms after six to ten days, due to the inflammatory response of the host to EBOV infection.[196] Initial symptoms such as fatigue, headache, fever, arthralgia, malaise, and myalgia are non-specific. However, within a few days, the signs of illness intensify, with nausea, vomiting, and diarrhea, leading to severe dehydration and electrolyte imbalance. Additionally, tissue hypoperfusion and coagulopathy are commonly observed, resulting in multiple organ dysfunction, including acute kidney and liver injuries (Figure 8).[197,198] Vasodilation and increased endothelial permeability caused by the migration of monocytes, macrophages, and neutrophils are important antiviral immune responses. However, if they occur systemically over a prolonged period, they can lead to hemorrhages. Disseminated intravascular coagulation (DIC) is a hallmark of severe EVD, characterized by widespread clotting in blood vessels, leading to organ damage, depletion of clotting factors, and severe bleeding.[199] Despite EVD being considered a viral hemorrhagic fever, bleeding abnormalities such as gum bleeding, hematemesis, and melena occur in fewer than half of the patients. In severe cases, the high replication rate of EBOV overwhelms the immune system, leading to high levels of inflammation with excess T-cell activation, hypercytokinemia ('cytokine storm'), and coagulopathy, results in multiple organ failure and ultimately the host's death.[200] Following the incubation period and upon exhibition of symptoms, body fluids become highly infectious, facilitating the transmission of the virus via direct contact to the next person or animal. Survival is often linked with extended convalescence with severe sequelae of EVD. Symptoms such as musculoskeletal pain, headache, encephalitis, and ocular complications (such as uveitis) have been reported and summarized as post-Ebola syndrome.[201] These symptoms may be partly explained by the virus's potential to persist in immune-privileged sites.[202] Consequently, body fluids, such as semen and breast milk, may remain infectious even after recovery. Therefore, the chances of transmission from survivors remains, contributing to the stigma faced by those who have recovered from EVD.[166,203,204]

1.18 Treatment and Vaccines

Prior to the major EBOV outbreak between 2013 and 2016 (Section 1.19), patients received only supportive care, including intravenous fluids, electrolyte balance maintenance, and medication for pain relief and symptom management. Recognizing the inadequacy of these

measures, substantial efforts have been dedicated to developing antiviral therapeutics and improving outbreak preparedness in endemic regions.[205]

Currently, the previous measures are complemented by antiviral therapies utilizing antibody cocktails such as Inmazeb (REGN-EB3) and Ebanga (mAb114), reducing mortality to around 34-35% in clinical trials compared to higher mortality rates in control groups (Pamoja Tulinde Maisha (PALM) trial).[206] These are monoclonal antibodies that target GP, preventing the virus from entering host cells and aiding the immune system in neutralizing the virus. Apart from that, antiviral drugs such as remdesivir are used under emergency conditions for Ebola treatment. Furthermore, transfusions of blood or plasma from recovered EVD patients, which contain antibodies against the virus, have also been utilized to increase survival rates. However, a substantial percentage of patients still succumb to the disease, especially those with high viremia at the time of hospitalization, warranting the need for novel and effective treatment strategies.[207]

To date, efforts put in vaccine development have resulted in the licensing of two vaccines.[208] In 2019, the first vaccine, called ERVEBO (rVSV-ZEBOV), was approved by the Food and Drug Administration (FDA) and the European Medicines Agency (EMA). It has been used in outbreak settings for at-risk populations and healthcare workers (ring vaccinations) and has proven to be highly effective in reducing mortality rates, particularly against *Orthoebolavirus zairense*. It is a replication-competent, live, attenuated recombinant vesicular stomatitis virus (rVSV) vaccine encoding the EBOV GP, manufactured by Merck.[209] In 2020, the second vaccine was approved for use under 'exceptional circumstances' by the EMA. However, it was used in 2019 under a research protocol during an outbreak in the DRC and proved to be effective in providing protection against *Orthoebolavirus zairense*. It is a two-dose vaccine regimen with Zabdeno (Ad26.ZeBOV) as the first dose, expressing the EBOV GP, and Mvabea (MVA-BN-Filo) as the second dose, expressing GPs from several filoviruses, including EBOV, SUDV, MARV, and TAFV (multivalent). The two components are an adenovirus-based vaccine and a modified Vaccinia Ankara virus (MVA)-based vaccine, respectively, which are manufactured by Johnson & Johnson.[210]

Effective management of EBOV infections and disease involves a combination of supportive care, antiviral therapies, and preventive vaccines. The two vaccines have proven effective in controlling outbreaks. However, broad-acting countermeasures for orthoebolaviruses other than EBOV are still not available. Continued research and development with a special interest in a universal *Orthoebolavirus* vaccine are crucial for advancing treatment options and enhancing the efficacy of preventive measures.[211]

1.19 *Orthoebolavirus* Outbreaks

Since the first recognized outbreak of EVD in 1976 in what is now the DRC,[123] many outbreaks of varying sizes have been reported in Central and Western Africa (Figure 9). Although most outbreaks can be attributed to EBOV, high case fatality rates (CFRs) have also been reported for Sudan virus (SUDV). Additionally, Bundibugyo virus (BDBV) and Taï Forest virus (TAFV) are pathogenic to humans, but their outbreaks have been limited to two and one, respectively. While some cases have been reported in other parts of the world, such as the United States of America (USA), the United Kingdom (UK), Spain, and Italy, most were imported from Africa or involved healthcare workers who came in close contact with EVD patients or infectious material.[127,212] The largest outbreak of EVD occurred in West Africa between 2013 to 2016, affecting Guinea, Liberia, and Sierra Leone. This epidemic resulted in over 28,000 cases and more than 11,000 deaths.[213] The rapid spread of the virus and high CFRs were facilitated by several factors, including weak surveillance and fragile public health infrastructure, poor infection control measures, and strained healthcare systems. Cultural practices, such as traditional burial rites involving close contact with the deceased, also played a critical role in the transmission of the virus.[214,215] Although recent outbreaks have been sporadic and could be controlled due to the use of newly available therapeutics and vaccines as well as prompt identification and isolation of cases, improved infrastructure, efforts in health education and community engagement, they continue to pose significant public health challenges with high CFRs. In August 2018, the DRC faced a substantial outbreak, primarily affecting the North Kivu and Ituri provinces. This outbreak was further complicated by the region's ongoing conflict and instability, which hindered efforts to contain the virus. Over 3,400 cases were reported, with more than 2,200 deaths (CFR: 66 %), making it the second-largest Ebola outbreak on record. The spread of the virus in this instance was exacerbated by factors such as population movement, distrust in health authorities, and attacks on healthcare workers and facilities. More recent outbreaks have increasingly been linked to relapse or sexual transmission, partially due to improved sequencing technology and availability, suggesting a persistent infection of EBOV in EVD survivors.[216,217] These include one outbreak in 2021 in Guinea with a CFR of 52.2 % and two in the DRC with CFRs of 50 % and 82 %, respectively. The most recent outbreaks were in 2022 in Uganda and the DRC. While the two outbreaks in the DRC comprised only six cases in total, the CFR was 100 %. The outbreak in Uganda was caused by SUDV, with 164 reported cases and a CFR of 34 %.[212]

Aside from the outbreaks possibly originating in persistence, most EVD outbreaks are likely the result of spillover events, a new introduction of the virus into the human community from an animal reservoir [(5)], followed by person-to-person transmission.[195,218] Due to an increase in

---

[(5)] Also called natural reservoir. Animal host where pathogens naturally reside and reproduces before the occurrence of spillover events

human-animal interactions through urbanization, deforestation, climate change, and destabilization by conflicts, RNA virus infections are emerging predominantly in affected regions.[219] This is compounded by the pervasive infrastructural underdevelopment, which contributes to the spread once a spillover occurs. In order to prevent future outbreaks, it is of great importance to identify and monitor the natural reservoirs of orthoebolaviruses.[220]
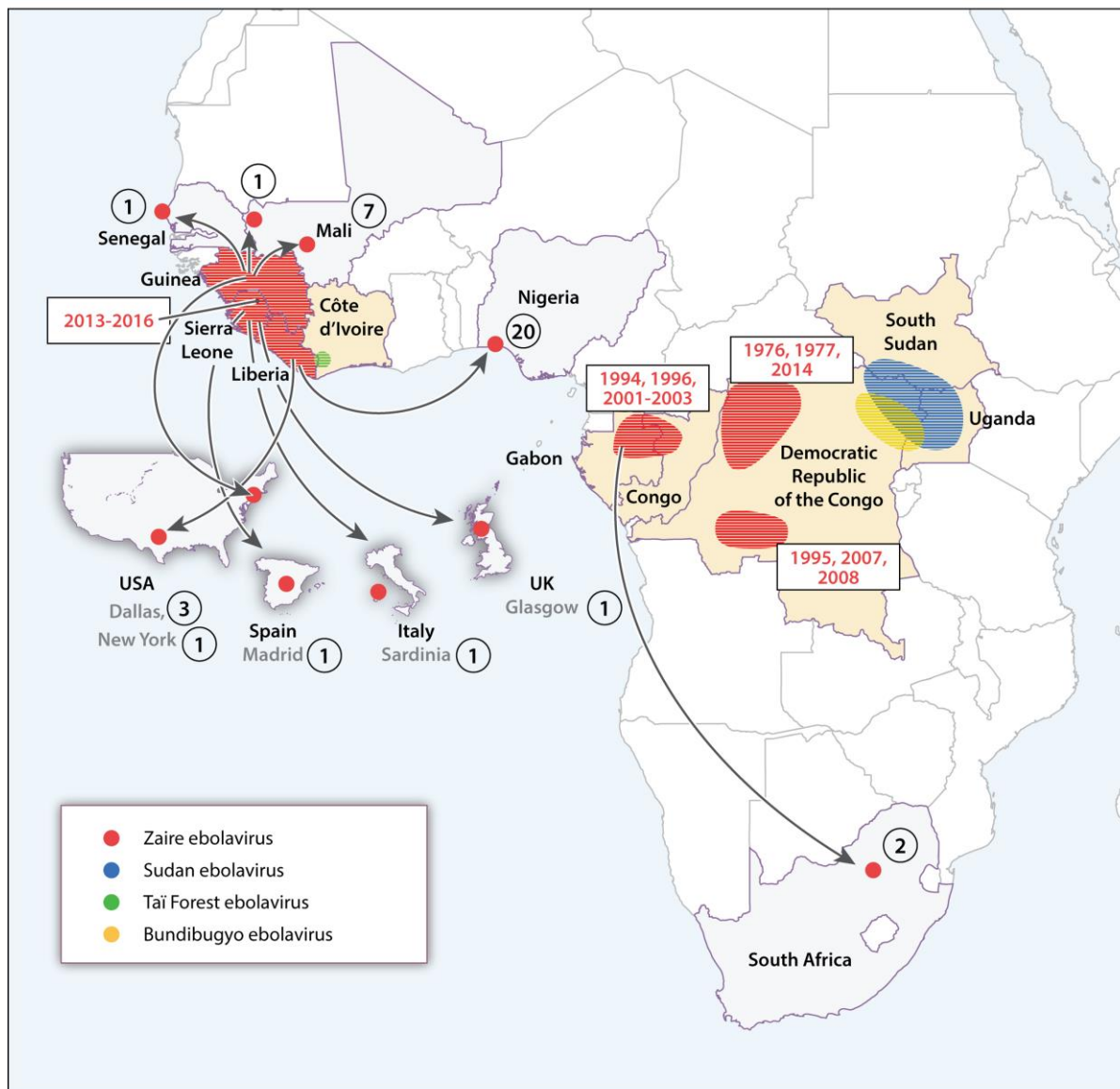
Figure 9: *Orthoebolavirus* Outbreaks in West and Central Africa (from 1976 to August 2016)

The map shows the geographic locations of all documented human outbreaks caused by four ebolavirus species within the equatorial region of Africa. Circled numbers represent EVD cases linked to the introduction of EBOV-infected individuals from Guinea, Sierra Leone, Liberia, or, in one case, Gabon, during the 2013–2016 West African epidemic. (Adapted from Basler *et al.*, 2017)

1.20 Ecology of Ebola Virus - Bats as Potential Reservoir

EBOV and other filoviruses are zoonotic pathogens, meaning they can infect not only humans but also other animals. Zoonotic pathogens can jump from a reservoir to other hosts in spillover events. A reservoir host is characterized as an infectable organism that is often resistant to the virus's associated disease and allows the virus to replicate and be transmitted to other hosts, including humans.[221] Humans or non-human primates (NHPs) function as intermediate or amplifying hosts or as dead-end hosts for the virus if the infection leads to the host's death. Despite increased efforts in more than 40 years of research, the reservoir of EBOV has not been identified. However, research points towards bats as natural reservoirs.[222,223] Belonging to the order of *Chiropteran*, bats represent approximately 20 % of all mammals with more than 1,400 known species habituated in various geographic areas and climate zones.[224] Bat colonies provide optimal sites for virus transmission due to their roosting habit with a high density and their ability to fly great distances creating perfect conditions for intra- and interspecies dissemination of the virus.[52,225] Nonetheless, the potential for bats as EBOV reservoir remains to be proven since the isolation of infectious viral particles or the recovery of whole viral genomes has been unsuccessful so far. However, Egyptian rousette bats (ERBs, *Rousettus aegyptiacus*) have been identified as reservoirs for another filovirus, MARV.[226] Additionally, complete genome sequences of Bombali virus (BOMV) were recently found in free-tailed bats (*Mops condylurus* and *Chaerephon pumilus*), although no infectious virus could be isolated, strengthening the argument that bats are the most likely natural reservoirs for orthoebolaviruses.[227,228] Intriguingly, Angolan free-tailed bats (AFBs, *Mops condylurus*) are being discussed as the origin of the EBOV epidemic in 2014. Although exposure to fruit bats is common in regions affected by EVD outbreaks, the index case (a 2-year-old boy in Meliandou, Guinea) may have been infected by playing in a hollow tree housing a colony of this insectivorous free-tailed bat species.[218,229] Studies have shown that this species can survive experimental infection asymptomatically. Moreover, a recent study investigated the permissiveness of AFBs to various filoviruses (EBOV, MARV, TAIV, and RESV), demonstrating only high and disseminated viral replication and infectious virus shedding of EBOV without clinical disease, while the other filoviruses failed to establish productive infections. Their findings also indicated horizontal and vertical transmission mechanisms that are expected of a reservoir host.[230]

1.21 The Special Immune System of Bats

Comparing the severe pathology of EVD in humans with the asymptomatic EBOV infections in bats raises important questions about the underlying reasons. Many research groups have investigated the immune system of bats, finding that while there are parallels to humans, the bat immune system is unique among mammals.[231] A homeostatic immune system is crucial for

every living organism, and in both bats and other mammals, this system is tightly regulated. Bats, however, appear to have an enhanced balance between defense and tolerance. An appropriate immune response is necessary to fight pathogens, but an excessive or dysregulated response can result in increased pathology. Thus, tolerating viruses at low levels could be the trade-off for restricting potential immunopathological responses.[232,233] Detailed immune mechanisms in bats are still being elucidated, but research over the last decades has uncovered multiple differences compared to other mammals, also attempting to explain their ability as natural reservoirs.[52]

One factor is that bats undergo hibernation with decreased body temperature and metabolic rate, possibly preventing viral clearance. Another factor is that the ability to fly, a unique feature among mammals, seems closely linked to their special immune system.[225] The high metabolic rate and increased ("fever-like") body temperature during flight are suggested to heavily influence immune responses.[234] Furthermore, evolutionary changes for adaptation to flight have been observed, including alterations in mitochondrial and nuclear oxidative phosphorylation genes and dampened inflammatory responses to stresses.[235] It is suggested that innate antiviral mechanisms in bats allow for early control of viral replication. This includes differences in IFN activation, such as baseline expression, kinetics, induction, or functions of antiviral genes in IFN signaling.[236] These extreme adaptations to hibernation and flight could have driven the observed differences in the immune system between bats and other mammals. Additionally, bats have enhanced autophagy, greater IgG diversity, unique structures within MHC-I and II, and express very high levels of heat-shock proteins, all potentially affecting the immune response.[52] Moreover, bats possess an additional toll-like receptor (TLR), TLR 13, previously identified only in rodents and bovines.[237] Conversely, adaptations to viral infections may have led to increased immunopathology during extracellular infections.[52,238] Despite these findings, much research is still needed to achieve a coherent understanding of the bat immune system.

1.22 Paleoviral Sequences in Bats

The absence of pathological processes in bats during virus infections is also suggested to be a result of 64 million years of co-evolution with viruses.[52,239,240] The discovery and ongoing research into endogenous viral elements in bat genomes are providing new insights into the immunological mechanisms that contribute to their unique immune system and their role as natural reservoirs for many viruses.[241] Bats have a high diversity of retroviral and non-retroviral endogenous sequences compared to other mammals, possibly excepting some rodents.[7] Although ERVs likely influence bat biology, the focus has shifted in recent decades to NIRVs due to the emergence of zoonotic and often fatal RNA viruses. These bat-NIRVs include sequences from borna-, orthobunya-, filo-, orthomyxo-, reo-, and rhabdoviruses. Some of these sequences are sufficiently preserved to retain potential functions.[242]

1.23 EBOV NIRVs in Bats

Multiple bat species harbor NIRVs, many of which are related to EBOV (NP- and VP35-NIRVs). The best-described filovirus NIRVs to date are VP35-NIRVs in mouse-eared bats (*Myotis*). These NIRVs are preserved as nearly full-length ORFs and potentially function as IFN antagonists, suggesting a suppressive effect on host immunity.[243,244] Other EBOV NIRVs are suggested to interfere with virus' assembly (primarily NP-NIRVs). Although their role is poorly understood, a correlation between the possession of NIRVs and resistance to the related virus or the disease it causes is being observed in bats, suggesting an involvement of NIRVs in immunity.[52,245]

The presence of EBOV NIRVs in genomes suggests a tight co-evolution of the host and the virus. Considering that all animals that harbor EBOV NIRVs could be potential EBOV reservoirs, it is crucial to further investigate their role in the ecology and transmission dynamics of the virus. For this, models are extremely important in basic research. Interestingly, both bats and mice possess EBOV NIRVs.[7,18,242] Although they can be infected with EBOV, neither species exhibits symptoms.[230,246]

1.24 *Mus musculus* as a Model Organism to Study NIRVs

Mus musculus, the common laboratory mouse, is a widely used model organism for studying various human diseases, including viral infections such as Ebola virus (EBOV). This species offers numerous advantages, including genetic similarity to humans, a well-characterized immune system, and the availability of sophisticated genetic and analytical tools.[246]

To analyze …

In the context of EBOV research, data have been derived from a combination of *in-vitro* studies, NHP models, human clinical data, and murine models. Human clinical data are the gold standard for understanding disease dynamics and treatment efficacy, yet they are challenging to obtain and often come post hoc. *In-vitro* studies allow for controlled experimentation on specific aspects of the virus and immune response. Despite promising advances in technologies such as organoids and organ-on-a-chip, *in-vitro* studies are often insufficient to capture the complexity of an entire organism's immune system. On the other hand, NHPs are closer to humans in terms of immune response, providing valuable insights, particularly when studying vaccine efficacy and disease pathology.[247–250] However, ethical considerations and logistical constraints limit their widespread use.

Recent research has increasingly focused on bats as potential EBOV reservoirs.[230] Although valuable data can be obtained from studying bats, conducting experiments on them poses significant challenges, which likely explains their limited use in experimental research. For

example, their maintenance and handling in laboratory settings are more complex compared to established mouse models and there is a lack of important reagents, such as bat-specific antibodies. All in all, mouse models remain invaluable for *in-vivo* studies.

Similar to bats, *Mus musculus* harbors a filovirus-like NIRV. This sequence aligns with the N-terminal region of EBOV NP, a highly conserved domain across *Mononegavirales*.[18,251,252] Other mammals also carry similar filovirus-like elements in this region (Figure 10). Notably, *Rattus norvegicus* has an identical NP-NIRV copy at the same genomic locus. Independent integration events in both species are highly improbable. This shared integration indicates a common ancestral event, with rat-mouse orthology placing the minimum age of NP-NIRV formation between 12 and 24 million years ago, reflecting prolonged co-evolution with ancestral filoviruses.[18]

The murine NP-NIRV is integrated as an intact ORF in reverse (3'-5'), similar to the negative-sense EBOV genome. It is flanked by LINEs, suggesting insertion via TE-mediated mechanisms. This makes the mouse an ideal model for investigating the function and evolutionary significance of EBOV NIRVs.
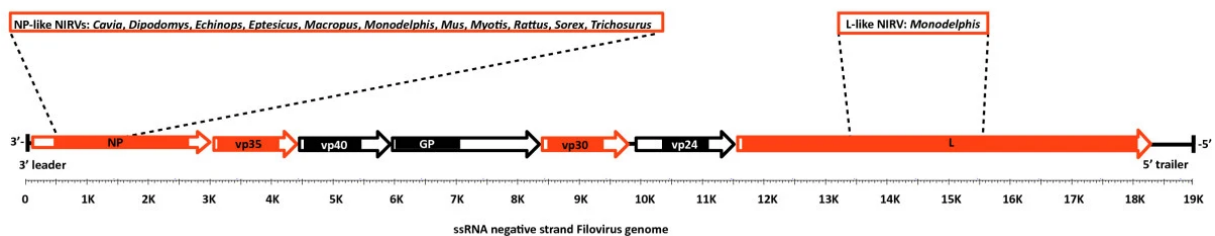
Figure 10: Filovirus Genome Map with Gene Order and Homology to Proposed Mammalian Filovirus-Like Elements.

Dashed lines mark the boundaries of NIRVs, highlighting a bias toward the N-terminal region of the NP gene. Mammalian genera with filovirus gene homology are listed above the genome map. Solid colors within the coding region arrows represent product size, while red shading indicates proteins linked to viral RNA within the ribonucleoprotein complex. (Adapted from Taylor *et al.*, 2010)

2 Objectives

This thesis aims to provide novel insights into the role of NIRVs and deepen the understanding of host-virus interactions throughout their co-evolution. Building on previous research that suggests a correlation between resistance to viral diseases and the presence of NIRVs, this project aims to characterize the role of the *Mus musculus* EBOV NP-NIRV in conferring resistance to EBOV disease in laboratory mice, as well as the underlying mechanisms. The study is driven by the hypothesis that EBOV-derived elements (NIRVs), embedded in the mouse genome but absent in humans, are presented as self-antigens during T cell maturation in the murine thymus. This process may confer immune tolerance to EBOV infection in mice.

Main objectives:

Evaluation of the Functions of the Murine NP-NIRV *in vitro*:

To investigate the functions of NP-NIRV, we aim to determine whether its expression directly impacts viral replication, potentially acting as a dominant-negative version of the EBOV NP. Additionally, we aim to explore the relationship between NP-NIRV and AIRE to better understand the molecular mechanisms involved.

Characterization of the Response to EBOV Infection in NIRV-Null Mice:

We have utilized CRISPR/Cas9[6] technology to generate NP-NIRV knockout (KO) mice (NIKI mice). The goal is to characterize these mice and examine the role of NP-NIRV in immune tolerance to EBOV infection, providing insights into how the absence of this NIRV affects the immune response.

---

[6] CRISPR = clustered regularly interspaced short palindromic repeats; Cas9 = CRISPER associated protein 9

3 Materials

The following chapter describes all materials used in this study.

3.1 Bacteria

Escherichia coli (E. coli) was used to amply plasmids in this study (Table 2).

Table 2: Bacteria

Bacteria strain	Properties	Reference
E. coli DH5α	chemically competent, Genotype: F⁻ Φ80*lac*ZΔM15 Δ(*lac*ZYA-*arg*F) U169 *rec*A1 *end*A1 *hsd*R17(r_k^-, m_k^+) *pho*A *sup*E44 *thi*-1 *gyr*A96 *rel*A1 λ⁻	Thermo Fisher Scientific Inc., Cat. # 18265-017

3.2 Mammalian Cell Lines

The following tables lists the mammalian cell lines (Table 3) that were used in this study. Table 4 lists all cell lines that were created from the Flp-In T-REx 293 host cell line containing a gene of interest (GOI). These cells were used in viral growth curve experiments. Vero E6 cells were used for virus amplification and virus titration (Section 4.3 and 4.9).

Table 3: Mammalian Cell Lines

Cell line	Properties	Reference
Flp-In T-REx 293	*Homo sapiens* (fetus), kidney, epithelial, adherent, SV40 T antigen, pFRT/lacZeo and pcDNA6/TR stably integrated	Invitrogen Thermo Fisher Scientific Inc., Cat # R78007
VERO C1008	*Cercopithecus aethiops* (adult), kidney, epithelial, adherent	ATCC [Vero 76, clone E6, Vero E5] (ATCC®CRL-1587)

Table 4: Flp-In T-REx 293 Cell Lines with GOI

Name of cell line	Properties
GFP	Stably expressing eGFP; loss of Zeocin resistance; Hygromycin resistance
NIRV	Stably expressing EBOV NP-NIRV; loss of Zeocin resistance; Hygromycin resistance
NIRV-GFP	Stably expressing a NIRV-P2A-eGFP construct; loss of Zeocin resistance; Hygromycin resistance
H1N1-NP	Stably expressing H1N1-NP with HA tag; loss of Zeocin resistance; Hygromycin resistance

3.3 Viruses

The following table displays the virus strains that was used in this study.

Table 5: Viruses

Virus	Properties	Reference
Orthoebolavirus zairense	Mayinga variant, passage 2	1976 Zaire outbreak variant, AF086833.2, GCA_000848505.1
Lassa mammarenavirus	Strain: Ba366, clustering with lineage IV variants	European Virus Archive Global partner site BNITM, isolated from *Mastomys natalensis*, GU979513.1 and GU830839.1

3.4 Mouse strains

All mice were bred in the animal facility of the Bernhard Nocht Institute for Tropical Medicine. Female mice between 5 and 15 weeks of age were used in this study. Samples from AIRE KO mice (thymic cDNA) were provided by Matsumoto *et al.* (Tokushima University). Experiments with animals were approved by the Committee on the Ethics of Animal Experiments of the federal state of Hamburg (Behörde für Gesundheit und Verbraucherschutz, Hamburg) under the approvals: 031/2018, 036/2019, N061/2021, 2021-T007 and N068/2023. A total of 274 mice were utilized in this study. Mice were handled and euthanized in accordance with the prescribed rules and regulations of the German Society for Laboratory Animal Science. The following table lists the mouse strains of this work.

Table 6: Mouse Strains

Mouse strain	Origin
C57Bl/6J	Jackson laboratories
NIKI643(Chr9_643bp_KO_B6J)	Jackson laboratories
NIKI814 (Chr9_814bp_KO_B6J)	Jackson laboratories
IFNAR$^{-/-}$ (B6(Cg)-Ifnar1tm1.2Ees/J)	Jackson laboratories
DEREG (*Foxp3^{DTR}, B6.129(Cg)-Foxp3tm3(Hbegf/GFP)Ayr/J*)	Jackson laboratories

NP-NIRV KO mice were generated using CRISPR/Cas9 technology. This mouse strain has no NP-NIRV sequence in chromosome 9 (deleted locus: Chr9: 73977099-7397765) and will be analyzed in comparison to C57BL/6J (WT) mice. The two NIKI mouse strains (643 and 814) have slightly different deletions. The number indicates the total of deleted base pairs (bp). The

strain was generated by The Jackson Laboratory (JAX) from C57BL/6J (JR 000664). The mice reproduce without complications and are completely healthy.

3.5 Primers

Table 7 and 8 lists all relevant primers used in this study. All primers were synthesized by biomers.net GmbH.

Table 7: Primers for PCRs

fw=forward; rev=revers, T_A = annealing temperature, univ = universal NP-NIRV primers

Name	Sequence (5'-3')	T_A [°C]	Size Amplicon
AIRE for AIRE rev	TCCCACCTGAAGACTAAGC ACCACTGGCTTTAGGCTGC	56.2	305 bp
GAPDH fw GAPDH rev	CGTATTGGGCGCCTGGTCA CACAGTCTTCTGGGTGGCAG	50.0	528 bp
NIRV fw (univ) NIRV rev (univ)	AGTCTATTCCTTCCGAAA AATCAATAAGCCTGAAAA	43.0	approx. 300 bp
mNIRVqRT fw mNIRVqRT rev	GCAGTTTCTTCCTTCCTAAACTGGTC CTCGCAAGAGACCAACCTTATGAAAG	57.0	126 bp

Table 8: Primers for Cloning of the Flp-In T-REx 293 Cell Lines

Lowercase: overhangs; uppercase: anneal; underlined: HA-Tag; fw = forward; rev = revers, T_A = annealing temperature

Name	Sequence (5'-3')	T_A [°C]	Size Amplicon
GFP fw	ctggctagcgtttaaacttaagc-TTACTTGTAAAGTTCGTCCATGCC	61.0	766 bp
GFP rev	cgggccctctagactcgagcggccgc-ATGTCCAAGGGCGAGGAAC		
NP-NIRV fw	ctggctagcgtttaaacttaagctt-ATGGGGCTGGGATTATTTTTAATTTATTG	61.0	327 bp
NP-NIRV rev	cgggccctctagactcgagcggccgc-TTAAATGTTTGTGATCATCTCAGTTG		
NIRV-GFP fw	ctggctagcgtttaaacttaagctt-ATGGGGCTGGGATTATTTTTAATTTATTG	61.0	1098 bp
NIRV-GFP rev	cgggccctctagactcgagcggccgc-TTACTTGTAAAGTTCGTCCATGCC		
HA-H1N1-NP fw	ctggctagcgtttaaacttaagctt-ATG<u>tacccttacgatgtaccggattacgca</u>-GCGACCAAAGGCACC	64.5	1548 bp
HA-H1N1-NP rev	cgggccctctagactcgagcggccgcTTAATTGTCGTACTCCTCTGCATTG		

3.6   Vectors and Constructs

The following tables show all vectors (Table 9) and constructs (Table 10) that were used for cloning of the Flp-In T-REx 293 cell lines. Table 11 lists all plasmids used for the transcription- and replication-competent virus-like particle (trVLP) system (Hoenen *et al.*).[253] The associated vector maps and maps of constructs are archived in the database of the research group Virus Immunology at the BNITM and will be shared upon request.

Table 9: Vector Systems

Vector	Properties	Size	Reference
pcDNA5/FRT	CMV promoter, T7 promoter, MCS, BGH pA, FRT site, hygR, SV40 pA, pUC origin, ampR	5070 p	Invitrogen Cat # V601020
pOG44	CMV promoter, SV40 pA, pUC origin, ampR, FLP ORF	5785 bp	Invitrogen Cat # V600520

Table 10: Constructs

Construct	Size	Size of Insert	Reference
pcDNA5/FRT/NIRV	5285 bp	327 bp	This study
pcDNA5/FRT/NIRV-GFP	6056 bp	1098 bp	This study
pcDNA5/FRT/GFP	5724 bp	766 bp	This study
pcDNA5/FRT/H1N1-NP	6506 bp	1548 bp	This study

Table 11: Vectors of the EBOV tetracistronic Minigenome[253]

Construct	Size	Reference
pTH2067_pCAGGS-luc2	6411 bp	Hoenen *et al.*
pTH5366_pT7.1-4cis-EBOV-vRNA-nluc	10,405 bp	Hoenen *et al.*
pTH5554_pCAGGS-EBOV-VP30_v1.1	5617 bp	Hoenen *et al.*
pTH5804_pCAGGS-EBOV-VP35_v1.1	6762 bp	Hoenen *et al.*

pTH5835_pCAGGS-EBOV-NP_v1.1	6970 bp	Hoenen *et al.*
pTH5895_pCAGGS-EBOV-L_v1.1	11,398 bp	Hoenen *et al.*
pTH5801_pCAGGS-T7opt	7412 bp	Hoenen *et al.*
pTH5900_pCAGGS-Tim1opt-v1.2	6162 bp	Hoenen *et al.*
pCAGGS (empty vector)	4801 bp	Hoenen *et al.*

3.7 Reagents

The following table lists all reagents that were used in this study.

Table 12: Reagents

Reagent	Company	Reference
BD Cytofix Fixation Buffer	BD Biosciences	554655
100 % isopropanol (2-Propanol)	Sigma-Aldrich Chemie GmbH	278475
4 % Formaldehyde	Biocyc GmbH & Co. KG	40060030551
Agarose Universal Agarose	Bio&SELL	B20.46.100
Ampicillin sodium salt	Sigma-Aldrich Chemie GmbH	10835242001
Antifade Mounting Medum with DAPI	Vectashield	H-1200
BD ELISPOT AEC Substrate	BD Biosciences	551951
Blasticidin S HCl	Gibco Thermo Fisher Scientific Inc.	R210-01
Bovine Serum Albumin (BSA)	Carl Roth GmbH + Co. KG	9048-46-8
CellTrace Violet	Invitrogen	C34557
Chloroform	Merck KGaA	102442
Collagenase I	Roche AG	5172969103
Collagen-I	Gibco Thermo Fisher Scientific Inc.	A10483-01
Complete Freund's Adjuvant (CFA)	Sigma-Aldrich Chemie GmbH	F5881
CutSmart-Buffer	New England Biolabs Inc.	B7204S
DMSO	Carl Roth GmbH + Co. KG	4720.20

DNase I	Roche AG	4716728001
Dulbecco's Modified Eagle Medium (DMEM) w: 4.5 g/L Glucose, L-Glutamine, w/o: Sodium pyruvate, w:3.7 g/L NaHCO3	PAN-Biotech GmbH	P04-03550
Dulbecco's Phosphate Buffered Saline (DPBS) w/o: Ca and Mg	PAN-Biotech GmbH	P04-361000
Enzyme EcoRI-HF	New England Biolabs Inc.	R3101L
Enzyme HindIII-HF	New England Biolabs Inc.	R3104L
Enzyme NotI-HF	New England Biolabs Inc.	R3189L
EtOH (Ethanol) ≥99,8 %,	Carl Roth GmbH + Co. KG	9065.3
Fetal Bovine Serum, qualified, heat inactivated	Gibco Thermo Fisher Scientific Inc.	10500064
Formalin solution, neutral, buffered, 10 %	Sigma-Aldrich Chemie GmbH	MKCQ0195
GelRed Nucleic Acid Gel Stain	Biotium	41003
GeneRuler DNA Ladder Mix	Thermo Fisher Scientific	SM0331
Glycerol	Carl Roth GmbH + Co. KG	3783.1
GoTaq Green Master Mix	Promega	M7123
ROTI Histofix, 4 % Formaldehyd, ready-to-use, phosphatgepuffert, pH 7	Carl Roth GmbH + Co. KG	P087.3
HRP Streptavidin	BD Biosciences	557630
Hygromycin B (50 mg/ml)	Gibco Thermo Fisher Scientific Inc.	10687010
HyPure Cell Culture Grade Water (endotoxin-free)	Cytiva	SH30529.FS
Isoflurane	Piramal Critical Care Deutschland GmbH	1,06231E+12
LB Agar (Luria/Miller)	Carl Roth GmbH + Co. KG	X969.2
LB Broth (Miller)	Sigma-Aldrich Chemie GmbH	L3522
Loading buffer 6X DNA Loading Dye	Thermo Fisher Scientific	R0611
Methyl cellulose (viscosity 400 cP)	Sigma-Aldrich Chemie GmbH	M0262
N,N-Dimethylformamid (DMF)	Carl Roth GmbH + Co. KG	68-12-2
NEBuilder HiFi DNA Assembly Master Mix	New England Biolabs Inc.	E2621L
N-Histofine Simple Stain MAX PO immune-enzyme polymer	Nichirei Biosciences Inc	414154F
Paraformaldehyde 37%	Carl Roth GmbH + Co. KG	CP10.4

Passive lysis buffer (5X)	Promega	E194A
Penicillin/Streptomycin (10,000 U/mL)	Gibco Thermo Fisher Scientific Inc.	15140122
PHA-L	Merck KGaA	431784-5MG
Red blood cell (RBC) lysis buffer (10x)	BioLegend	420301
Roswell Park Memorial Institute medium (RPMI) 1640 (+L-Glutamine)	Gibco Thermo Fisher Scientific Inc.	11875093
Tetramethylbenzidine (TMB)	Mikrogen Diagnostics	10008
TransIT-LT1 Transfection Reagent	Mirus Bio	MIR 2305
Triton X-100	Carl Roth GmbH + Co. KG	3051.2
TRIzol Reagent	Ambion Thermo Fisher Scientific	15596018
Trypan Blue Stain 0.4 %	Gibco Thermo Fisher Scientific Inc.	15250-061
Trypsin – EDTA solution	Sigma-Aldrich Chemie GmbH	R001100
Zeocin Selection Reagent	Gibco Thermo Fisher Scientific Inc.	R250-05

3.8 Media

The following part describes the different media that was used to culture cells.

3.8.1 Bacterial Growth Medium

For culturing bacterial cells, lysogeny broth (LB) powder was dissolved in double-distilled water (ddH$_2$O). Before use, the LB-medium was autoclaved (121 °C for 20 min at 2 bar). Sterile heat-sensitive additives such as Ampicillin (Amp) were added after the medium had cooled to <55 °C. For solid medium 1,5 % (w/v) Agar-Agar was added to the LB-medium before autoclaving (Table 13). After sterilization the agar was poured into petri dishes under a safety cabinet and left there until solidification. Agar plates and medium were stored at 4 °C.

Table 13: Bacterial Growth Medium

Medium	Application	Possible Additions	Antibiotics
LB	*E. coli*	for solid medium 1,5 % (w/v) Agar-Agar	0.1 % (v/v) Amp

3.8.2 Mammalian Cell Growth Medium

For mammal cell lines Dulbecco's Modified Eagle's Medium (DMEM) complemented with 10 % or 5 % Fetal Calf Serum (FCS) was used. For the infection process DEMEM with FCS

was used. After an infection DMEM with 2,5 % FCS was used. To prevent bacterial contaminations Penicillin und Streptomycin (P/S) was added. For splenocytes culture during Enzyme-linked immune absorbent spot (ELISpot) assays RPMI 1640 medium with 10 % FCS was used (Table 14).

Table 14: Mammalian Cell Growth Medium

Medium	Application	FCS in % (v/v)	Antibiotics
DMEM	Vero	5 % or 10 %	1 % (v/v) P/S
	Flp-In T-REx 293	5 % or 10 %	1 % (v/v) P/S, 1 % (v/v) Zeocin, 1 % (v/v) Blasticidin
	Flp-In T-REx 293 with inserted GOI	5 % or 10 %	1 % (v/v) P/S, 1 % (v/v) Hygromycin B, 1 % (v/v) Blasticidin
	During infections	0 %	1 % (v/v) P/S
	After infections	2.5 %	1 % (v/v) P/S
RPMI	Splenocytes (ELISpot assay)	10 %	-

3.9 Consumables

The following table lists all consumables used in this study.

Table 15: Consumables

Consumables	Company	Reference
25ml Reservoir, Sterile, SureFlo, Four Sleeves of 50 per Case, Polystyrene	Integra Biosciences	4382
96 Well Cell Culture Plate (sterile, V-bottom, with lid)	Greiner Bio-One	651 180
Carbon Steel Scalpel Blade (No 11, Sterile)	Swann Morton	0203
CryoPure Tube 1.6ml white	Sarstedt AG & CO. KG	72.380
Disposal bags	Sarstedt AG & CO. KG	86.1197
EASYstrainer Cell strainer 70 µm, for 50 mL tubes, blue, sterile	Greiner Bio-One	542070
GOT-PIII test plates	Fujifilm	9903140ES
Luna Cell Counting Slides	Logos biosystems	L12001
Lysing Matrix B	MP Biomedicals	116540425

Microscopic Cover Glasses	Glaswarenfabrik Karl Hecht GmbH & Co. KG	41001112
Microscopic slides	Paul Marienfeld GmbH & Co. KG	1216332
Microtest Plate 96 Well,R	Sarstedt AG & CO. KG	82.1582
Micro tube 2.0ml	Sarstedt AG & CO. KG	72.691
Micro tube 2.0ml PP	Sarstedt AG & CO. KG	72.693
MultiScreenHTS IP Filter Plate, 0.45 μm, 8-Well Strips (ELISpot plates)	Merck Millipore	M8IPS4510
Multivette 600 CAT-Gel	Sarstedt AG & CO. KG	15.1674
Omnican 100	B. Braun	9151141S
Polystrene round-bottom tube with cell-strainer cap (5 mL)	Falcon	10585801
SafeSeal tube 1.5ml	Sarstedt AG & CO. KG	72.706
TC Flask T25, Stand., Vent. Cap	Sarstedt AG & CO. KG	83.3910
TC Flask T75, Stand., Vent. Cap	Sarstedt AG & CO. KG	83.3911
TC Plate 6 Well, Standard,F	Sarstedt AG & CO. KG	83.3920
TC Plate 12 Well, Standard,F	Sarstedt AG & CO. KG	83.3921
TC Plate 24 Well, Standard,F	Sarstedt AG & CO. KG	83.3922
Tube 15ml, 120x17mm, PP	Sarstedt AG & CO. KG	62.554
Tube 50ml, 114x28mm, PP	Sarstedt AG & CO. KG	62.547
V-bottom plate, polypropylene low-binding	Greiner Bio-One	651201

3.10 Kits

The following table lists all kits used in this study.

Table 16: Kits

Kits	Company	Reference
BD Cytofix Fixation Buffer	BD Bioscience	554655
Flp-In T-REx Core Kit	Invitrogen	K650001
iScript cDNA Synthesis Kit	Bio-Rad Laboratories	1708890
LEGENDplex Mouse Anti-Virus Response Panel (13-plex) with Filter Plate	BioLegend	740621

Nano-Glo Dual-Luciferase Reporter Assay System	Promega	N1610
NucleoSpin Gel and PCR Clean-up	Macherey-Nagel GmbH & Co. KG	740609,25
NucleoSpin Plasmid, Mini Kit	Macherey-Nagel GmbH & Co. KG	740588,25
NucleoBond Xtra Midi EF, Midi Kit	Macherey-Nagel GmbH & Co. KG	740420.50
NucleoBond Xtra Maxi EF, Maxi kit	Macherey-Nagel GmbH & Co. KG	740424.50
ultraView Universal DAB Detection Kit	Ventana	760-500
Zombie NIR Fixable Viability kit	BioLegend	423105

3.11 Antibodies

The following tables list all antibodies used in this study.

3.11.1 Antibodies and Dyes for Flow Cytometry and FACS

Tables 17 list displays the antibody panel for the analysis of immune cells in murine lung tissue and Table 18 shows the panel for FACS of TECs.

Table 17: Panel for Immune Cell Composition in Murine Lungs During EBOV infections

Marker	Color	Clone	Company	Reference
CD11b	Alexa 488	M1/70	BioLegend	101217
Ly6C	APC	HK1.4	BioLegend	128016
Ly6G	BV650	1A8	BioLegend	127641
F4/80	PerCPCy5.5	BM8	BioLegend	123128
CD11c	BV421	N418	BioLegend	117343
CD3	BV711	17A2	BioLegend	100241
CD4	PECy7	GK1.5	BioLegend	100422
CD19	BV570	6D5	BioLegend	115535
CD8a	BUV395	53-6.7	BD Bioscience	563786
Dead cells	Zombie NIR	-	BioLegend	423106

44

Table 18: FACS Panel for TECs

Marker	Color	Clone	Company	Reference
EpCAM	PE	G8.8	eBioscience	12-5791-81
Ly-51	PE-Cy 7	6C3/BP-1	BioLegend	108314
CD45.2	PerCP Cy 5.5	104	BioLegend	109828
mTECs	UEA I/FITC	-	Vector Laboratories	FL-1061
Dead cells	Zombie NIR	-	BioLegend	423106
MHC II (IA/IE)	APC	M5/114.152	BioLegend	107614

3.11.2 Antibodies for Immunofocus Assay

Table 19 includes the antibodies used for the immunofocus assay.

Table 19: Antibodies for Immunofocus Assay

Antibody	Company
Polyclonal mouse anti-EBOV primary antibody	in-house (BNITM)[254]
Sheep anti-mouse (IgG H+L) HRP-conjugated	Jackson Immuno Research Laboratories, Inc.

3.11.3 Antibodies for Immunofluorescence Microscopy Staining

Tables 20 displays the antibodies used for the immunofluorescence microscopy staining.

Table 20: Antibodies for Immunofluorescence Microscopy

Antibody	Company
Goat anti-Mouse IgG (H+L) Cross-Adsorbed Secondary Antibody, Alexa Fluor 647	Invitrogen

3.11.4 Antibodies for ELISpot Assay

The capture and detection antibodies of the ELISpot assay are listed in the following table.

Table 21: Antibodies for ELISpot Assay

Antibody	Company
Mouse IFN-γ ELISPOT Capture Antibody (51-2525KZ)	BD Biosciences
Mouse IFN-γ ELISPOT Detection Antibody (51-1818KA)	BD Biosciences

3.11.5 Peptides for ELISpot Assay

The following table lists the peptides used in the ELISpot assay. For peptide synthesization GenScript Biotech Corporation was commissioned.

Table 22: Peptide Sequences

Name	Sequence
GFP	HDFFKSAMPEGYVQE
EBOV NP	LSFASLFLPKLVVGE
NIRV	LIYCSFFLPKLVKGG

3.12 Laboratory Equipment

The following table lists all devices and equipment used in this study.

Table 23: Laboratory Equipment

Laboratory equipment	Company
5415C Microcentrifuge	Eppendorf
AID iSpot (ELISpot reader)	Advanced Imaging Devices GmbH
Axio Imager M1 (microscope)	Zeiss
BD FACS Aria IIIu	BD Biosciences
BD LSRII Fortessa flow cytometer with an autosampler (HTS)	BD Biosciences
Centrifuge 5810 R	Eppendorf
Consort EV231 Electrophoresis Powersupply	Consort bvba

Cytek Aurora 5-Laser Spectral Flow Cytometer	Cytek Biosciences
Electrophoresis chamber model 40-1214-R	PEQLAB Biotechnologie GmbH
Eppendorf Thermomixer C	Eppendorf AG
EVOS FL Auto Imaging System (microscope)	Invitrogen
FastPrep 24 5G (Organ shredder)	MP Biomedicals
Fuji DRI-CHEM NX500i system	Fuji
Gel iX20 Imager	Intas Science Imaging Instruments GmbH
GloMax Navigator Microplate Luminometer with Dual Injectors and Pumps	Promega
Innova 4400 Incubator Shaker	New Brunswick Scientific Co.
Luna II automated Cell counter	Logos biosystems
MACS separators	Miltenyi Biotec
Microcentrifuge, VWR Micro Star 17 R	VWR
NanoDrop 2000	Thermo Fisher Scientific
Sunlab 3D shaker SU1030	Sunlab
T100 Thermal Cycler	Bio-Rad Laboratories
Ventana Benchmark XT	Ventana Medical Systems
Vortex mixer	Thermo Scientific

3.13 Software

The following table lists all software used in this study.

Table 24: Software

Software	Company
Adobe Photoshop (version 24)	Adobe
AID multiSpot	AID Autoimmun Diagnostika GmbH
Biorender.com	BioRender
ChatGPT	OpenAI
FACSDiva Software	BD Bioscience

Fiji	Open source
FlowJo, V10.9	FlowJo LLC
GraphPad Prism 10	GraphPad Software
Legendplex/Qognit software	BioLegend
Microsoft Office	Microsoft Corporation
NEBuilder Assembly tool	New England Biolabs (NEB)
Snapgene	Insightful Science
SpectroFlo version 3.1.0	Cytek Biosciences
Zotero	Open source

4   Methods

The following section describes all methods used in this study.

4.1   Mammalian Cell Culture

In this study, two mammalian cell lines were used: Vero E6, derived from kidney epithelial cells of the African green monkey, and Flp-In T-REx 293, a Human Embryonic Kidney (HEK) 293T cell line (Table 3). Both cell lines were cultured in 75 cm² flasks with 10 ml of DMEM (Table 14) and maintained at 37 °C with 5 % CO_2. Cells were passaged at 80 % confluency, with a 1:10 ratio, twice per week. The process involved washing cells with phosphate-buffered saline (PBS), detaching them with trypsin, inhibiting trypsin with DMEM (5% FCS) for a total volume of 10 ml, and transferring 1 ml of cells to new flasks containing DMEM (5 % FCS). Each cell line was discarded after 40 passages, followed by preparation of a fresh low-passage line (Section 4.1.4).

4.1.1   Determination of Mammalian Cell Counts

For cell counting, 10 µl of the cell suspension was mixed with 10 µl of trypan blue solution. Next, 10 µl of this mixture was pipetted onto a cell counting chamber, which was then inserted into the automated cell counter. The cell concentration was displayed as cells per ml (cells/ml).

4.1.2   Plating of Mammalian Cell Lines

For subsequent experiments, cells were cultured in well plates by seeding an appropriate number (Table 25) into each well and incubating them in DMEM at 37 °C with 5 % CO_2. A confluency of 80 % was targeted for transfections, while a complete monolayer was required for titrations.

Table 25: Cell Numbers for Well Plates

Well Plate	Vero E6	Flp-In T-REx 293	
	For Monolayer	For Transfection	For Monolayer
6	2×10^6	5×10^5	2×10^6
24	1×10^6	-	-

4.1.2.1 Collagen Coating of Well Plates

To ensure cell adherence during certain procedures, plates were pre-coated with 400 µl of collagen-I per well, diluted 1:30 in PBS. To prevent polymerization, the collagen solution was kept on ice. Plates were incubated with collagen for 1 hour at 37 °C, then washed twice with 2 ml PBS per well. Residual PBS was carefully removed, and plates were allowed to dry

completely under a sterile hood. Once dried, plates were sealed with parafilm, packed in a sterile bag, and stored at 4 °C until use.

4.1.3   Cryopreservation and Storage of Mammalian Cell Lines

To store cells, all cells of a cell culture flask were collected, centrifuged at 500 x g for 5 minutes, and re-suspended for a final concentration of $1x10^6$ cells/ml in FCS containing 10 % (v/v) dimethyl sulfoxide (DMSO). Cells were then stored at -80 °C for short-term storage or in liquid nitrogen for long-term preservation.

4.1.4   Thawing of Mammalian Cell Lines

Cells were retrieved from -80 °C or liquid nitrogen storage. The contents of one vial were mixed with pre-warmed DMEM (37 °C) and centrifuged at 500 x g for 5 minutes to remove DMSO. The cell pellet was then re-suspended in warm DMEM containing 10 % FCS and seeded into a cell culture flask (T25). After incubating overnight at 37 °C with 5 % CO_2, the medium was replaced.

4.2   Bacterial Cell Culture

4.2.1   Cultivation of *E. coli*

The *E. coli* strain DH5α was cultivated in sterile test tubes with 5 ml of LB medium, supplemented with selective antibiotics such as ampicillin (0.1 % (v/v)). Cultures were incubated shaking (120 rpm) at 37 °C for 16 hours. Following this, larger cultures could be initiated in Erlenmeyer flasks using the preculture.

4.2.2   Generation of *E. coli* Stocks

Cryo-cultures of successfully cloned plasmids were prepared as glycerol stocks in cryotubes. A bacterial culture was incubated overnight in the appropriate antibiotic-supplemented medium, then diluted 1:1 with 50 % glycerol. The cryo-cultures were stored at -80 °C. Additionally, bacterial strains were plated on solid media and stored at 4 °C for approximately two weeks.

4.3   Virus Amplification

LASV and EBOV were amplified on 60 % confluent VeroE6 cells. One day after seeding VeroE6 cells in DMEM with 5 % FCS and 1 % P/S, cells were infected with a multiplicity of infection (MOI) of 0.1 for each virus at 37 °C for 1 hour. After infection, the virus-containing medium was removed and replaced with DMEM containing 2.5 % FCS and 1 % P/S. Cells were incubated for 4 days (LASV) or 7 days (EBOV) at 37 °C with 5 % CO_2. Supernatant was then harvested after centrifugation (2000 x g, 10 min, 4 °C) and stored at -80 °C. Viruses were passaged a maximum of two to three times on VeroE6 cells before use in experiments.

4.4 Molecular Biological Methods

4.4.1 RNA-Extraction

RNA extraction was performed using TRIzol Reagent. Cells were centrifuged at 1500 x g for 5 minutes, and the pellet was resuspended in 1 ml of TRIzol. Samples were incubated for 5 minutes at room temperature, then mixed with 0.2 ml chloroform per 1 ml TRIzol, shaken for 15 seconds, and incubated for an additional 3 minutes at room temperature. Samples were then centrifuged at 12,000 x g for 15 minutes at 4 °C, and the aqueous phase was transferred to a new 1.5 ml tube. Next, 0.5 ml of 100 % isopropanol was added per 1 ml TRIzol. After 10 minutes at room temperature, samples were centrifuged again at 12,000 x g for 15 minutes at 4 °C. The supernatant was discarded, and the pellet was washed with 1 ml of 75 % ethanol, followed by centrifugation at 7,500 x g for 5 minutes at 4 °C. The supernatant was removed, and the pellet was air-dried for 5-10 minutes. Finally, the RNA pellet was resuspended in 20-50 µl of RNase-free water, depending on pellet size, and stored at -80 °C.

4.4.2 Isolation of Plasmid-DNA

Plasmid DNA was isolated using a commercial kit (NucleoBond Xtra Midi or Maxi EF, Machery-Nagel). An overnight culture of *E. coli* containing the plasmid was cultivated in 400 ml of LB media in a shaker at 37 °C, and cells were harvested 16 hours later by centrifuging at 12,000 x g for 15 minutes. The alkaline lysis method was applied following the manufacturer's instructions, ensuring endotoxin-free plasmid preparation suitable for transfection into mammalian cell lines. The final eluate was stored at -20 °C. During the cloning process of plasmids, plasmids were isolated from 5 ml LB cultures using the NucleoSpin Plasmid Mini kit (Machery-Nagel).

4.4.3 Polymerase Chain Reaction (PCR)

Polymerase Chain Reaction (PCR) was employed for the specific amplification of DNA fragments, conducted in thermocyclers under conditions tailored to amplicon size, polymerase, and primer specifications (Table 7 and 8). Annealing temperatures (T_a) were derived from the primer melting temperature (T_m) using the formula $T_{ann} = T_m - 5$ °C. A general PCR program applied in this study is detailed in Table 27. GoTaq Green Master Mix was used, with DNase-free water, appropriate primers, and DNA samples added to the pre-mixed master mix (Table 26).

Table 26: Pipetting Scheme for a 50 µl PCR with GoTaq

25 µl	GoTaq Master Mix
1 µl (each)	Primer (1:10)
1 µl	DNA template
ad 50 µl	ddH$_2$O

Table 27: General PCR Program

Reaction step	Temperature in °C	Time in min:sec
Initial Denaturation	95	05:00
Denaturation	95	00:30
Annealing	$T_a = T_m - 5$ °C	00:30
Elongation	72	X*
Final Elongation	72	05:00

x35 (Denaturation, Annealing, Elongation)

* Elongation time is depending on the size of the amplicon and was calculated for each primer pair (Table 7 and 8). For the Taq-Polymerase a speed of 1000 nucleotides per minute was assumed.

4.4.4 Synthesis of Complementary DNA

To convert RNA into complementary DNA (cDNA), the iScript cDNA Synthesis Kit was used, following the manufacturer's protocol. The kit includes a reaction mix, reverse transcriptase, and nuclease-free water. The standard reaction scheme is outlined in Table 28 the PCR program is detailed in Table 29.

Table 28: Reaction Scheme for cDNA Synthesis

4 µl	5x iScript Reaction mix
1 µl (each)	Reverse transcriptase
1 µl	RNA template
ad 20 µl	ddH$_2$O

Table 29: Reaction Protocol for cDNA Synthesis

Reaction step	Temperature in °C	Time in min:sec
Priming	25	05:00
Reverse transcription	46	20:00
Inactivation	95	01:00

4.4.5   Agarose-gel electrophoresis

DNA fragments size was assessed via gel electrophoresis. Agarose gels at 1-2 % (w/v) concentration in 1x Tris-acetate-EDTA (TAE) buffer (TAE 50x: Table 31) were prepared (Table 30) based on expected fragment sizes (Table 7 and 8). Samples were mixed with loading buffer and run for 60-90 minutes at 100-120 V in an electrophoresis chamber containing 1x TAE buffer. The agarose gel matrix allowed fragments to separate according to size. PCR samples were loaded immediately after PCR completion. Voltage was applied using a Consort EV231 device. A DNA marker (Supplementary Figure 11) was used to estimate fragment sizes. GelRed Nucleic Acid Gel Stain in the gel enabled visualization of the amplified fragments in a gel documentation system (Gel iX20 Imager).

Table 30: Composition 1 % Agarose Gel

1,5 g	Agarose
150 ml	1x TAE Buffer

add GelRed Nucleic Acid Gel Stain after boiling up (1:10,000)

Table 31: TRIS-Acetate-EDTA-Puffer (TAE-Puffer) (50x)

2 M	TRIS
0,1 M	EDTA

4.4.6   DNA Concentration Determination

DNA concentration was measured photometrically with a NanoDrop 2000. Impurities such as carbohydrates, peptides, phenols, or aromatic compounds were detected at 230 nm, while proteins were measured at 280 nm. A 260/280 nm ratio between 1.8 and 2.0 indicated a pure DNA sample, and a 260/230 nm ratio above 2.1 suggested minimal contamination.

4.5 Establishment of Flp-In T-REx 293 Cell Lines Stably Expressing a GOI

The following section outlines the generation of Flp-In T-REx 293 cell lines that stably express a GOI. Briefly, the GOI is cloned into a plasmid. This plasmid, along with a flippase-expressing plasmid, is co-transfected into the Flp-In T-REx 293 host cell line. Stable transfectants are then selected using hygromycin B.

4.5.1 Cloning Strategy

The following part describes the methods used for cloning the plasmids for the generation of the Flp-In T-REx 293 cell lines.

4.5.1.1 Primer Design

Primers were designed to generate DNA fragments containing the GOI with overhangs complementary to the ends of the linearized plasmid (pcDNA5/FTR) for GOI insertion. Additionally, the primers were designed to regenerate restriction sites flanking the insert during assembly. SnapGene software (Insightful Science) and the NEBuilder Assembly tool (New England Biolabs) were used for this step. The primer sequences are listed in Table 8.

4.5.1.2 Generation of GOI DNA Fragments for Assembly

PCR was performed using primers and template DNA to amplify DNA fragments containing the GOI for subsequent assembly. Amplicon specifications are provided in Table 8, with general PCR instructions detailed in Section 4.4.3. PCR products were run on an agarose gel (Section 4.4.5), and the band corresponding to the GOI was excised and purified using a DNA purification kit according to the manufacturer's instructions. The purified PCR product was then ready for assembly with the linearized vector.

4.5.1.3 Restriction

To linearize the vector for assembly, the plasmid pcDNA5/FRT was digested with restriction enzymes in CutSmart-Buffer. The enzymes used were: HindIII, NotI and EcoRI (New England Biolabs). The digestion reaction mix is detailed in Table 32. The reaction was incubated at 37 °C for 20 to 60 minutes and then heat-inactivated at 80 °C to stop enzyme activity, using a thermo-mixer. After digestion, the reaction mix was separated by electrophoresis, and the corresponding band for the linearized vector was excised from the agarose gel and purified using a DNA purification kit according to the manufacturer's instructions.

Table 32: Restriction Reaction-Mix (50 µl)

2 µl	DNA (1 µg/µl)
6 µl	CutSmart-Buffer
1 µl	Restriction enzyme
ad 50 µl	ddH$_2$O

4.5.1.4 Cloning of pcDNA5/FRT/GOI

For the assembly of DNA fragments, NEBuilder HiFi DNA Assembly Master Mix was used. The insert (PCR product) and the linearized vector were mixed in a 1:2 ratio with 5 µl of Assembly Master Mix, and the volume was brought to 10 µl with ddH$_2$O, ensuring the total amount did not exceed 0.2 pmol. The reaction was incubated at 50 °C for 60 minutes. Subsequently, 5 µl of the reaction mix was used for bacterial transformation.

The assembly process utilizes a combination of enzymes: an exonuclease first generates single-stranded 3' overhangs, facilitating the alignment of fragments with complementary sequences at the overlap region. A polymerase then fills the gaps in the aligned fragments, while DNA ligase seals any breaks in the assembled DNA. Additionally, the assembly process regenerates restriction sites, ensuring the insert remains flanked by the appropriate sites. The result is a fully sealed, double-stranded DNA molecule ready for transformation into *E. coli*.

4.5.2   Heat Shock Transformation

Competent *E. coli* DH5α cells were used to amplify the constructs. Briefly, 5-10 µl containing 1 µg of DNA was added to the competent cells and incubated on ice for 30 minutes. A heat shock was then applied for 90 seconds at 42 °C in a thermo-mixer, followed by another 2-minute incubation on ice. After adding 1 ml of LB medium (without antibiotics), the mixture was incubated at 37 °C for 60 minutes. Next, 100 µl of the culture was plated on selective LB-agar and incubated overnight at 37 °C. As the plasmid carries ampicillin resistance genes, only successfully transformed clones grew on the selective medium.

4.5.3   Identification and Verification of *E. coli* Clones

Antibiotic-resistant clones were selected from agar plates and cultured overnight in 5 ml of selective LB medium. Following plasmid isolation using a kit, clones were verified for correct insert size by enzyme digestion and subsequent electrophoresis. Promising candidates were sent for sequencing via commercial services. Cryo-cultures were then prepared to amplify successfully cloned plasmids.

4.5.4 Co-Transfection of pcDNA5/FRT/GOI and pOG44

Plasmids were purified using a kit with an endotoxin removal step. The pOG44 plasmid, containing a flippase (FLP) recombinase, enables recombination between Flp recognition target (FRT) sites on both the GOI-containing plasmid and the host cell line. Both genes, *FLP* and *FRT* are originally derived from *Saccharomyces cerevisiae*. The pcDNA5/FRT/GOI to pOG44 ratio was 1:9.

The Flp-In T-REx 293 host cell line was seeded in 2 ml DMEM (10 % FCS) in 6-well plates 24 hours before transfection to reach 70 % confluency by transfection day. The DNA and transfection reagent (TransIT-LT1) were diluted in DMEM (Table 33), mixed immediately, and incubated for 15 minutes at room temperature. The mixture was then added dropwise to each well of a 6-well plate (WP), and the plate was gently rocked for even distribution. After 24 hours of incubation (37 °C, 5 % CO_2), cells were detached and transferred to a fresh 6-well plate, with each well plated into a separate 10 cm culture dish to optimize hygromycin B selection by reducing cell density. This medium selection targeted clones that successfully integrated the GOI into the cell genome.

Table 33: Co-Transfection. Amounts per Well (6WP)

0.2 µg	pcDNA/5/FRT/GOI
1.8 µg	pOG44

mix with 7,5 µl TransIT-LT1 in 250 µl DMEM (0 % FCS)

4.5.5 Selection Process

Twenty-four hours after transfection and transfer to 10 cm culture dishes, the medium was replaced to eliminate floating dead cells. Fresh medium (DMEM with 10 % FCS, 1 % P/S) containing hygromycin B (100 µg/ml) and blasticidin (15 µg/ml) was used. Clones with successful GOI integration lost resistance to zeocin while gaining resistance to hygromycin B. The Flp-In T-REx System utilizes a tetracycline (Tet) repressor for controlled expression, and blasticidin maintained selection pressure on the Tet repressor. Over several days, cultures were observed, with regular medium changes, until surviving clone colonies could be isolated.

To expand the clones, colonies were first seeded into 12-well plates, then transferred to T25 and T75 culture flasks. Besides hygromycin B resistance, PCR analyses on both cDNA and gDNA were conducted to confirm GOI expression and integration. Sequencing of the PCR products was performed using a commercial sequencing service. Finally, cryo-cultures were prepared and stored in liquid nitrogen for long-term preservation.

4.6 Transcription- and Replication-Competent Virus-like Particle (trVLP) System

The trVLP system, developed by Hoenen *et al.* and based on a minigenome system, enables studies on EBOV, a BSL-4 pathogen, in a BSL-2 setting.[253] This system replicates nearly all aspects of the EBOV life cycle. Unlike other systems, the trVLP model includes a tetracistronic minigenome that contains EBOV proteins VP40, GP1,2, and VP24, alongside a nanoluciferase (also: NanoLuc or NLuc) reporter gene (Figure 11). Only plasmids expressing viral proteins NP, VP35, VP30, and L are transfected into cells. The genetic material (tetracistronic minigenome) is incorporated into the nucleocapsid, and complete VLPs are released into the supernatant. This supernatant, containing the VLPs, can be used to infect a new batch of cells previously transfected with plasmids, allowing for passaging across multiple cycles (Figure 12). To assess transcription efficiency, firefly luciferase plasmids were co-transfected, and for replication efficiency, nanoluciferase activity was measured.
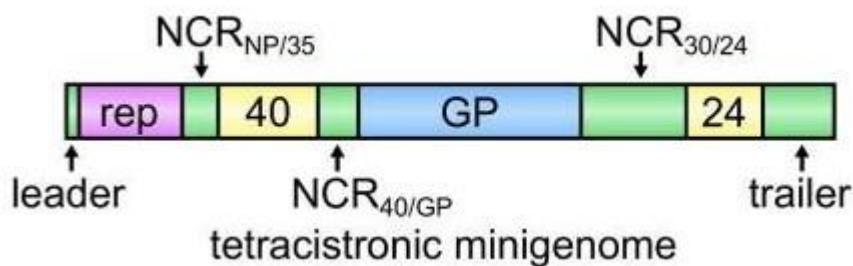
Figure 12: Structure of the Ebola Virus Tetracistronic Minigenome

Coding regions for Ebola virus proteins are indicated in yellow (VP40 and VP24) and blue (GP1,2) boxes, while non-coding regions (NCRs) are represented in green, with specific labeling for leader and trailer regions. Subscripts indicate the viral NCR used to join coding regions. The coding region for the reporter gene (rep) is highlighted in purple. (Adapted from Hoenen *et al.*)

4.6.1 Transfection of Producer Cells

The first batch of cells producing VLPs is referred to as the producer cell (p0). Flp-In T-REx 293 cells were seeded in 2 ml DMEM (5 % FCS, 1 % P/S) in 6-well plates to achieve 70 % confluency on the day of transfection. Collagen-coated plates were used to prevent cell detachment due to frequent media changes (Section 4.1.2.1). TransIT-LT1 was used as the transfection reagent. Table 34 details the plasmids and amounts transfected into the producer cells. In addition to the viral proteins, a plasmid expressing T7 polymerase (for initial transcription of the minigenome) and a plasmid expressing firefly luciferase reporter were transfected.

Table 34: Producer Cells (p0), Transfection Amounts per Well (6WP)

0,25 μg	Minigenome (cis-GP-VP40-VP24-NLuc)
0,125 μg	NP
0,125 μg	VP35
0,075 μg	VP30
1 μg	L
1 μg	T7
0,5 μg	Firefly luciferase

mix with 7,5 µl TransIT-LT1 in 250 µl DMEM (0 % FCS)
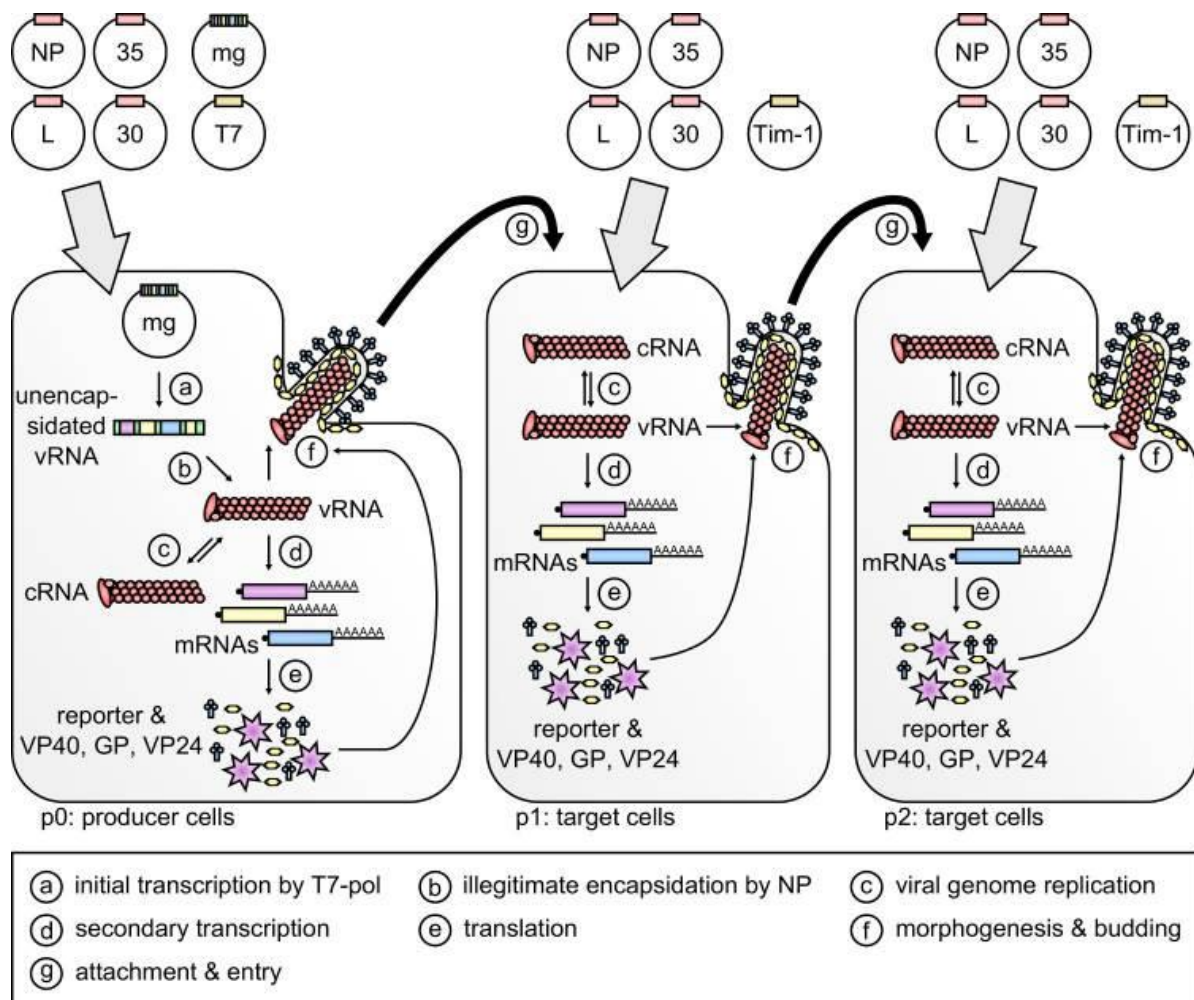
Figure 13: Schematic of trVLP Assay

Cells are transfected with expression plasmids encoding EBOV nucleocapsid proteins (NP, VP35, VP30, L), a tetracistronic minigenome (mg), and T7 polymerase. This setup enables stages including initial transcription (a), encapsidation (b), genome replication (c), and transcription (d), followed by translation (e). mRNAs for VP40, GP1,2, and VP24 are also transcribed from the tetracistronic minigenome, allowing the formation of trVLPs (f). These trVLPs subsequently infect target cells (g) pre-transfected with nucleocapsid protein plasmids (NP, VP35, VP30, and L) and the cellular EBOV attachment factor Tim-1, resulting in genome replication, transcription, and further trVLP production for subsequent infection cycles. (Adapted from Hoenen *et al.*)

The transfection reagent and DNA were mixed immediately in DMEM (0 % FCS) and incubated for 20 minutes at room temperature. After incubation, the mixture was added dropwise to each well, and the plate was gently rocked to ensure even distribution. After 24 hours of incubation (37 °C, 5% CO_2), the medium was replaced with 4 ml fresh DMEM (5 % FCS, 1 % P/S). Forty-eight hours later (72 hours post-transfection), the supernatant was collected to infect the next batch of target cells (passage 1), and the cells were harvested for the luciferase assay (Figure 13).
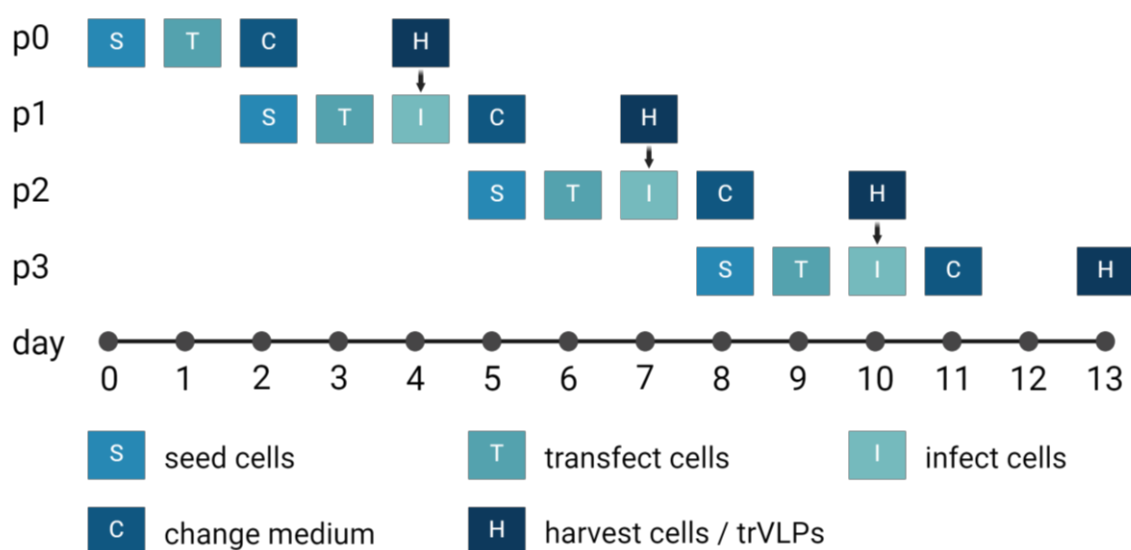
Figure 14: Timeline of trVLP Assay for 3 Consecutive Passages

Key procedural steps: seeding cells (s), transfecting cells (t), infecting cells (i), performing medium changes (c), and harvesting cells and trVLPs (h). Arrows indicate transitions between passages (infection of new batch of target cells with supernatant containing trVLPs).

4.6.2   Transfection of Target Cells

All subsequent cell batches after the producer cell are referred to as target cells and are numbered according to their passage (p1 to p3). Target cells are seeded to achieve 70 % confluency by the next day for transfection (Figure 13). P1 is seeded one day after the transfection of p0. On the following day, the target cells are pre-transfected. Table 35 outlines the plasmids and amounts used for the transfection of target cells. Only plasmids expressing NP, VP35, VP30, L, firefly luciferase reporter, and T7 polymerase are transfected. Additionally, a plasmid expressing Tim-1 is included to enhance the infection rate of the VLPs, as Tim-1 acts as an attachment factor for filoviruses.

The transfection procedure for target cells was identical to that of the producer cells. After a 24-hour incubation period (37 °C, 5 % CO_2), the medium was replaced with 4 ml fresh DMEM

(5 % FCS, 1 % P/S). Forty-eight hours later (72 hours post-transfection), the supernatant containing the VLPs was collected and used to infect the next batch of target cells (passage 2). The resulting VLPs could then be used to infect subsequent generations of target cells. To assess background activity, a -L control (plasmid expressing L, the polymerase was substituted with an empty plasmid) was included.

Table 35: Target Cells (p1 to X), Transfection Amounts per Well (6WP)

0,125 µg	NP
0,125 µg	VP35
0,075 µg	VP30
1 µg	L
1 µg	T7
0,25 µg	Tim-1
0,5 µg	Firefly luciferase

mix with 7,5 µl TransIT-LT1 in 250 µl DMEM (0 % FCS)

4.6.3   Infection of Target Cells

The supernatant from the producer cells (and later also from target cells) contains the trVLPs which were used to infect the next generation of target cells (p1, p2, p3). 24 h after the pre-transfection of the target cells, the supernatant from the producer cells was collected and centrifuged at 800 x g for 5 min (Figure 13). The medium on the to-be-infected target cells was replaced by 3 ml of the supernatant containing the trVPLs. After the incubation (24 h, 37 °C, 5 % CO_2), the medium was exchanged with 4 ml fresh DMEM (5 % FCS, 1 % P/S). 48 h later (72 h post transfection) the supernatant was used to infect the next batch of cells (target cells, passage 1) and the cells were harvested for the luciferase assay.

The supernatant from the producer cells (and later from target cells) contains the trVLPs, which are used to infect the next generation of target cells (p1, p2, p3). Twenty-four hours after pre-transfection of the target cells, the supernatant from the producer cells was collected and centrifuged at 800 x g for 5 minutes. The medium on the target cells to be infected was replaced with 3 ml of the supernatant containing the trVLPs. After a 24-hour incubation (37 °C, 5 % CO2), the medium was exchanged with 4 ml fresh DMEM (5 % FCS, 1 % P/S). Forty-eight hours later (72 hours post-transfection), the supernatant was used to infect the next batch of target cells, and the cells were harvested for the luciferase assay.

4.6.4 Luciferase Assay

After removing the supernatant, the cells were lysed in 500 µl passive lysis buffer per well. Following a 15-minute incubation at room temperature, the samples were transferred into tubes and stored at –20 °C until measurement.

To detect luciferase activities, a commercial kit (Nano-Glo Dual-Luciferase Reporter Assay System, Promega) was used according to the manufacturer's instructions. The kit measures firefly and NanoLuc reporter activities in two separate steps. The assay was performed using a luminometer equipped with a dual auto-injection system. Injector 1 delivered the ONE-Glo EX reagent, which activates the firefly signal, while injector 2 delivered the NanoDLR Stop & Glo reagent, which extinguishes the firefly signal and activates the NanoLuc signal. Samples and reagents were brought to room temperature and measured in 96-well plates.

4.7 Immunofluorescence Microscopy Staining

In the scope of the experiments with the trVLP system, immunofluorescence staining of the transfected cells was performed.

4.7.1 Samples Preparation

6-well plates with sterile glass coverslips were coated with collagen (Section 4.1.2.1). Cells were seeded into these wells, growing on the coverslips, and the experiment was conducted as described (Section 4.6). After removing the supernatant with the VLPs, the cells were fixed in 1 ml formalin solution (10 %) for 20 minutes. The coverslips were stored in their respective wells in 1 ml PBS at 4 °C until staining.

4.7.2 Staining of Coverslips

For staining, the coverslips were transferred to 24-well plates containing 500 µl of 0.5 % Triton X-100 in PBS to permeabilize the cells. After 30 minutes at room temperature, cells were washed twice with 1 ml of PBS. Next, the coverslips were treated with 500 µl of PBS containing 1 % BSA for 30 minutes to block nonspecific signals. After another washing step, cells were stained overnight at 4 °C with 200 µl of EBOV-NP antibody (in-house, 1:100 in PBS). Following this, cells were washed again with PBS and stained for 2 hours at room temperature with 200 µl of secondary antibody (anti-mouse AF647, 1:100 in PBS). Finally, the coverslips were transferred upside down onto glass slides using mounting medium staining for DAPI. Images were taken with the Axio Imager M1 and processed and analyzed using Fiji.

4.8 Multicycle-Replication Assay of EBOV in Flp-In T-REx 293 Cell Lines

The following part outlines the procedure for performing a multicycle-replication assay of EBOV to measure its replication kinetics in the Flp-In T-REx 293 cell lines. Twenty-four hours

before infection, cells were seeded in collagen-coated 6-well plates with DMEM (5 % FCS, 1 % P/S, 1 % tetracycline) to reach approximately 70 % confluency.

4.8.1   Infection of Cells with EBOV

The infection of cells with EBOV was performed in a biosafety level 4 (BSL-4) laboratory at BMITM. Cells were infected with EBOV at MOI of 0.1 and 0.01. After removing the supernatant, the cells were washed with 500 µl PBS per well. Then, 200 µl of DMEM (0 % FCS) containing EBOV was added and incubated for 1 hour at 37 °C and 5 % CO_2. Following incubation, the supernatant was removed and replaced with 5 ml of DMEM (2.5 % FCS, 1 % P/S, 1 % tetracycline). The cells were then incubated at 37 °C and 5 % CO_2 and sampled daily for 14 days (Section 4.8.2).

4.8.2   Sampling Process

Each day, 1 ml of supernatant was collected from each well, centrifuged at 10,000 x g for 5 minutes at room temperature, and transferred to a new tube. Samples were stored at -80 °C until infectious viral particles were quantified (Section 4.9). Each well was replenished with 1 ml of fresh DMEM (2.5 % FCS, 1 % P/S, 3 % Tetracycline).

4.9   Immunofocus assay

For titration, 1 x 10^6 Vero cells were seeded in 24-well plates. 96-well dilution plates were prepared with 130 µl DMEM (0 % FCS), leaving the first and last columns empty. 180 µl of the sample was added in duplicates to the first column, and 60 µl were serially diluted across columns (Dilutions -1 to -5). The medium was removed from the Vero cells, and 200 µl of each dilution was added to the wells. After one hour of incubation at 37 °C, the medium was replaced with 1 ml of overlay medium, consisting of methylcellulose and DMEM with 5% FCS mixed at a 1:2 ratio (viscosity: 400 cP). Cells were incubated for seven days at 37 °C. Plates were then treated with 4 % formaldehyde for 60 minutes to inactivate the virus, followed by three washes with tap water. The volume of all reagents used in the following steps was 200 µl per well. After inactivation, the plates were treated with 0.5 % Triton X-100 for 30 minutes at room temperature (shaking), washed, and then blocked with PBS containing 5 % FCS for 1 hour on a shaker. The blocking solution was removed, and the cell monolayer was incubated overnight at 4 °C with an in-house-generated mouse polyclonal anti–pan-Ebolavirus NP primary antibody (1:2000). After washing, a secondary anti-mouse antibody at a 1:5000 dilution was added for 1 hour at room temperature to detect infected cell foci (for antibodies see Tabel 19). Plates were washed again. Finally, Immunoblot TMB substrate in a 1:2 water mix was added and incubated at room temperature in the dark until focus-forming units (FFU) were visible. Viral titers were quantified after drying the plates.

4.10 Animal Experiments

The following section describes methods and procedures used in various animal experiments of this study. Details of the different strains of *Mus musculus* used can be found in Table 6.

4.10.1 Animal Handling

The mouse lines were bred in the animal facility of the BNITM and transferred to rooms designated for animal experiments. Mice were housed in conventional cages and kept in individually ventilated cages (IVCs) in groups of up to four animals, with autoclaved, low-dust woodchip bedding and nesting material after weaning. The cages are equipped with enrichment materials, such as retreat housing and cardboard tubes. Autoclaved tap water and germ-free food pellets are provided *ad libitum*. Hygiene monitoring is conducted quarterly according to Federation of European Laboratory Animal Science Associations (FELASA) guidelines. To acclimate the animals to the BSL-4 laboratory environment, they are transferred there at least one week before the experiment. The facility maintains a day-night cycle to mimic natural conditions. During the experiments, animals were monitored daily for signs of illness or discomfort (e.g., hunched posture, rough coat, weight loss). Mice were euthanized via isoflurane overdose followed by cervical dislocation at the end of the experiment, for organ collection, or upon reaching termination criteria (e.g., weight loss >20 %).

4.10.2 Infection of Mice

In this study, mice were infected intranasally (i.n.) to mimic the natural infection route. Each mouse received 20 µl of pure DMEM containing 10,000 FFU of EBOV applied to the nostrils. Before inoculation, the mice were anesthetized with isoflurane. All animal experiments involving EBOV were conducted in the BSL-4 laboratory at BNITM.

4.10.3 Immunizations of Mice

To generate peptide-specific T cells, mice were immunized via subcutaneous (s.c.) route with Complete Freund's Adjuvant (CFA) to enhance the immune response. The peptides, synthesized by GenScript and dissolved in Dimethylformamide (DMF), were administered at a dose of 100 µg peptide in 100 µl PBS/CFA (1:1 ratio) per mouse. An additional group receiving only CFA served as a control. Fourteen days later, the spleens were harvested for *ex-vivo* experiments.

4.10.4 Administration of Diphtheria Toxin (DT)

To deplete Tregs in DEREG mice, DT was administered via intraperitoneal (i.p.) injection. The DT stock solution was diluted with PBS. Mice were given 0.5 µg DT per gram of body weight one day before infection, followed by 0.25 µg/g on days 1 and 3 post-infection.

4.10.5 Blood Draw and Serum Collection

Blood was drawn from infected animals two to three times weekly via the tail vein. Prior to sampling, animals were warmed under an infrared lamp to dilate the veins. Mice were then restrained, and a small incision was made with a scalpel blade. Approximately 20 µl of whole blood was collected into 980 µl of DMEM with 1 % Heparin and stored at -80 °C until titration. For serum collection, whole blood was placed in serum tubes, incubated for 20-30 minutes at room temperature, centrifuged at 12,000 x g, and stored at -80 °C. Additionally, cardiac punctures were performed at endpoints to collect blood under anesthesia just before euthanasia.

4.11 Clinical Parameters

Serum aspartate aminotransferase (AST) levels were quantified using GOT/AST Fuji DRI-CHEM slides in Fujifilm in a DRI-CHEM NX500 analyzer. Serum samples were diluted 1:10 in water before analysis. The measurement range was 10-1000 U/L.

4.12 Multiplex Fluorescence-Encoded Bead-Based Assay

Cytokine and chemokine levels in serum samples were analyzed using a multiplex bead-based assay kit (LEGENDplex Mouse Anti-Virus Response Panel) with fluorescence-encoded beads. This panel enabled the simultaneous quantification of 13 mouse proteins by flow cytometry: IFN-γ, CXCL1 (KC), TNF-α, CCL2 (MCP-1), IL-12p70, CCL5 (RANTES), IL-1β, CXCL10 (IP-10), GM-CSF, IL-10, IFN-β, IFN-α, and IL-6.

The kit was used according to manufacturer's instructions. Briefly, infectious serum samples were first inactivated by mixing with assay buffer containing Triton X-100 to a final concentration of 1 % and incubating at room temperature for 20 minutes. This step was performed under BSL-4 conditions. In a 96-well plate, inactivated samples, beads, and detection antibodies were mixed in a 2:1:1 ratio. Plates were incubated overnight on a shaker at 650 rpm at 4 °C in the dark. The next day, SA-PE was added to each well in a volume equal to that of the beads or antibody and incubated for 30 minutes at room temperature on a shaker, also in the dark. Plates were then centrifuged at 1000 x g for 5 minutes and washed twice with 200 µl of wash buffer. Finally, samples were resuspended in wash buffer and analyzed using a BD LSRII Fortessa flow cytometer with an autosampler (HTS) for well plates. Data analysis was performed using the Legendplex analysis Qognit software provided by BioLegend.

4.13 Organ Harvesting

In this study, organs were collected from mice either for titrations and histology or for further analysis by flow cytometry or PCR. Following euthanasia, each selected organ (spleen, liver, lung, kidney, thymus, brain, heart, intestine, and eye) was removed and placed in a tube with ice-cold PBS. Organs were then treated with DNase I and collagenase I at 37 °C for 20 minutes

to aid tissue dissociation. Next, the organs were passed through a cell strainer into a fresh tube containing PBS to obtain single-cell suspensions. The tubes were centrifuged at 500 x g for 5 minutes, after which the supernatant was discarded. Red blood cell (RBC) lysis buffer, diluted 1:10 with ddH$_2$O, was added for 3 minutes to remove residual RBCs, followed by inactivation with 25 ml PBS. After a second centrifugation at 500 x g for 5 minutes, the supernatant was discarded, and the pellet was resuspended in 100-400 µl PBS, adjusted to pellet size. Samples were then transferred into 1.5 ml or, for larger samples, 2 ml tubes. These prepared samples were suitable for staining in flow cytometry or fluorescence-activated cell sorting (FACS) or for RNA extraction.

4.14 Sample Preparation for Flow Cytometry

For flow cytometry or FACS sorting, single-cell suspensions of lung cells were stained for viability with Zombie NIR for 30 minutes at room temperature, washed twice with PBS, and blocked with Fc receptor blocking solution for 20 minutes at room temperature. Cells were then washed with PBS, centrifuged again, and the supernatant discarded. Cells were stained with an antibody cocktail consisting of the multiparametric flow cytometry panel in Table 17 in the dark for 30 minutes at room temperature. Cells were fixed using the BD Cytofix Fixation Buffer with 500 µl of fixation solution containing 4 % paraformaldehyde (PFA) for 60 minutes at room temperature. This step also inactivated the virus. Samples were then centrifuged at 500 x g for 5 minutes and the supernatant was removed. After a final wash, the cell suspension was resuspended in PBS, passed through a sieve into FACS tubes, and stored at 4 °C until analysis. Samples were acquired using an Aurora flow cytometer and analyzed with FlowJo software.

4.15 Fluorescence-Activated Cell Sorting (FACS)

In this study, an antibody panel (Table 18) was developed for sorting mTECs and cTECs from *Mus musculus* thymus samples. Cell sorting was conducted using the FACSAria IIIu (BD Biosciences) equipped with three excitation lasers (488 nm, 531 nm, and 635 nm). The following section describes the antibodies, antigens, and additional dyes employed.

Zombie NIR was used to distinguish live and dead cells; as a non-permeant dye in live cells and permeant only in cells with compromised membranes, it served as a live/dead indicator and emits a signal similar to APC/Cy7. The PerCP/Cyanine5.5 anti-mouse CD45.2 antibody targeted CD45.2, an alloantigen found on Ly5.2-positive mouse strains (e.g., C57BL/6). For labeling MHC II molecules on antigen-presenting cells, the APC anti-mouse I-A/I-E antibody was applied. EpCAM (CD326) marked epithelial cells, and Ly-51, a cell-surface glycoprotein, specifically targeted cortical epithelial cells. Lastly, Ulex europaeus agglutinin I (UEA I), which binds to α-linked fucose residues, was included for its specific affinity to the murine thymus medullary region, as established by Farr and Anderson (1985).[255]

4.16 ELISpot Assay

To evaluate the immune response of mice against EBOV NP-NIRV, an ELISpot assay was conducted, quantifying cytokine secretion (IFN-γ) at the single-cell level. This assay aimed to determine if NIRVs elicit an active immune response or tolerance. C57BL/6J mice were immunized with peptides (Table 22) combined with CFA, while a control group received only CFA. After 14 days, spleens were harvested, and splenocytes were cultured *in vitro*. After re-stimulation with 10 µg of each peptide, administered separately to check for cross-reactivity, IFN-γ secretion was quantified using antibodies (Table 21). Phytohemagglutinin (PHA-L) was used as a positive control.

In this protocol, ELISpot plates were pre-activated with 40 µl EtOH (35 %), washed with 200 µl PBS per well, and incubated overnight at 4 °C with 50 µl capture antibody in PBS (5 µg/ml). The following day, plates were washed and blocked with 1 % BSA in PBS (200 µl per well) for 1 hour at room temperature. Then, 200,000 splenocytes per well were seeded and re-stimulated with peptides. Plates were incubated overnight at 37 °C with 5 % CO_2 in RPMI medium containing 10 % FCS. On day three, plates were washed and treated with 50 µl detection antibody (1 µg/ml in PBS with 0.1 % BSA) for 1 hour at room temperature. After additional washing, 100 µl horseradish peroxidase (HRP), diluted 1:200 in PBS, was added and incubated for 1 hour at room temperature. Plates were then washed, and 100 µl BD ELISPOT AEC Substrate was added per well. The reaction was halted by adding ddH_2O once spots appeared, and plates were allowed to air-dry. Spots were quantified with an ELISpot reader.

4.17 Histology and Immunohistochemistry

Immunohistochemistry staining and hematoxylin and eosin (H&E) staining was performed by Susanne Krasemann (Institute for Neuropathology, University Medical Center Hamburg-Eppendorf, Hamburg, Germany). Mouse tissue samples were fixed in 4 % formaldehyde solution for at least 72 h at room temperature to inactivate the virus, dehydrated, and then processed for paraffin embedding. Sections were subjected to H&E staining according to standard procedures. Immunohistochemical detection of activated microglia/macrophages was performed as follows: Tissue sections were subjected to antibody-specific antigen retrieval using the Ventana Benchmark XT. Sections were blocked in PBS with 10 % FCS and afterwards incubated with the primary antibodies for rat anti–mouse IBA1 (Ionized calcium-binding adaptor molecule 1). Bound primary antibodies were detected with anti-mouse, anti-rabbit or anti-rat N-Histofine Simple Stain MAX PO immune-enzyme polymer and stained with DAB substrate using the ultraView Universal DAB Detection Kit (Ventana). Tissues were counterstained with hematoxylin. Images were acquired with the Leica DMD108 digital microscope.

4.18 Bioinformatical Methods

This study employed the Basic Local Alignment Search Tool (BLAST) from the National Center for Biotechnology Information (NCBI) to identify NIRVs in mammals. BLAST detects regions of local sequence similarity, comparing nucleotide or protein sequences to databases and evaluating match significance. Specifically, a tBLASTn search was used to compare a protein sequence against a translated nucleotide database, while BLASTp compared a protein sequence directly to a protein database. Searches for sequence similarity to filoviruses used protein sequences from genes of EBOV (AF086833.2) as a query with tBLASTn in databases of NCBI (such as Nucleotide collection (nr/nt)). Filoviruses (taxid:11266) were excluded from the search. Additionally, the BLAST-like alignment tool (BLAT), which applies a pairwise sequence alignment algorithm, was utilized to search for the NP-NIRV within the *Mus musculus* genome. For this genome search, the Ensembl genome browser for vertebrates was used.[256]

4.18.1 *In-silico* Analysis of Thymic MHC-II Peptides

To investigate the murine immune peptidome, a BLASTp (NCBI) search was conducted on a published dataset of low-abundance peptides presented by MHC-II molecules in the murine thymus.[257] The search was restricted to non-redundant (nr) *Mononegavirales* protein sequences using default parameters. Sequences with expect values of $E \leq 1$ were retained for MHC-II epitope prediction through the Immune Epitope Database (IEDB) tools. MHC-II binding predictions (allele: H2-IAb) were made using the IEDB analysis resource NetMHCIIpan_ba (ver. 4.1) tool.[258] Results were quantified and then compared against a dataset of the human immune peptidome.[259]

4.19 Statistics

Statistical analyses were done using Graphpad Prism software. All data are presented as mean $\pm$ standard error of the mean ($\pm$SEM). For comparison of survival curves, log-rank (Mantel-Cox) tests were used. For multiple comparisons, nonparametric one-way ANOVA (Kruskal-Wallis test) or two-way ANOVA (weight, AST levels, and viremia) was used. Significance levels are presented as follows: *, $P \leq 0.05$; **, $P \leq 0.01$; ***, $P \leq 0.001$; and ****, $P \leq 0.0001$.

4.20 Other Software Applications

GraphPad Prism was used for statistical analysis and graph generation, while Microsoft Word and Excel were applied for general documentation and figure creation. PowerPoint and biorender.com were used to design figures. Histological and immunohistochemical images were arranged with Adobe Photoshop. Flow cytometry data, collected with BD FACSDiva software, was analyzed in FlowJo, and Fiji was used to process microscope images. SnapGene

supported sequence analysis. Finally, ChatGPT-4 assisted in proofreading and enhancing readability of this thesis.

5 Results

This thesis focuses on a filovirus-like NIRV inserted into the *Mus musculus* genome and is structured into two key parts: (1) evaluation of the functions of the NP-NIRV in infected cells, and (2) the analysis of the role of NP-NIRV on the immune response to EBOV. The study is based on the hypothesis that murine NIRVs are presented as self-antigens during T cell maturation in the thymus, thereby conferring immune tolerance to EBOV infection.

5.1 Characterization of the Murine NP-NIRV

Previous *in-silico* studies identified a filovirus-like sequence in *Mus musculus* that shares similarity to EBOV NP.[18] This study demonstrates that this filovirus pseudogene is conserved as an intact ORF, expressed at the RNA level, and further investigates its potential role and function.

To characterize the insertion site of the NP-NIRV in the murine genome, we performed a bioinformatic analysis using a the pairwise sequence alignment algorithm known as BLAST-Like Alignment Tool (BLAT). The murine NP-NIRV was identified on Chromosome 9, at the genomic position 9:73977099-73977655 (Supplementary Figure 1). We also observed LINEs flanking the NP-NIRV, which suggests an involvement of TEs in its insertion mechanism (Supplementary Figure 2). The NP-NIRV itself was found to be integrated as an intact ORF in reverse orientation (3'-5') with a length of 276 bp (Supplementary Figure 3).

The EBOV NP and NP-NIRV share a conserved 15-amino-acid region ('SLFLPKLVVGEKACL' in EBOV-NP and 'SFFLPKLVKGGGACL' in NP-NIRV; Figure 14 and Supplementary Figure 4). The high conservation of this region, observed across NP-NIRVs in other species such as bats, rodents and marsupials allowed us to design universal NP-NIRV PCR primers (Table 7) for the identification of NP-NIRVs in mice and the discovery of additional NIRVs in bat species without available annotated genomes, such as *Mops condylurus*.[260] *In-silico* analyses of these 15 amino acid peptides also suggested binding of mouse MHC-II molecules with similar affinity values for the NP and NIRV-derived peptides (Figure 14).

Furthermore, a short motif, 3'-TTATTAGG-5', located near the start of the NP-NIRV codon was discovered (Supplementary Figure 3). This motive was assigned to a putative AIRE binding site (TTATTA-box).[261,262] AIRE promotes the expression of TRAs in mTECs, which is an important checkpoint for T-cell selection.[66] The potential relationship between AIRE and the NP-NIRV was further explored within this study.

Peptide Alignment of Most Conserved Region (Mouse/EBOV)

```
NP-NIRV: SFFLPKLVKGGGACL  (Percentile Rank=18.0)
EBOV NP: SLFLPKLVVGEKACL  (Percentile Rank=39.0)
```

Figure 15: Alignment of Most Conserved Region (Mouse/EBOV) with Predicted MHC-II Affinity
Amino acids that are identical between the Mouse and EBOV peptides are marked in yellow. A small, numbered percentile rank indicates high affinity (0-100). The MHC-II binding predictions (allele: H2-IAb) were generated on 10/22/2024 using the IEDB analysis resource NetMHCIIpan_ba (ver. 4.1) tool.

5.2 Evaluation of the Functions of the NP-NIRV *in vitro*

The NP-NIRV represents an ancient viral remnant of filovirus NPs integrated into the *Mus musculus* genome, with its functional roles remaining largely unexplored. The NP of filoviruses is critical for viral replication and nucleocapsid and ribonucleoprotein formation.[263]

Based on the alignment between murine NP-NIRV and EBOV NP, we hypothesize that NP-NIRV may interact with EBOV NP or mimic its function. To investigate this, we evaluated the functional properties of NP-NIRV using *in-vitro* assays to assess its potential influence on IB formation and viral replication. Employing a tetracistronic minigenome (trVLP system) as described by Hoenen *et al.* (Figure 11 and 12)[253] along with cell lines stably expressing the NP-NIRV, we aimed to uncover whether NP-NIRV plays an active role in these critical processes.

5.2.1 Generation of Cell Lines

We generated cell lines stably expressing NP-NIRV using the Flp-In 293 T-REx system, which allows for rapid creation of stable cell lines with homogeneous expression. Co-transfection of the Flp-In human embryonic kidney (293) cell line with an Flp-In expression vector containing the GOI and a Flp recombinase vector ensures targeted integration into a single, transcriptionally active FRT site, resulting in consistent gene expression across all cells.

We generated cell lines expressing the murine NP-NIRV, a NP-NIRV-GFP construct, and eGFP under a CMV promoter, referred to as NIRV, NIRV-GFP and GFP cell line, respectively. The GFP cell line served as a control to assess the effects of NP-NIRV expression by comparing it to a cell line expressing only GFP. The NIRV-GFP construct comprises the NP-NIRV sequence connected via a porcine teschovirus 2A (P2A) auto-proteolytic site to the downstream eGFP gene. Regulated by the same promoter, this construct produces two distinct proteins through ribosome skipping, facilitated by the P2A linker sequence.

Upon GOI integration, the cells lost zeocin resistance and gained hygromycin B resistance, allowing for the selection of successfully modified cells. This ensures survival of only those cells with stable integration. Green fluorescence in the NIRV-GFP and GFP cell lines confirmed GOI expression, though a lower GFP signal was observed in NIRV-GFP cells compared to the GFP-only line (Supplementary Figure 5). Notably, we detected GOI expression even in the absence of tetracycline, although the system utilizes a repressor that induces expression in presence of tetracycline. Nonetheless, all experiments were performed using cell lines cultured with medium containing 1 mg/ml tetracycline. NP-NIRV expression was further validated by PCR on mRNA in both NIRV and NIRV-GFP cell lines (Supplementary Figure 6), and correct GOI integration was confirmed by sequencing across all cell lines.

5.2.2 NP-NIRV Does Not Impact IB Formation

The filovirus NP oligomerization is crucial for the formation of IBs, which are the primary sites of viral replication and transcription. We hypothesized that NP-NIRV might affect IB formation by interacting with EBOV NP, thereby influencing viral replication. To test this, we compared IB formation with an EBOV minigenome system in the presence and absence of NP-NIRV *in vitro*. IB formation was assessed via immunofluorescence staining of NP in cell monolayers transfected with the trVLP system.

Flp-In T-REx 293 cells were seeded on coverslips and transfected with the plasmids of the trVLP system. To ensure successful transfection, efficiency was verified by co-transfection with a firefly luciferase reporter, providing a quantifiable measure of transfection success and consistency (Supplementary Figure 7). The verification was critical to ensure that any observed differences in IB formation were attributable to the presence or absence of NP-NIRV, rather than variability in transfection success.

Three days post-transfection, supernatant containing trVLPs was transferred to the next passage of pre-transfected cells (p1), and passaging continued until p3. Fixed monolayers were stained using an anti-EBOV NP antibody (magenta) to identify IBs, defined as concentrated sites of NP within cells, while nuclei were stained with DAPI (blue). IB formation was consistently observed in all cell lines across all passages (p3: Figure 15; p0-p2: Supplementary Figures 8-10).

We included a control without polymerase L to confirm that viral replication and transcription depend on L, ensuring that observed effects were not due to non-specific activity. This control also verified the proper functioning of the trVLP system. We also observed the formation of inclusion bodies (IBs) in the absence of L, as anticipated, since NP can independently drive IB formation. Additionally, a control without NP showed that NP transfection was essential for IB formation, as its absence completely inhibited the process across all cell lines. This finding also

indicates that NP-NIRV could not substitute for NP in forming IBs, as we did not observe IB formation in cell lines expressing the NP-NIRV.
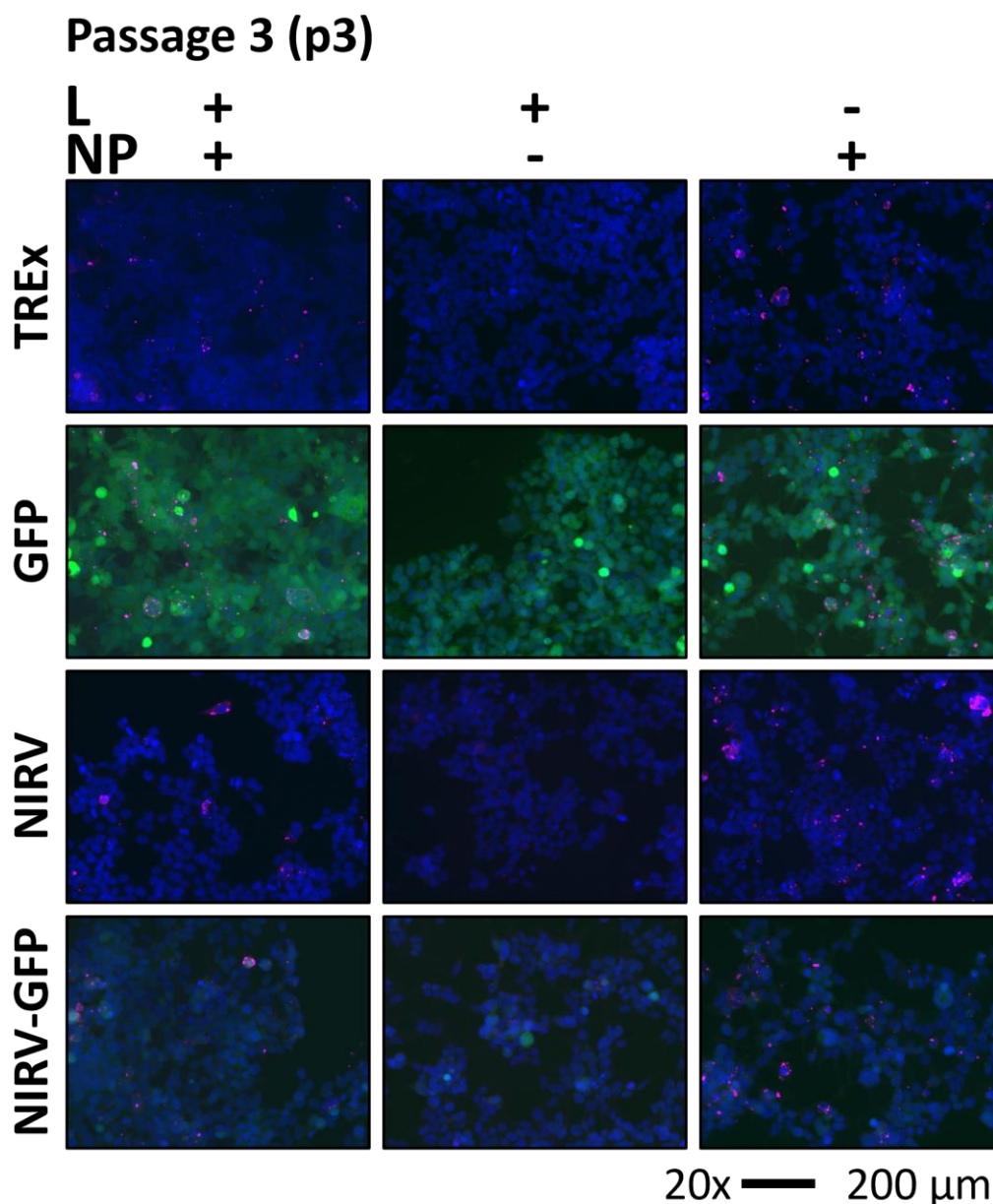
Figure 16: Inclusion Body Formation in 293 Cell Lines (p3)

Immunofluorescent staining of Flp-In T-REx host cell line (TREx) and Flp-In T-REx cell lines stably expressing GFP, NP-NIRV, NP-NIRV-GFP construct transfected with trVLP system. DAPI staining (Blue) and EBOV NP staining (Magenta). L = Plasmid expressing EBOV polymerase, NP = Plasmid expressing EBOV-NP, "+" = transfected, "-" not transfected. Representative pictures of passage 3.

5.2.3 Impact of NP-NIRV on trVLP Production of EBOV Minigenome System

The presence of IBs in cell lines expressing NP-NIRV suggests that the NP-NIRV does not interfere with IB formation, though it may still influence other viral processes. Beyond its role in IB formation, NP interacts with VP35 (polymerase co-factor) and VP30 (transcription activator) to facilitate filovirus RNA synthesis. Additionally, the interaction of NP with VP24 is essential for nucleocapsid assembly and genome packaging. NP also encapsidates the viral RNA genome, forming the ribonucleoprotein (RNP) complex, which protects the viral RNA from degradation. This multi-functional role of NP highlights the potential for NP-NIRV to impact other viral mechanisms.

To explore whether the expression of NP-NIRV affected viral replication, we used a minigenome system containing a nanoluciferase reporter gene, allowing us to quantify replication and transcription in the presence or absence of the NP-NIRV in Flp-In T-REx 293 cell lines. As functional trVLPs can bud, infect new cells, and subsequently initiate a new replication cycle, we measured reporter activity over two passages (p0 to p2). Supernatant collected three days post-transfection was used to infect pre-transfected cells in the subsequent passage. This approach aimed to indirectly assess whether NP-NIRV interacts with other viral proteins, potentially affecting trVLP production and minigenome replication. As a transfection control, we utilized co-transfection of a plasmid encoding a firefly luciferase reporter gene (Supplementary Figure 7).

We observed reduced nanoluciferase activity in the NIRV cell line, but not in the NIRV-GFP cell line, where activity levels were similar to those in the Flp-In T-REx 293 host cell line (TREx) and the GFP cell line (Figure 16). The difference in reporter activity between the NIRV and NIRV-GFP cell lines, both expressing NP-NIRV, suggests that NP-NIRV, but not the NP-NIRV-GFP construct affects the minigenome. Repeating the experiment with an influenza NP-expressing cell line confirmed that the reduction in trVLP production was specific to NP-NIRV and not due to viral nucleoproteins in general.
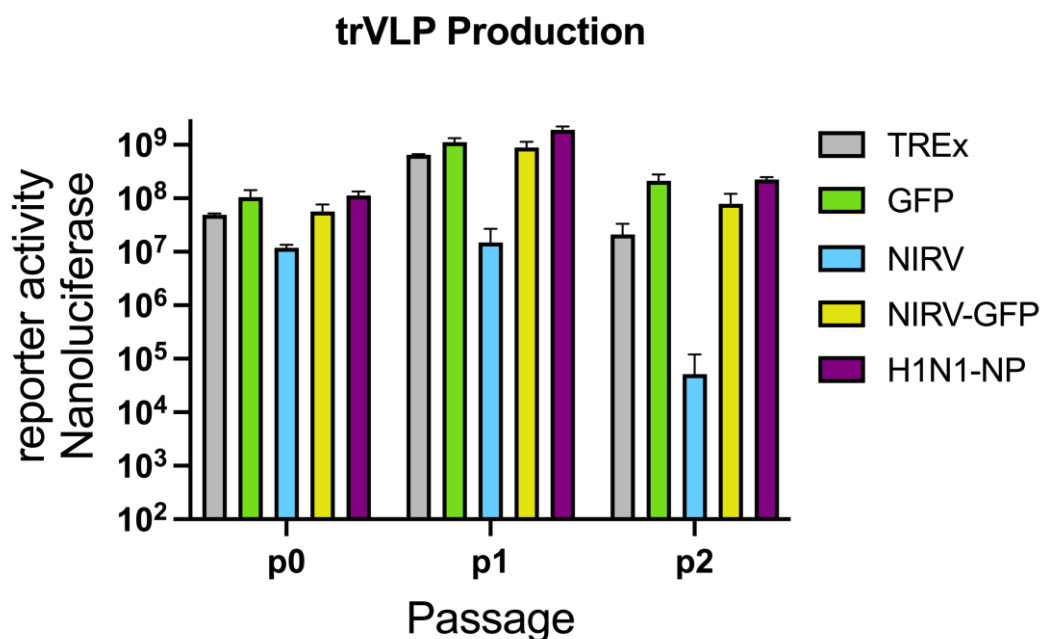
trVLP Production

Figure 17: Production of trVLPs in 293 Cell Lines

Reporter activity (nanoluciferase) representing the production of trVLPs in cells of Flp-In T-REx host cell line (TREx) and Flp-In T-REx cell lines stably expressing GFP, NP-NIRV, NP-NIRV-GFP construct or H1N1-NP from passage p0 to p2. Differences between reporter activity of cell lines were non-significant (Kruskal-Wallis test). Bars represent mean value ± SEM of two independent experiment with triplicates.

5.2.4   NP-NIRV Does Not Inhibit EBOV Replication in Cell Culture

To clarify the minigenome data we decided to investigate the potential impact of NP-NIRV on viral replication using authentic EBOV in a multicycle replication experiment.

We infected the TREx, NIRV, NIRV-GFP, and GFP cell lines with EBOV (Mayinga variant) at low MOI of 0.1 and 0.01. Using lower MOIs allows for better observation of viral replication dynamics by preventing rapid and synchronized infection of all cells. Samples were collected daily over a 14-day period, and the infectious viral particles in the supernatant were quantified using an immunofocus assay. This assay detects viral antigen-expressing cells using EBOV NP-specific antibodies. These clusters of infected cells, called focus forming units (FFUs), are counted to determine the concentration of infectious particles in the sample.

The resulting growth curves showed similar multicycle replication curves across all cell lines, regardless of NP-NIRV or NP-NIRV-GFP expression (Figure 17). We concluded that NP-NIRV expression in EBOV-infected cells does not affect wild type (WT) EBOV replication.
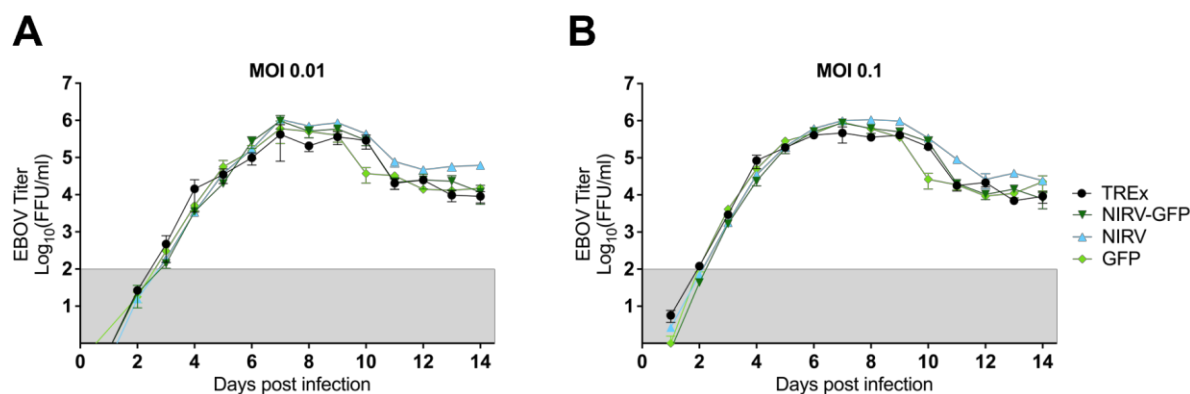
Figure 18: EBOV Replication in 293 Cell Lines

Infection of Flp-In T-REx host cell line (TREx) and Flp-In T-REx cell lines stably expressing NP-NIRV, NP-NIRV-GFP construct and GFP with an MOI of 0.01(**A**) and MOI of 0.1 (**B**) over a duration of 14 days. Samples were taken every day. Viral titers were measured via immunofocus assay. Grey area marks detection limit. Differences between viral titers of cell lines were non-significant (two-way ANOVA). Representative graphs of two independent experiments with triplicates.

5.2.5 Expression of the NP-NIRV in *Mus musculus*

To investigate the biological role of mouse NP-NIRV, we first assessed its tissue-level expression. Widespread expression would suggest a general cellular function, while site-specific expression might indicate tissue-specific roles.

RNA was extracted from various organs of WT mice (C57BL/6J), converted into cDNA, and subjected to subsequent PCR analysis using universal NP-NIRV primers (Table 7). We identified a PCR product of the predicted size (~300 bp) in the spleen, kidney, and thymus, with weaker expression detected in the heart and intestine (Figure 18A). Glyceraldehyde 3-phosphate dehydrogenase (GAPDH) served as a control (Figure 18B).

A

B
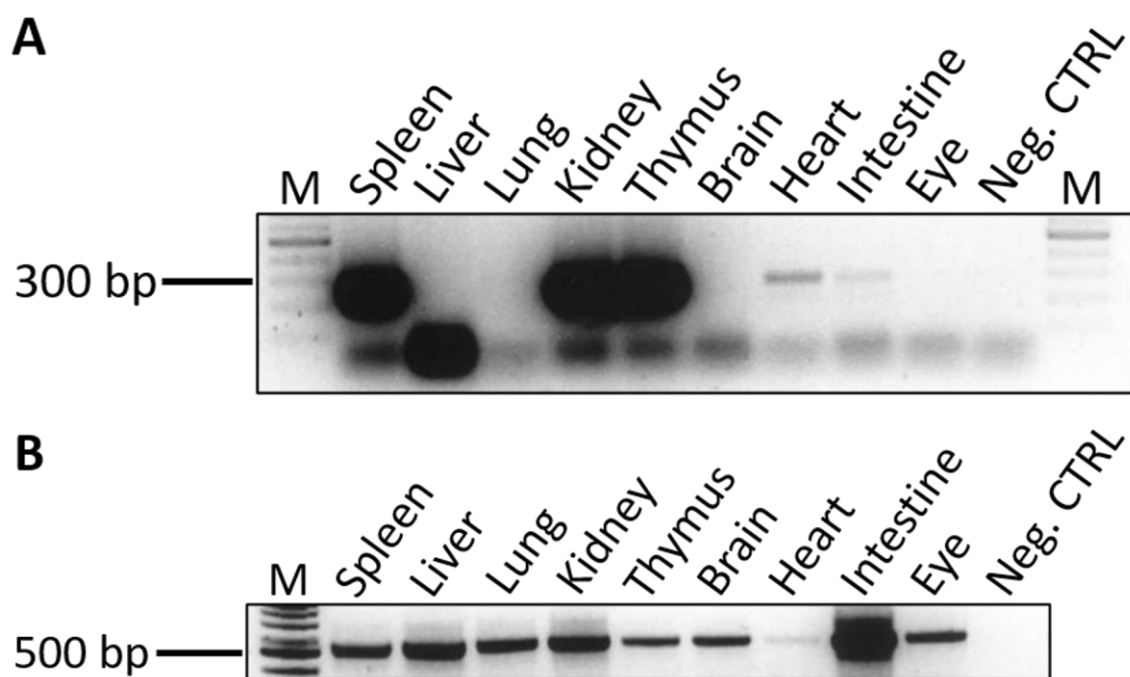
Figure 19: Detection of NP-NIRV Expression in Mouse Organs

PCR for NP-NIRV, strong bands observed for spleen, kidney and thymus, faint bands for heart and intestine(**A**). PCR with GAPDH primer, bands observed for all organs (**B**). "M" indicates lane with marker: GeneRuler DNA Ladder Mix (Supplementary Figure 11). Representative of three independent experiments is shown.

To further dissect the expression of the NP-NIRV in the murine thymus, we next performed cell sorting of the two main types of TECs, namely, cTECs and mTECs. cTECs are primarily responsible for the positive selection of progenitor T cell, while mTECs are involved in negative selection and the establishment of central tolerance, presenting self-peptides to developing T cells under the regulation of transcription factors such as AIRE.[70] Our FACS sorting gating strategy is shown in Figure 19A, and the antibody panel used for sorting is listed in Table 18. The cells were first sorted by size (FSC) and granularity or smoothness (SSC), with only live cells being considered for further analysis. In the next step, we excluded cells expressing CD45.2 (hematopoietic marker) to focus on non-hematopoietic cells. We then selected cells expressing MHC-II, confirming their epithelial nature by assessing the expression of EpCAM. Finally, based on the expression level of UEA-1 lectin and Ly51, TECs were separated into subpopulation of mTECs (UEA$^+$Ly51$^-$) and cTECs (UEA$^-$ Ly51$^+$) (Figure 19A). After sorting, RNA was extracted from TEC subpopulations and converted into cDNA for PCR analysis of NP-NIRV expression.

NP-NIRV expression was detected in mTECs but not in cTECs (Figure 19B), indicating that NP-NIRV expression is restricted to mTECs. The PCR for GAPDH showed strong expression

across all TEC samples, confirming successful cDNA synthesis and RNA quality across all samples (Figure 19C).

As described above, an important feature of mTECs is their expression of AIRE, a transcription factor that promotes the expression of a wide array of TRAs, which are typically absent in the thymus. Peptides derived from these antigens are then presented by mTECs to progenitor T cells during the negative selection process, contributing to central immune tolerance by eliminating T cells that could react against self-antigens (e.g., insulin, myelin) or induce their conversion into Tregs. A PCR using primers against AIRE indicated expression in mTECs but not cTECs, validating the purity achieved during sorting (Figure 19D).
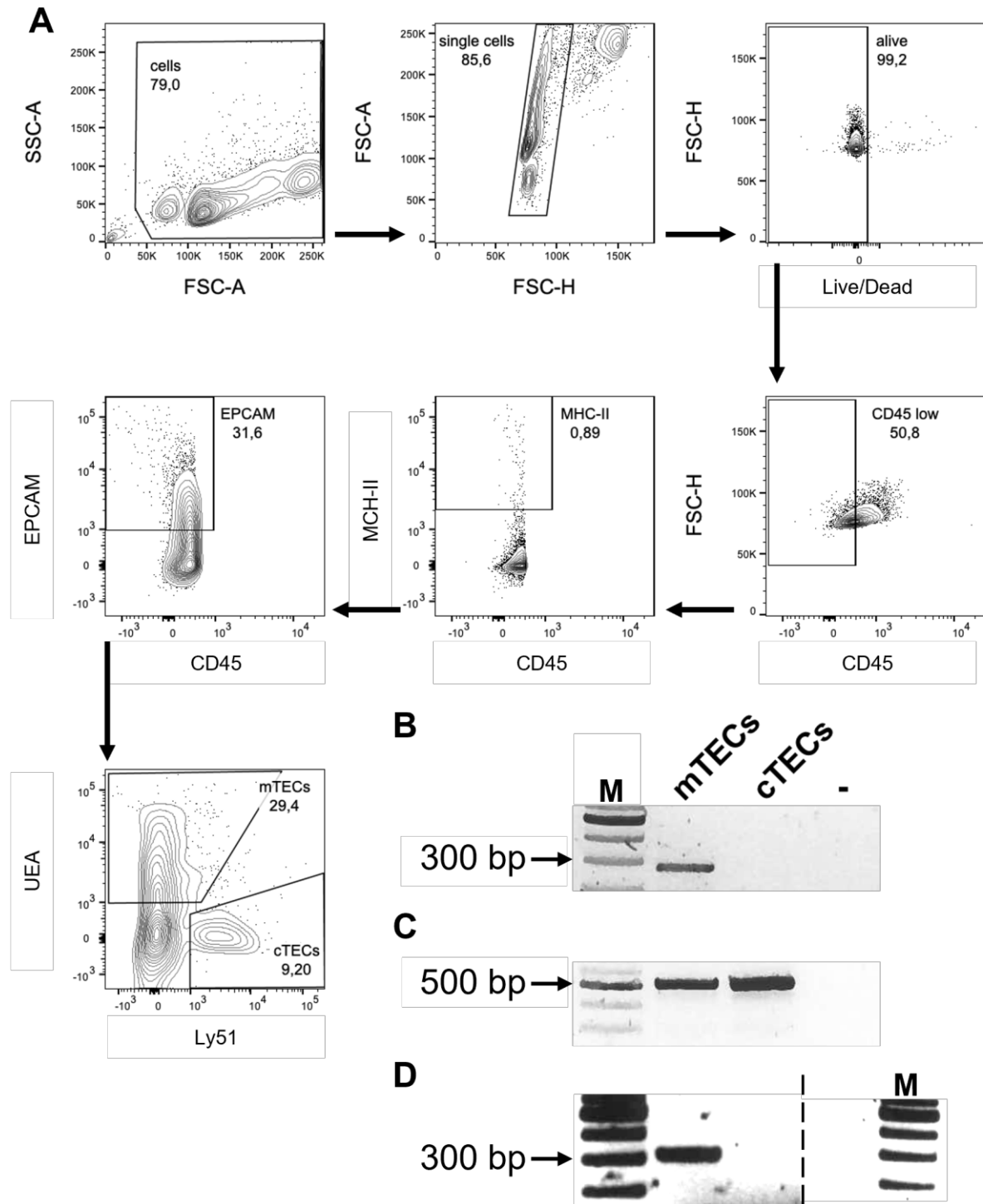
Figure 20: Detection of NP-NIRV Expression in Sorted mTECs

Sorting strategy for mTEC and cTEC isolation. Plots shown are representative of three independent experiments **(A)**. Expression of NP-NIRV, detection of NP-NIRV in mTECs but not in cTECs **(B)**. Expression of GAPDH **(C)**. Expression of AIRE **(D)** "–" = negative control. 1.5 % agarose gel. "M" indicates lane with marker: GeneRuler DNA Ladder Mix (Supplementary Figure 11); PCR with GAPDH primer. Representative of three independent experiments.

5.2.6 AIRE Knock-Out Mice Lack NP-NIRV Expression

The unique expression of the NP-NIRV in mTECs and the presence of an AIRE binding site in this pseudogene led us to hypothesize that the NP-NIRV could be expressed in thymic mTECs as a self-peptide under the control of AIRE. To test this hypothesis, we analyzed thymic cDNA from AIRE KO mice (AIRE$^{-/-}$) for NP-NIRV expression. While GAPDH was clearly expressed in both WT (AIRE$^{+/+}$) and AIRE KO mice, NP-NIRV was not detected in thymus tissue from AIRE KO mice (Figure 20 A and B). This finding suggests that AIRE is required for NP-NIRV expression in the thymus. As a control, a PCR confirmed AIRE's expression exclusively in WT mice (Figure 20C).
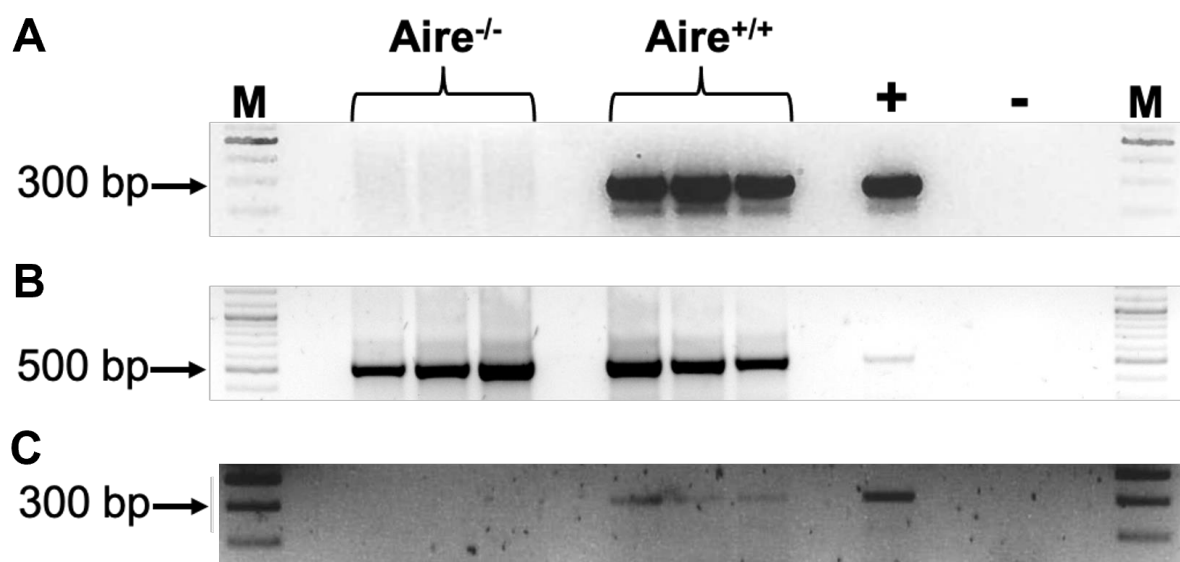
Figure 21: No Detection of NP-NIRV Expression in AIRE KO Mice

Expression of NP-NIRV, detection of NP-NIRV in Aire$^{+/+}$ (WT) but not in Aire$^{-/-}$ (KO) (**A**). Expression of GAPDH (**B**) "+" and "–" indicates lane with positive and negative control, respectively. "M" indicates lane with marker: GeneRuler DNA Ladder Mix (Supplementary Figure 11); Representative of three independent experiments is shown.

5.2.7   NP-NIRV Peptide Stimulation Leads to Low-Level Secretion of IFN-γ

To further explore NP-NIRV's potential role in immune tolerance, we examined the immune response of mice immunized with NP-NIRV-derived peptides. The aim was to determine whether immunization would trigger a typical CD4 Th1-type response against a foreign peptide or a reduced Th1 response characteristic of tolerance to self-peptides.

Mice were immunized with peptides derived from the most conserved region of NP-NIRV and EBOV NP, using GFP-derived peptides as a control for a foreign antigen (Table 22). Peptides were administered subcutaneously with CFA, and an adjuvant-only negative control group was included. Fourteen days post-immunization, spleens were harvested, and single-cell suspensions (splenocytes) were prepared. The splenocytes, containing T cells and antigen-presenting cells, were re-stimulated *ex-vivo* with the peptides to stimulate peptide-specific T cell responses. To assess CD4 Th1-type T cell responses, we conducted an ELISpot assay to detect antigen-specific T cells producing IFN-γ (Figure 21A).

Splenocytes from mice immunized with the GFP peptide exhibited a strong IFN-γ response upon re-stimulation with GFP, as evidenced by a high number of spots per well in the ELISpot assay (Figure 21B). This confirms that the GFP peptide is recognized as a foreign antigen, which aligns with expectations, since GFP is not a naturally occurring protein in mice and its presence likely triggers an immune response due to its non-self-nature.

In contrast, splenocytes from mice immunized with peptides derived from EBOV NP or NP-NIRV exhibited a reduced IFN-γ response when re-stimulated with their respective peptides (Figure 21C and D). The adjuvant-only control group (CFA) showed no detectable IFN-γ production, except for a slight response to GFP and a strong response to the positive control (Figure 21E), confirming low background noise and assay functionality.

The reduced IFN-γ production in response to NP and NP-NIRV peptide re-stimulation, compared to GFP and the positive control, indicates a more tolerogenic immune response. These findings suggest that these filovirus-like peptides may be recognized as self-peptides by the murine immune system, potentially contributing to immune tolerance mechanisms.
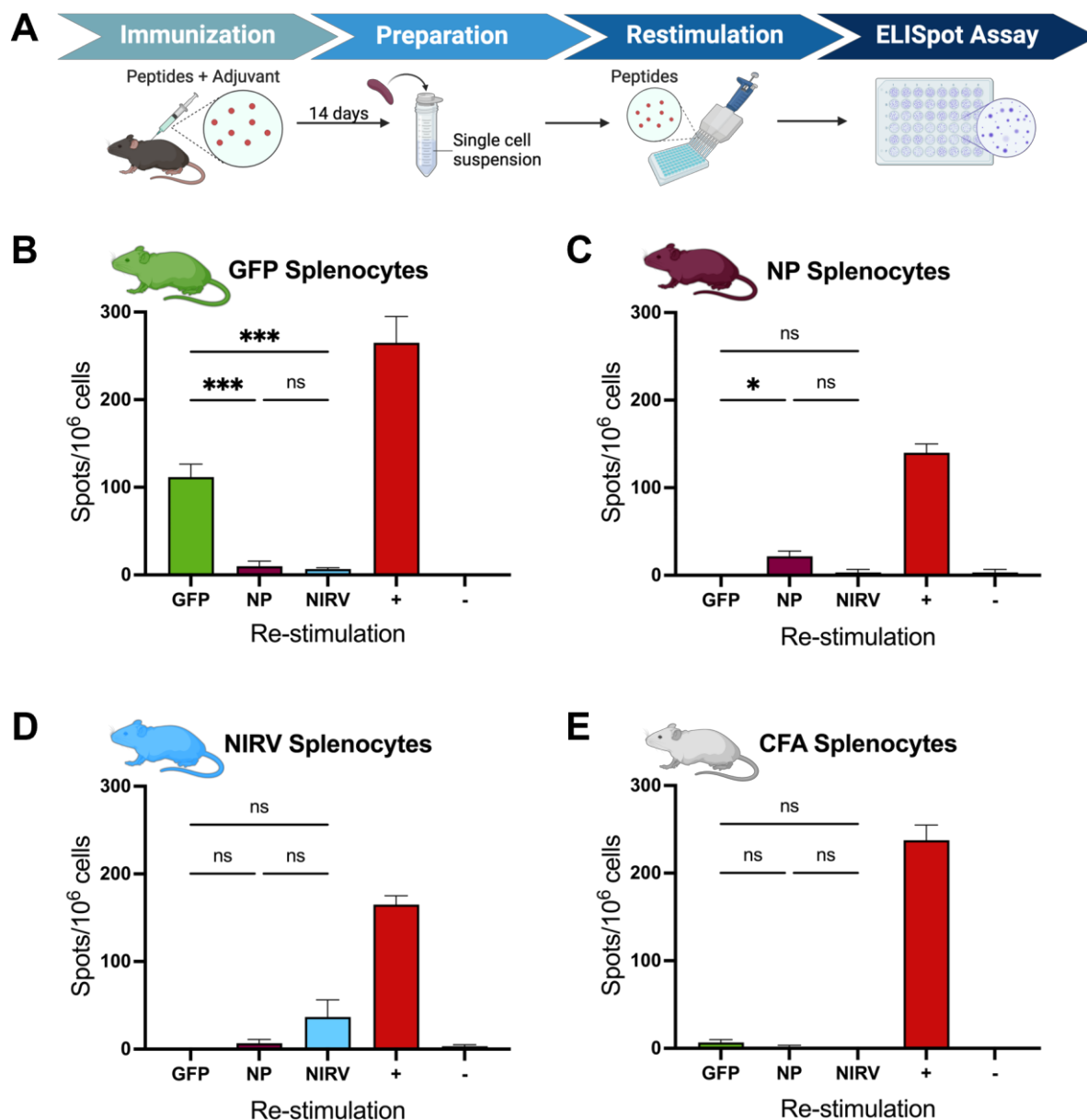
Figure 22: ELISpot Assay for IFN-γ with Re-stimulated Mouse Splenocytes

Schematic of ELISpot Assay with immunization of mice (**A**). Mice (n=1) were immunized s.c. with either GFP, NP, NIRV peptides in combination with CFA as adjuvant. An adjuvant-only group was implemented as control. Re-stimulation (in triplicates) with peptides of splenocytes from mice immunized with GFP (**B**), NP (**C**), NIRV (**D**) peptides and adjuvant-only group (**E**). Lectin served as positive control (+) for the re-stimulation. Number of spots were calculated for $1x10^6$ cells. Stars (*) represent significant differences (one-way ANOVA). Graphs represent mean value of triplicates ± SEM. Representative of four independent experiments is shown.

5.3   Characterization of NIKI mice in Response to EBOV Infection

To investigate the role of NP-NIRV in EBOV pathogenesis, we employed a mouse model featuring NP-NIRV KO (NIKI) mice. This *in-vivo* approach complements our *in-vitro* assays, which only partially reflect the complexity of immune processes.

NIKI mice on a C57Bl/6J background were generated using CRISPR-Cas technology in collaboration with The Jackson Laboratory (JAX). Two strains, NIKI 643 and NIKI 814, were produced with distinct deletions in the NP-NIRV region. Both strains maintained a WT phenotype throughout breeding, confirming their suitability for studies on NP-NIRV's role in viral pathogenesis and immune regulation.

5.3.1   EBOV Infection of NIKI Mice

In our initial experiment with NIKI mice, we aimed to evaluate their response to EBOV infection in comparison to WT (C57Bl/6J) and interferon-α/β receptor KO (IFNAR$^{-/-}$) mice. WT mice, while susceptible to EBOV infection, do not develop disease signs and typically clear the virus within nine days. Conversely, IFNAR$^{-/-}$ mice, which lack IFN-I signaling, are highly susceptible to EBOV infection, reaching euthanasia criteria within two weeks post-infection, making this a 100 % lethal model.[246,264] Since EBOV is predominantly transmitted through contact with infectious body fluids and enters the host through mucosal surfaces or skin lesions, we decided to infect the mice intranasally (i.n.) with 10,000 FFU of EBOV to simulate respiratory mucosal infection. Mice were monitored daily for signs of morbidity over a 21-day period, with body weight recorded each day. This timeline allows for the assessment of the incubation period, disease progression of EBOV infection, and any potential delayed effects. Additionally, blood samples were collected every three days to assess viremia and AST levels in serum.

All mice, except for the IFNAR$^{-/-}$ mice, survived the infection, with no notable differences in weight loss or AST levels between the two NIKI strains and the WT group (Figure 22A, B and D). This indicates that NIKI mice exhibit behavior similar to WT mice during EBOV infections. However, viremia was detected in the NIKI mice, peaking on day 7, similar to the viremia levels seen in IFNAR$^{-/-}$ mice, while no viremia was observed in WT mice (Figure 22C). Upon observing significant weight loss due to EBOV infection, the IFNAR$^{-/-}$ mice were euthanized for ethical considerations. Their high levels of viremia and elevated AST levels highlight the critical role of the IFN-I response in controlling EBOV infection, as the absence of this signaling pathway exacerbated disease progression.
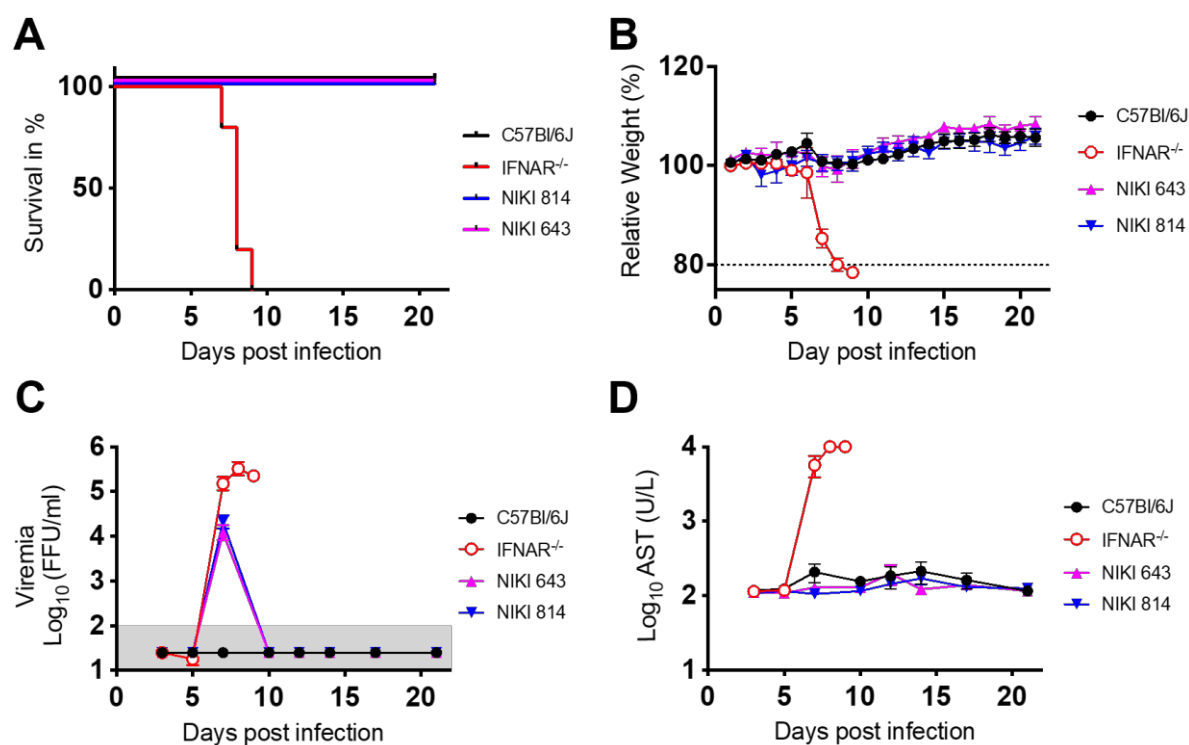
Figure 23: Infection of NIKI Mice in Comparison to WT and IFNAR^{-/-} Mice

Mice (n=5) were infected i.n. with 10,000 FFU of EBOV. Mice were monitored for survival (**A**) and relative weight loss. Animals that fell below an initial weight of 80 % (dotted line) were sacrificed (**B**). Viremia in blood (**C**), and AST activity (**D**) were measured at indicated time points. The limit of detection for viremia in blood is shaded in grey. Differences in weight and ASTs between NIKI and WT mice are non-significant. Differences in viremia between NIKI and WT mice were significant on day 7 ($p<0.0001$) (two-way ANOVA). Graphs represent mean value $\pm$ SEM.

5.3.2 Similar Responses Observed in NIKI and WT Mice During EBOV Infections

Following the initial infection experiment, we aimed to further investigate the early phase of EBOV infection in NIKI mice. To achieve this, we used a comprehensive set of assays to assess inflammation, specifically measuring cytokine and chemokine levels while analyzing immune cell infiltration. These analyses were performed using flow cytometry and histology to provide a comprehensive understanding of the immune response dynamics in NIKI mice during EBOV infection.

We compared WT and NIKI mice, with IFNAR$^{-/-}$ mice as a positive control for heightened inflammation. All mice (n=9/strain) were infected i.n. with 1,000 FFU of EBOV. Three mice per strain were euthanized on days 3, 6, and 9 post infection to monitor disease progression over time. This time-course study allowed for the tracking of temporal changes in immune response, inflammation, and viral load, providing insights into the kinetics of EBOV infection in NIKI, WT, and IFNAR$^{-/-}$ mice. Additionally, three uninfected mice per strain were included as baseline controls. Blood samples were collected at the experimental endpoint via heart puncture, and viral titers were measured using an immunofocus assay.

Although NIKI 814 showed viremia at day 6 post-infection, neither NIKI strains maintained sustained levels of viremia over the course of infection (Figure 23A). These results suggest that similar to WT mice, NIKI mice controlled virus dissemination. As expected, IFNAR$^{-/-}$ mice exhibited progressive increases in viremia, indicating their inability to control the infection due to the lack of a functional IFN-I response. Viral titers in organs were similar between WT and NIKI mice (Figure 23B). We measured viral loads in the spleen, liver, lung, and kidney. IFNAR$^{-/-}$ mice showed high titers in the spleen, liver, and kidney on both days 6 and 9.

In NIKI 814 mice, viral particles were detected in the spleen, while none were observed in NIKI 643 or WT mice. No Infectious viral particles were detected in the liver of NIKI and WT mice at any time point, indicating that these strains effectively controlled the infection and prevented detectable EBOV dissemination. Titers in the kidneys increased across all strains over the course of the experiment, with NIKI mice showing slightly higher levels than WT mice on day 9. Lung titers rose from day 3 to day 6, then declined in NIKI and WT mice but peaked in IFNAR$^{-/-}$ mice on day 9. NIKI 814 mice exhibited elevated levels of infectious viral particles in the lung compared to slightly lower levels in WT mice on day 3, while NIKI 643 mice had titers similar to IFNAR$^{-/-}$ mice on day 6. By day 9, NIKI mice had lung titers comparable to those of WT mice. The elevated titers in the lung were expected due to the intranasal infection route.
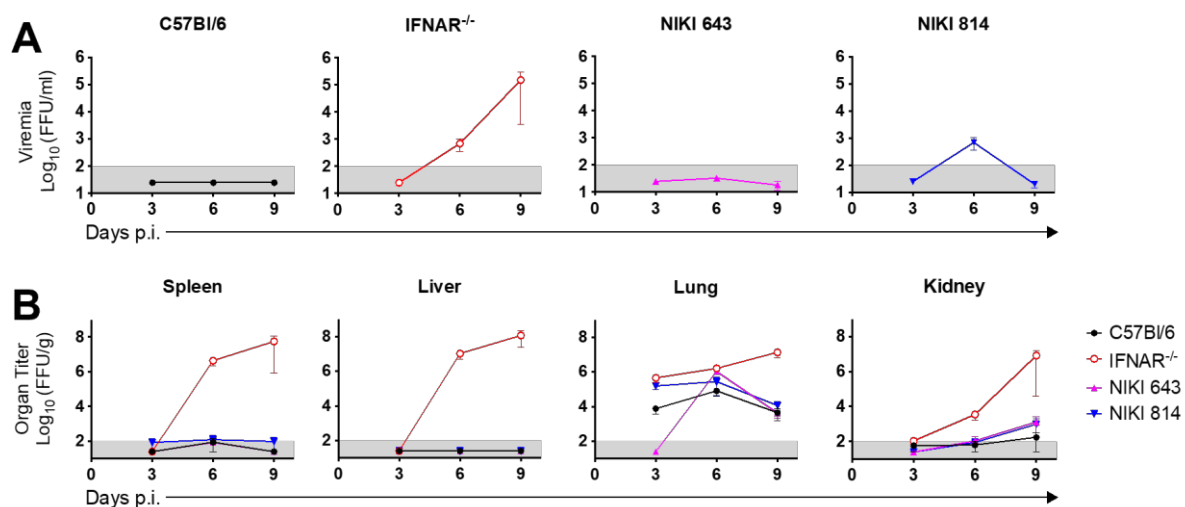
Figure 24: Time Course Study of Mice During EBOV Infection

Mice (n=9) were infected i.n. with 10,000 FFU of EBOV. 3 Mice per strain were euthanized at Day 3, 6 and 9. Mice were monitored for survival and relative weight loss (not shown). Only IFNAR$^{-/-}$ fell below an initial weight of 80 % (dotted line) and were euthanized. Viremia in blood (**A**), and viral replication in spleen, liver, lung and kidney (**B**) were measured at indicated time points. The limit of detection for viremia in blood is shaded in grey. Differences in viremia between NIKI and WT mice were non-significant (two-way ANOVA). Differences in virus titers in organs between NIKI and WT mice were non-significant (Kruskal-Wallis test). Graphs represent mean value ± SEM.

To investigate possible differences in inflammation between NIKI mice and WT mice upon EBOV infection, we sought to assess the infiltration of immune cells at infection sites by flow cytometry, evaluation of serum cytokine levels and immunohistochemistry.

The flow cytometry analysis of immune cells in lung tissue demonstrated a noticeable increase in neutrophil frequency in IFNAR$^{-/-}$ mice on days 6 and 9 post-infection, indicating an inflammatory immune response (Figure 24A). This increase was not observed in NIKI and WT mice, suggesting reduced inflammatory responses in these strains. While neutrophil levels in NIKI 814 mice were lower than in IFNAR$^{-/-}$ mice, they were higher than in both NIKI 643 and WT mice on day 9. However, the differences were not statistically significant (Kruskal-Wallis test). The frequency of CD3$^+$ cells was consistent between NIKI and WT mice (Figure 23B), whereas in IFNAR$^{-/-}$ mice, CD3$^+$ cell frequency declined from day 6 to day 9, possibly reflecting an increased neutrophil proportion. B cell frequencies decreased across all strains at a similar rate as the infection progressed (Figure 23C).

In sum, the lack of significant differences between NIKI and WT mice speaks to the similarity in behavior of NIKI and WT mice during EBOV infections.
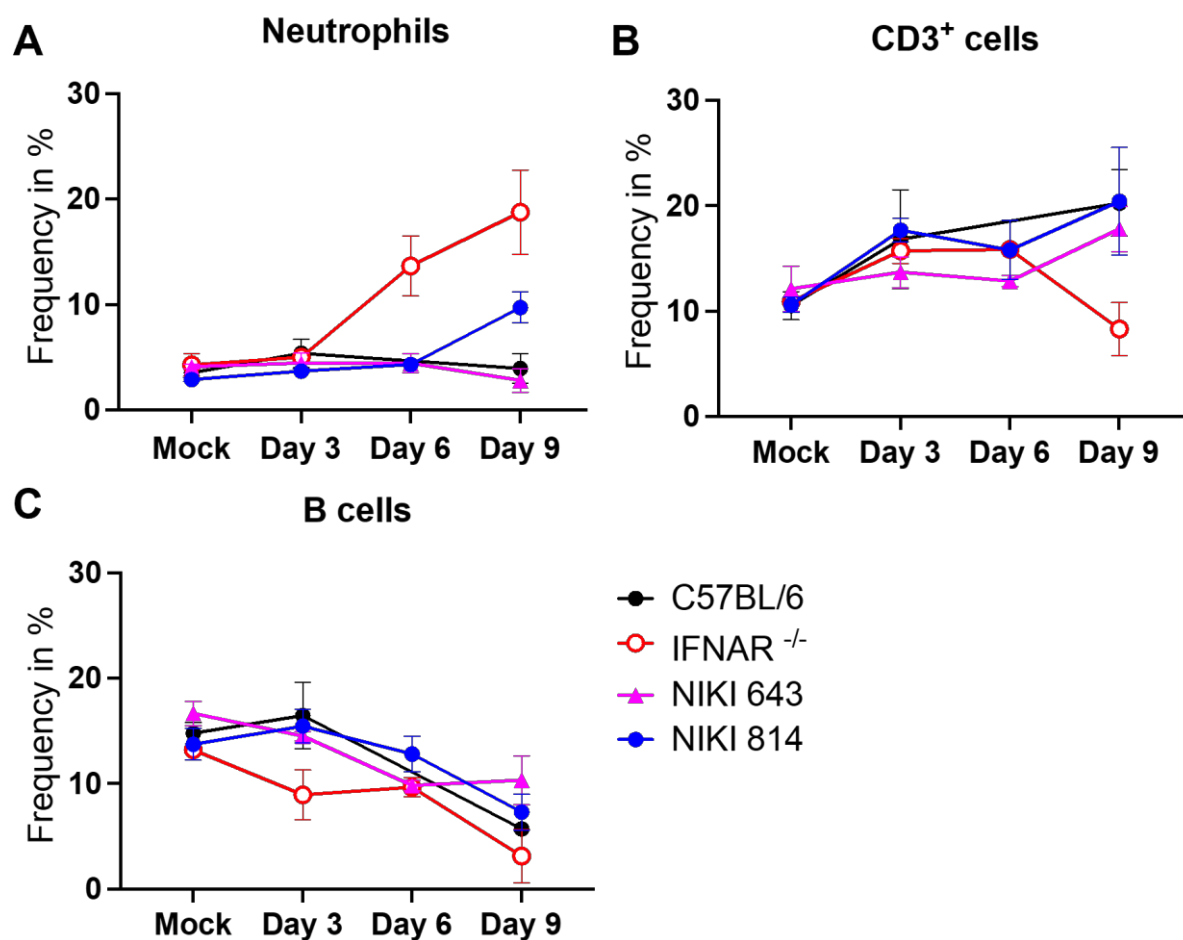
Figure 25: Frequency of Cells in Lung Tissue of Mice During EBOV Infection

Mice (n=9) were infected i.n. with 10,000 FFU of EBOV. 3 Mice per strain were sacrificed at Day 3, 6 and 9. 3 uninfected mice per strain (Mock) served as baseline control. Lung tissue was homogenized to single cell suspension and stained for flow cytometry analysis. Frequency of singlets was calculated for neutrophiles (**A**), CD3^{+} cells (**B**) and B cells (**C**). Differences between NIKI and WT mice were non-significant (Kruskal-Wallis test). Graphs represent mean value ± SEM.

To further evaluate the inflammatory response against EBOV infection in all three mouse strains, serum cytokine and chemokine levels were analyzed. Samples were collected from both uninfected (Mock) and infected mice at all time points (day 3, 6 and 9) and examined using a multiplex fluorescence-encoded bead-based assay, with flow cytometry readouts. Data were normalized using min-max normalization, scaling cytokine values between 0 and 100 (Figure 25). This approach allowed for direct comparison of inflammatory profiles between different time points and mouse strains.

No inflammation was detected in uninfected mice or on day 3 post-infection, establishing a baseline and indicating that early stages of EBOV infection do not induce a significant inflammatory response. By day 6, two out of three IFNAR$^{-/-}$ mice exhibited elevated levels of IFN-γ, CXCL1 (KC), IFN-α, and IL-6, consistent with their compromised immune response due to the lack of IFN-I signaling. In contrast, NIKI and WT mice maintained low cytokine and chemokine levels, suggesting a more regulated cytokine response compared to the heightened inflammation seen in IFNAR$^{-/-}$ mice.

On day 9, most IFNAR$^{-/-}$ mice exhibited high levels of IFN-γ, TNF-α, CCL2 (MCP-1), CCL5 (RANTES), CXCL10 (IP-10), and IL-10, with one mouse showing additional increases in IL-1β, IFN-β, and IL-6. Meanwhile, NIKI and WT mice maintained low inflammatory markers, with only sporadic increases in individual markers. Overall, compared to WT mice, the lack of the NP-NIRV expression in NIKI mice did not result in enhanced inflammation in response to EBOV infection.
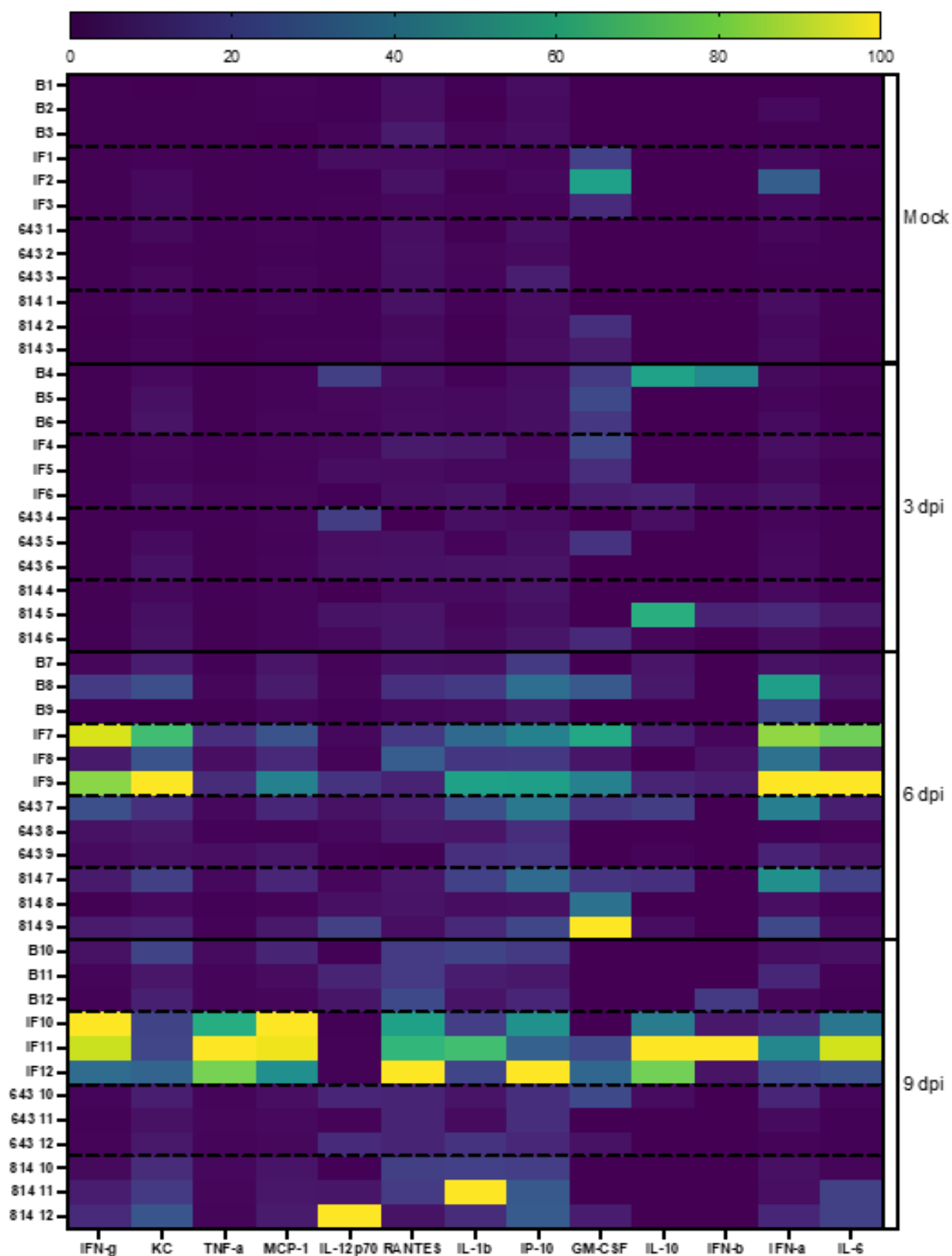
Figure 26: Cytokine Response of Mice During EBOV Infection

Mice (n=9) were infected i.n. with 10,000 FFU of EBOV. 3 Mice per strain were sacrificed at Day 3, 6 and 9. 3 uninfected mice per strain served as baseline control (Mock). Dotted lines separate strains, lines separate Mock animals and days post infection (dpi). Cytokine data was normalized using min-max normalization, which normalized cytokine values between 0 and 100. B = C57Bl/6; 643 = NIKI 643; 814 = NIKI 814; IF = IFNAR$^{-/-}$. Number indicates individual mouse.

Finally, we assessed inflammation in the three mouse strains via tissue immunohistochemistry analysis at necropsy. We used antibodies against IBA1, a marker that is upregulated upon macrophage/microglia activation (Figure 27).[265] The level of inflammation in tissue sections was subsequently analyzed using a blinded scoring system ranging from 0 to 5, where 5 represents the highest level of inflammation (Figure 26).

We did not observe major differences in inflammation and pathology in the kidneys between NIKI and WT mice (tissue sections not shown). In contrast, IFNAR$^{-/-}$ mice exhibited the expected elevated levels of inflammation compared to low levels in NIKI and WT mice (Figure 26B).

In the lungs of IFNAR$^{-/-}$ mice, we observed a significant increase in IBA1-positive cells on day 6, which intensified on day 9, indicating elevated pathology with areas of necrosis (Figure 27). NIKI mice displayed moderate inflammation on day 6, which further increased on day 9, especially around the pulmonary alveoli and blood vessels. Conversely, WT mice exhibited minimal IBA1-positive cells on days 3 and 6; however, on day 9, inflammation in WT mice reached levels comparable to those in NIKI mice.

These findings suggest that lung inflammation is more pronounced in IFNAR$^{-/-}$ mice compared to NIKI and WT mice, aligning with our other data. The delay in inflammation in WT mice compared to NIKI mice indicates slightly different dynamics of the EBOV infection. Both strains appear to control early inflammation more effectively, whereas IFNAR$^{-/-}$ mice experience more severe and sustained pathology.
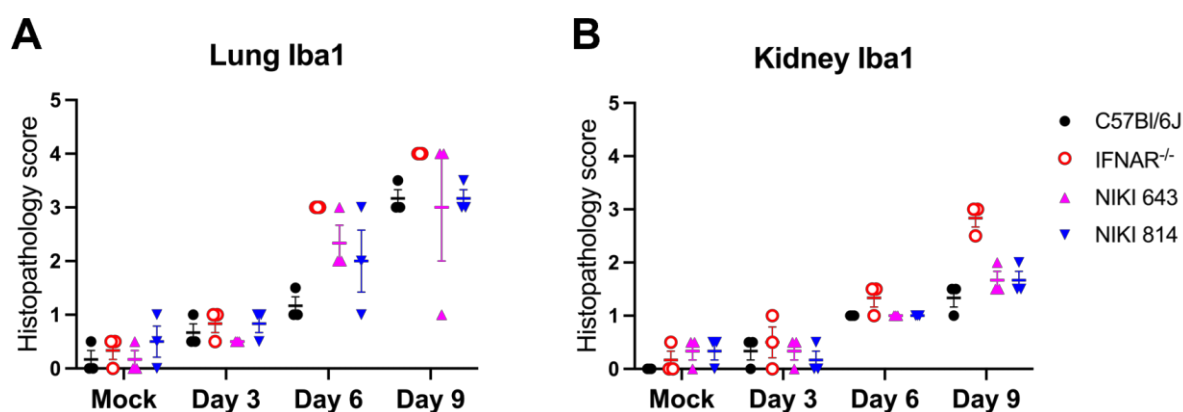
Figure 27: Histopathology Scoring of Lung Tissue from Mice During EBOV Infection
Mice (n=9) were infected i.n. with 1,000 FFU of EBOV. 3 Mice per strain were sacrificed at Day 3, 6 and 9. 3 uninfected mice per strain served as baseline control (Mock). Histopathological score (ordinal method, values of 0 to 5) for Iba1-positive cells in lung sections shows elevated levels for NIKI mice compared to C57Bl/6J (WT) mice on day 6 post infection **(A)** and slightly elevated levels on day 9 in the kidney. Graphs represent mean value ± SEM.
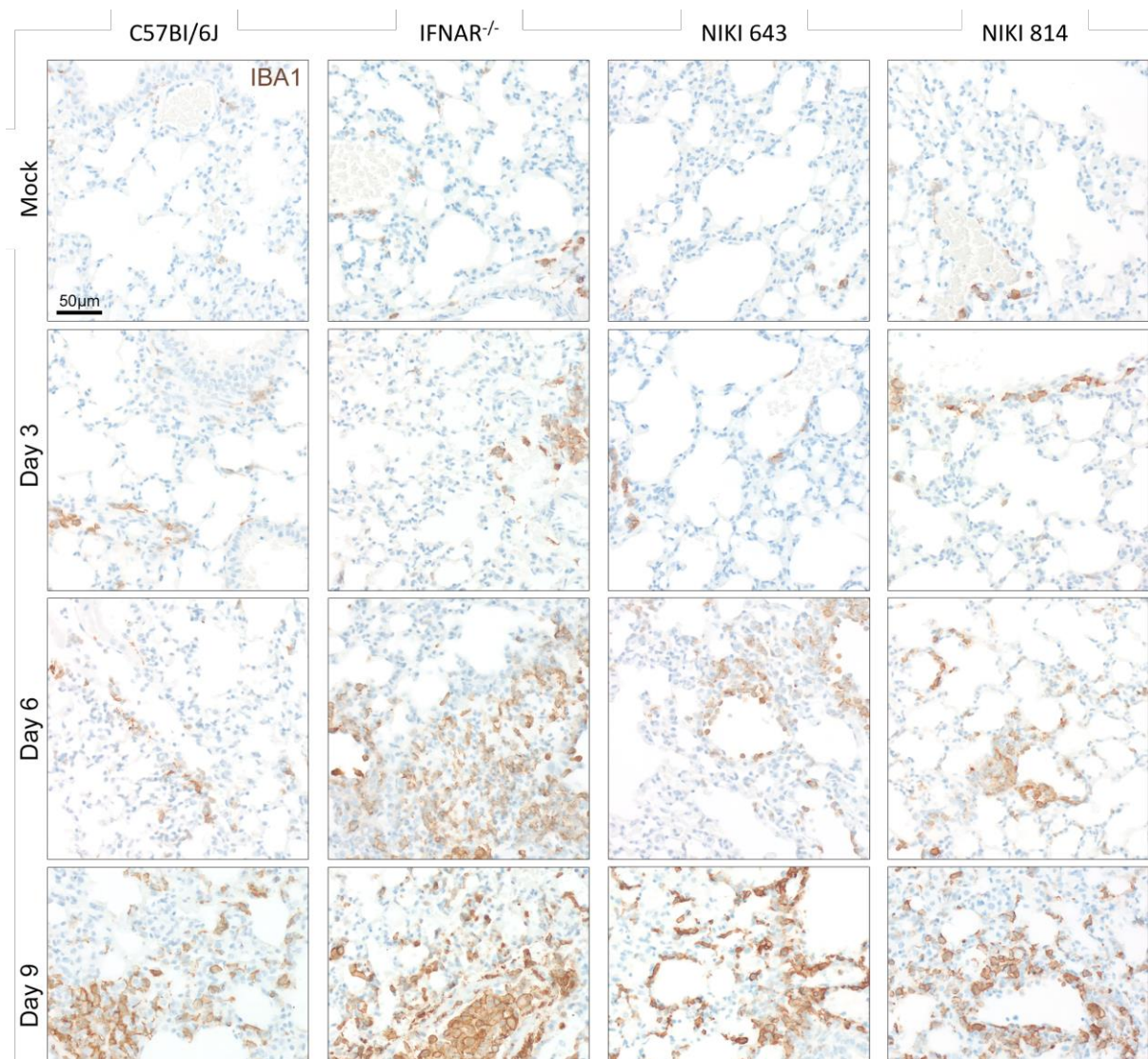
Figure 28: IBA1 Staining of Lung Tissue Sections from Mice During EBOV Infection

Histopathological findings in tissue sections of Mice (n=9) infected i.n. with 1,000 FFU of EBOV. 3 Mice per strain were sacrificed at Day 3, 6 and 9. 3 uninfected mice per strain served as baseline control (Mock). Brown indicates staining with anti-Iba1 antibodies in the tissue sections.

5.4 Identification of Other *Mononegavirales* NIRVs in Mice

Despite the absence of NP-NIRV expression in NIKI mice, we observed no differences in pathogenesis or inflammation compared to WT mice. One possible explanation is that other NIRVs, in addition to NP-NIRV, may also be presented in the murine thymus and contribute to T cell selection. Given the high conservation of NP within the order *Mononegavirales*, which includes the family *Filoviridae*, NP-derived NIRVs across this order could modulate T cell responses against filoviruses and related viruses. To test this hypothesis, we used a published data set of low-abundance peptides presented by MHC-II molecules in the murine thymus by Padma P. Nanaware *et al.*[257] and performed a BLASTP (NCBI) search, comparing them to *Mononegavirales* sequences. After quantifying hits with an E value of 1 or lower, we used the Immune Epitope Database (IEDB) to identify known immune epitopes and used IEDB tools to predict their binding potential to MHC-II molecules (Figure 28).

The BLAST E-value represents the number of expected hits of similar quality (score) that could occur by chance. Given the small size of peptide sequences, we set a higher E-value threshold. The conserved region of the NP-NIRV in *Mus musculus* has an E-value of 0.5 when compared to EBOV NP. To put this into perspective, the entire putative protein product of NP-NIRV exhibits an E-value of 8e-05 (8×10^{-5}), demonstrating a highly significant similarity and low probability of occurring by chance.
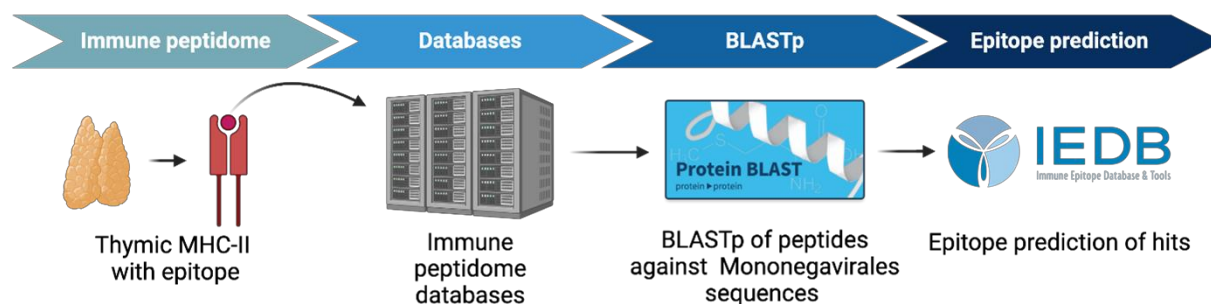
Figure 29: Schematic of *in-silico* Analysis of Immune Peptidome

MHC-II bound peptides from published databases were blasted (BLASTP, NCBI) against *Mononegavirales* sequences. Immune Epitope Database (IEDB) was used to confirm hits as MHC-II epitopes.

We identified over 500 hits for *Mononegavirales* sequences, including *Paramyxoviridae*, *Rhabdoviridae*, *Nyamiviridae*, *Pneumoviridae*, *Filoviridae*, and *Lispiviridae* (Figure 29), suggesting that a range of virus-like peptides could influence immune tolerance and modulate responses against a wide range of viruses in mice.

In contrast, analysis of human thymic data yielded fewer *Mononegavirales* hits, with no matches for *Pneumoviridae*, *Filoviridae*, or *Lispiviridae*.[259] However, the human data did contain hits for *Bornaviridae* and *Artoviridae*, suggesting that virus-like peptides may contribute to immune tolerance in humans, albeit to a lesser extent than in mice, and that the involved virus families differ between species.
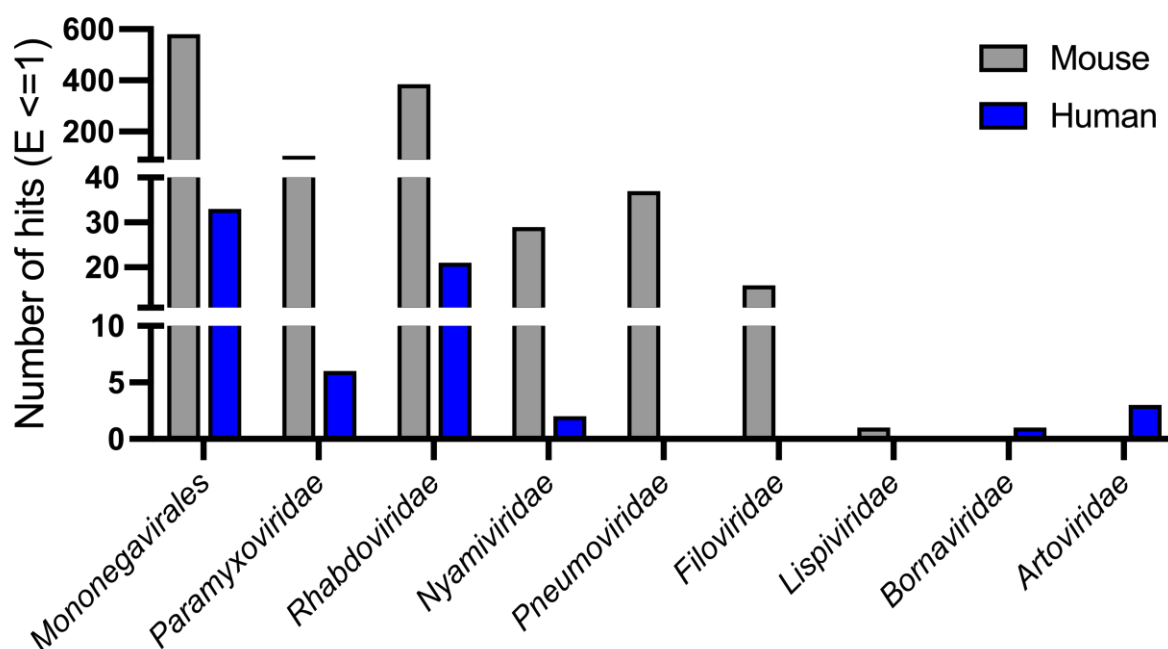
Figure 30: *In-silico* **Analysis of Murine and Human Immune Peptidome**
BLASTp (NCBI) of peptidome eluted from mouse thymus (**A**). BLASTp of peptidome eluted from human thymus (**B**). Only hits of organisms with an E value of <=1 were counted. The first bar (*Mononegavirales*) displays the total number of hits within the order and is broken down into individual family taxa hits.

5.5   EBOV Infection in Treg-Depleted (DEREG) Mice

To further test the hypothesis that multiple NIRVs could be modulating T cell responses against filoviruses in mice, we next sought to assess the effect of regulatory CD4 T cell depletion in mice.

A key mechanism of immune tolerance involves converting self-reactive T cell progenitors into Tregs. As a result, mature Tregs with TCRs specific to self-peptides circulate throughout the body and utilize several mechanisms to prevent effector T cell responses against self-antigens.[70] Our *in-silico* analysis identified multiple MHC-II peptides in the murine thymus that resemble *Mononegavirales* sequences, leading us to hypothesize that *Mus musculus* harbors various *Mononegavirales*-specific Tregs. These Tregs might react to *Mononegavirales* antigens and could be activated during EBOV infection due to epitope similarities. Thus, we aimed to explore the role of Tregs in EBOV infections, hypothesizing that their absence could influence disease outcomes.

We utilized DEREG mice, which are genetically modified to allow for the conditional depletion of FOXP3-expressing Tregs upon the administration of diphtheria toxin (DT).[266] In these mice, FOXP3-expressing cells express the DT receptor, making them selectively susceptible to DT (Figure 30B).

Treg-depleted mice were infected with EBOV and monitored for 21 days. Blood and serum samples were collected to assess viremia and AST levels (Figure 30A). To determine if the effects were specific to EBOV or generalizable to other viral infections, we included a control group of mice infected with Lassa virus (LASV, *Arenaviridae*), a virus outside the *Mononegavirales* order. Uninfected (Mock), Treg-depleted mice served as a control to investigate potential side effects of DT administration and the associated loss of FOXP3-expressing cells.

EBOV-infected DEREG mice exhibited significant weight loss compared to untreated infected mice; a pattern not observed during LASV infection (Figure 30C). These findings indicate that Tregs play an important role in modulating early immune responses specific to EBOV infection. DT injections were discontinued after day 3. Weight loss in EBOV-infected DEREG mice peaked on day 8 and subsequently began to regain weight continuously until the end of the experiment, possibly reflecting the recovery of Treg populations. However, AST levels remained elevated in these mice compared to the other control groups, and viremia peaked on day 18, while it remained undetectable in untreated infected mice throughout the experiment (Figures 30D and 30E). These findings indicate that Treg depletion may impair effective clearance of EBOV.
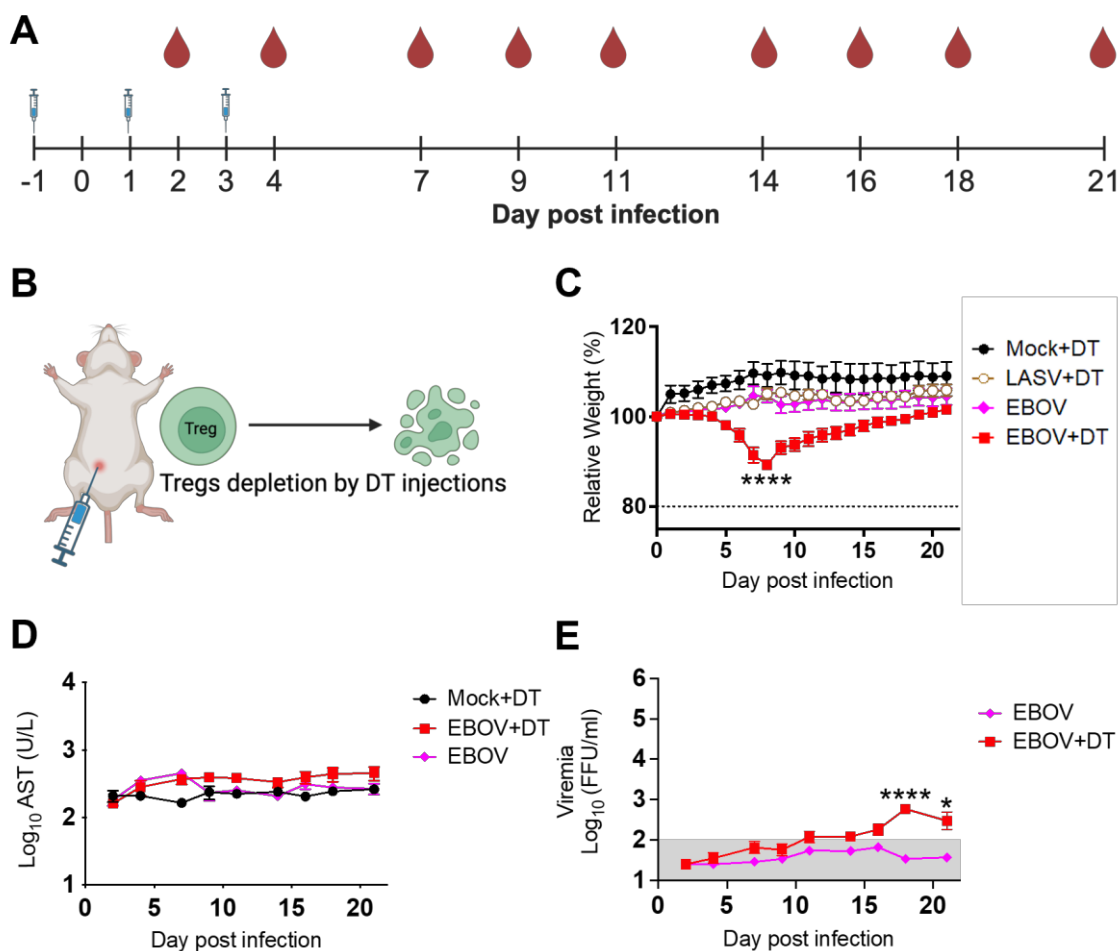
Figure 31: EBOV Infection in Treg-Depleted (DEREG) Mice

Mice (n=6) were infected i.n. with 10,000 FFU of EBOV. Schematic of the experiment with timepoints for DT injections (daily from day 0 until day 7) and blood drawings (**A**). Tregs are depleted through i.p. DT injections in C57BL/6-Tg(Foxp3-DTR/EGFP) (**B**). Mice were monitored for relative weight loss (**C**). Viremia in blood (**D**), and AST activity (**E**) were measured at indicated time points. The limit of detection for viremia in blood is shaded in grey. Differences in AST levels were non-significant. Significant differences are indicated by stars (*) (two-way ANOVA). Differences in weight (between LASV+DT and EBOV+DT) were significant between day 5-19 but the most drastic differences were observed on day 8 (as indicated). Graphs represent mean value ± SEM.

6 Discussion

Paleoviral sequences remain largely understudied despite their recognized evolutionary significance.[1,7] Over recent decades, numerous EVEs have been identified across species, but their functions, particularly those of NIRVs, are still poorly characterized.[18,30,50] Furthermore, the reasons for the stark differences in EBOV pathogenicity between humans and species such as bats and rodents remain incompletely understood.

This thesis aims to address these gaps by investigating the potential role of a murine NP-NIRV in promoting immune tolerance to EBOV infections in mice. By doing so, it contributes to a deeper understanding of the evolutionary impact of paleoviral sequences, particularly in the context of EBOV-host interactions.

Our findings suggest the involvement of NP-NIRV in immune tolerance mechanisms. Additionally, we provide evidence for the crucial role of Tregs during EBOV infections in mice and propose that additional NIRVs present in the mouse genome and derived from viruses of the order *Mononegavirales* may also contribute to immune tolerance.

6.1 NP-NIRV Does Not Affect Inclusion Body Formation or WT EBOV Replication in Cell Culture

The NP-NIRV is integrated as an intact ORF in the genome of *Mus musculus*, and we argued that if it is translated into a protein, it could function as a dominant negative form of the EBOV NP, potentially affecting NP functions such as IB formation and viral replication.

We generated stable cell lines expressing NP-NIRV, NP-NIRV-GFP (with P2A linker sequence), and a GFP control. However, the intensity of fluorescence was lower in the NP-NIRV-GFP line compared to the GFP-only line. This reduction can be explained by the ribosome skipping mechanism, which, as shown in other studies, can cause the ribosome to fall off the mRNA approximately 60% of the time at the 2A site. This leads to a decrease in the expression of the downstream GFP protein by about 70%, depending on the construct.[267,268]

Notably, GOI expression was detected in cell lines cultured in the absence of tetracycline, despite regulation by a Tet-repressor. This may be attributed to the use of FCS in the culture medium, as most FCS lots contain residual tetracycline, likely due to its presence in the feed of donor animals. Consequently, basal-level GOI expression may occur even when using tetracycline-reduced FCS.

Although we lacked a specific antibody to confirm NP-NIRV protein translation, evidence at the mRNA level confirmed the presence of NP-NIRV in both NP-NIRV and NP-NIRV-GFP cell lines. Additionally, the sensitivity to zeocin of altered cell lines and their resistance to

hygromycin B, as well as DNA sequencing confirmed a successful integration of the respective GOI.

In combination with the cell lines, we employed an established tetracistronic EBOV minigenome system to assess the impact of NP-NIRV expression on IB formation.[253] Notably, similar levels of IBs were observed in cell lines expressing NP-NIRV or NP-NIRV-GFP when compared to the empty host cell lines and the GFP cell line, suggesting that NP-NIRV does not interfere with IB formation. This observation aligns with sequence alignment results, indicating that NP-NIRV overlaps with the N-terminal region of EBOV NP but not with regions critical for IB formation (Figure 31).[269] Functional studies demonstrate that the N-terminal 450 amino acids of EBOV NP, conserved across *Mononegavirales*, are important for NP-NP interactions necessary for IB formation.[251] However, these studies examined larger segments of the N-terminal region, not specifically the overlapping NP-NIRV area. Other studies also identify regions in the C-terminal and central domains of EBOV NP as essential for full IB functionality, which do not align with NP-NIRV.[269]
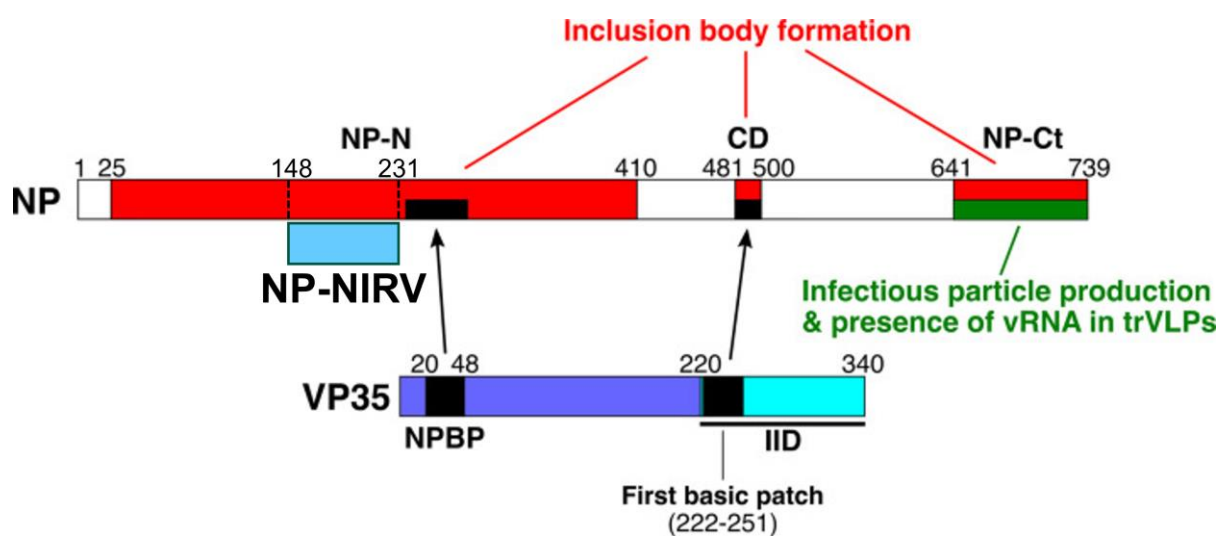
Figure 32: Identified NP Functions with Murine NP-NIRV Alignment

Illustration of NP functions. Full-length NP and VP35 proteins are shown, with NP regions defined as follows: NP-N (amino acid 1–412), NP-Ct (amino acid 641–739), and the central domain (CD, amino acid 481–500). Red boxes mark regions necessary for IB formation. NP-Ct is required for NP-induced IB formation, but this requirement is bypassed when VP35 is co-expressed. Similarly, while NP-N and NP-Ct support IB formation, mutation of the CD does not abolish it, as NP-Ct and CD complement each other. The green box indicates the region critical for producing infectious trVLPs and retaining viral RNA in purified trVLPs. Black regions highlight NP binding peptide (NPBP) and its binding site in NP, as well as VP35's first basic patch and its binding site, the CD. Murine NIRV (blue box) aligns with EBOV NP (amino acid 148 -231). (Adapted from Miyake *et al.*, 2020)

To evaluate NP-NIRV's potential effect on viral replication, we quantified trVLP production by measuring luciferase expression using the tetracistronic EBOV minigenome system. Reduced luciferase activity in the NP-NIRV cell line indicated that NP-NIRV may suppress trVLP production. Notably, although both the NIRV and NIRV-GFP cell lines express NP-NIRV, luciferase activity was higher in the NIRV-GFP cell line. A possible reason for this could be RNA interference. The NP-NIRV-GFP construct exists as a larger RNA molecule before ribosome skipping separates it into two proteins. Thus, the larger NP-NIRV-GFP RNA may not interfere with viral replication as effectively as the smaller NP-NIRV RNA molecule expressed in the NIRV cell line.

While the minigenome system is useful for modeling EBOV biology under BSL-2 conditions, it only partially replicates the replication cycle of the authentic virus. To address this and to clarify the minigenome data, we quantified the production of infectious viral particles from WT EBOV in the presence of NP-NIRV. Our results indicated that NP-NIRV does not affect EBOV replication, implying that the observed effects in the trVLP system are specific to the minigenome model and do not translate to WT virus replication in cell culture. This is in contrast to a study on a bornavirus NIRV-encoded protein in the thirteen-lined ground squirrel, which demonstrated an inhibitory effect on BDV replication. It interfered with BDV polymerase activity and colocalized with viral components in the nucleus, likely inhibiting replication by integrating into the viral ribonucleoprotein complex.[45] Like our study, the researchers employed a minigenome system and later confirmed their findings with WT BDV in cell lines expressing the BDV NIRV. The larger size and greater similarity of the BDV NIRV to current bornavirus proteins may account for stronger inhibitory effects on viral replication relative to the murine NP-NIRV (35 kDa BVD NIRV and putative 11 kDa NP-NIRV).

Given the assumption that the murine NP-NIRV has been inherited over millions of years for a specific purpose, the lack of an effect on WT EBOV replication in our experiments suggests that it may serve a different role. Indeed, our findings support the central hypothesis of this study—that NIRVs contribute to immune tolerance. In this context, it appears that the size of NIRVs may not be the determining factor. Rather, small, conserved peptide sequences shared between NIRVs and viral proteins likely play a critical role.

6.2   NP-NIRV's Role in Immune Tolerance

In *Mus musculus*, we detected NP-NIRV at the mRNA level predominantly in the spleen, kidney, and thymus. While traces of expression were found in other organs, the primary activity of NP-NIRV seems confined to tissues associated with immune functions, implying a specialized role in these organs. The thymic expression of NP-NIRV is particularly noteworthy, given the organ's vital role in central tolerance. Our findings revealed NP-NIRV expression specifically in mTECs, while absent in cTECs. This selective expression implies NP-NIRV's potential involvement in the negative selection process, crucial for eliminating autoreactive T cell progenitors.

Furthermore, NP-NIRV exhibits characteristics consistent with TRAs, which are typically expressed in specific organs, such as insulin in the pancreas. In the thymus, the expression of TRAs serves to educate progenitor T cells to not attack self-peptides and is regulated by transcription factors, such as AIRE, which is predominantly expressed in mTECs but not in cTECs.[65,270] The putative AIRE binding site within the NP-NIRV sequence and the absence of NP-NIRV expression in thymic tissue from AIRE KO mice, strongly suggesting that AIRE is needed for NP-NIRV expression in the thymus.[261]

The expression of AIRE has also been reported in extrathymic cells, such as DCs in lymph nodes, suggesting that these cells may express AIRE-regulated genes and contribute to maintaining immune tolerance beyond the thymus.[271,272] This could potentially explain the detection of NP-NIRV expression in organs rich in immune cells. Alternatively, NP-NIRV may serve a unique role in the spleen and kidney, meriting further investigation.

Overall, our *in-vitro* results revealed NP-NIRVs dependence on AIRE for expression and its selective presence in mTECs while being absent in cTECs, providing strong support for the hypothesis that NP-NIRV plays a role in immune tolerance through its presentation during the negative selection of the central tolerance mechanism.

6.3   A Conserved NIRV-Derived Peptide Sequence of EBOV NP in Mice Might Be Recognized as Self

The NP-NIRV and EBOV NP share a highly conserved region, and if NP-NIRV-derived peptides foster immune tolerance, they could induce a reduced T cell response, indicating their recognition as self in mice. Our ELISpot assays confirmed this, showing lower T cell activity and decreased IFN-γ production in response to conserved NP-NIRV and EBOV NP peptides, in contrast to the robust Th1 response elicited by GFP peptides. These findings suggest that murine immune systems may recognize filovirus-like peptides as self, prompting a tolerogenic response and supporting NP-NIRV's role in promoting immune tolerance.

The ELISpot assay, while effective at quantifying the number of cytokine-producing cells, does not offer detailed insight into the magnitude of cytokine production per cell. This limitation could be significant when the level of cytokine production influences the nature of the immune response. Additionally, the results of the assay are heavily dependent on the peptide sequences used for stimulation. If these peptides do not adequately mimic naturally processed antigens or are not optimally presented by MHC molecules on APCs, the assay may fail to accurately reflect the true immune response.

The peptides used in this study were 15 amino acids long, a typical length for MHC-II peptides.[273,274] *In-silico* analysis suggested a low binding affinity for MHC-II molecules, indicating that APC interactions likely engaged CD4 T cells. To gain a more comprehensive understanding of the T cell response, it may be valuable to investigate the polyclonal response using overlapping peptides from the entire EBOV NP. Alternatively, an *in-silico* analysis of EBOV NP could help pre-select relevant regions, filtering out less interesting areas before conducting the ELISpot assay.

Another limitation of the ELISpot assay is that, while it identifies antigen-specific T cells based on cytokine production, it does not provide insight into the specific TCR affinities or specificities involved in antigen recognition. To address this limitation, TCR sequencing of reactive T cells could be performed, allowing for a deeper understanding of the specificity and diversity of the T cell response.

Combining this approach with flow cytometry and functional assays, including those targeting Tregs, could provide a more comprehensive analysis of the immune response. Both bats and mice exhibit filovirus-specific antibody and T cell responses. If NIRVs facilitate immune tolerance by promoting the recognition of viral-like peptides as self-antigens, investigating the corresponding antibody and T cell responses could elucidate whether viral peptides resembling NIRVs evoke a tolerogenic response, thus diminishing or altering antibody and T cell activation.

Despite our attempts to develop an NP-NIRV-specific tetramer or pentamer for T cell analysis via flow cytometry, commercial production proved unfeasible due to technical limitations in generating stable complexes. Advancements in this technology could potentially allow for precise identification and characterization of NP-NIRV-specific T cells, enhancing our understanding of immune tolerance mechanisms and the role of NP-NIRV in modulating T cell responses.

6.4 NP-NIRV KO Mice Exhibit Similar Behavior to WT Mice

To investigate the role of NP-NIRV in EBOV pathogenesis, we utilized a mouse model which does not express NP-NIRV (NIKI mice). While no significant differences between NIKI and WT mice were observed, the similar viremia levels between NIKI and IFNAR^{-/-} mice on day 8 led us to hypothesize that relevant immune events might occur during the early phase of the infection. Neutrophil and T cell infiltration in infected tissues present in IFNAR^{-/-} mice suggests an excessive immune response that may explain exacerbated disease severity and impaired viral control. In many viral infections, elevated lung neutrophil counts often correlate with increased disease severity, and a high neutrophil-to-lymphocyte ratio is typically associated with poorer outcomes, signaling an imbalanced immune response.[275,276] However, this was not observed in NIKI and WT mice.

It is important to note that our interpretations rely on analyzing the relative frequencies of cell populations, rather than their absolute numbers. This approach allows us to assess the proportional representation of specific immune cell types within the overall population, providing insight into shifts in immune cell balance. However, it may overlook absolute changes in cell counts that could impact the immune response.

Serum cytokine and chemokine profiles further confirmed the similarity between WT and NIKI mice. Due to the intranasal infection route and the typical incubation period for EBOV, both groups exhibited low analyte levels on day 3, indicating minimal viral dissemination and a likely localized infection within the lungs. This aligns with the usual onset of symptoms in IFNAR^{-/-} mice.[177,264] By days 6 and 9, WT and NIKI mice maintained low cytokine levels, contrasting with the elevated inflammatory response observed in IFNAR^{-/-} mice.

Notably, IFNAR^{-/-} mice exhibited elevated levels of IFN-α and IFN-β. While these cytokines are generally regulated by a feedback loop involving the IFN receptor, they can also be produced via alternative or compensatory pathways.[277–280] This receptor-independent secretion may lead to unchecked IFN production, heightening inflammation without the typical antiviral response mediated by IFN signaling.[281–284] In the context of EBOV infection in IFNAR^{-/-} mice, this may contribute to further immune dysregulation and increased disease severity.

The detection of cytokines and chemokines in this experiment was restricted to serum retrieved via heart puncture. Examining these analytes in local environments, such as the lung, could provide additional insights and reveal different patterns.

Our histopathological findings in the lungs and kidneys are consistent with our data. The increase in inflammation observed in the lungs of all subjects over the course of infection can be attributed to the intranasal infection route.

Although the scoring was conducted using blinded histopathological analysis, sample preparation could have introduced bias, as only small tissue samples rather than the entire lung were analyzed. This limitation may explain the outlier in NIKI 643 mice on day 9, where the tissue sample size was considerably smaller than that of other samples in this study.

Overall, the behavior of NIKI mice largely mirrors that of WT mice, with only minor differences that could be attributed to slight variations in the dynamics of infection among individual mice or random heterogeneity in sample collection, such as tissue sections. Our findings indicate that the loss of the NP-NIRV in mice does not result in increased morbidity. This suggests that NP-NIRV does not play a significant role in protecting against EBOV infection under the conditions tested.

6.5 *In-silico* Analysis of Immune Peptidomes Reveals a Diverse Range of *Mononegavirales*-like Peptides

In-silico analysis revealed no additional EBOV NP NIRVs in the genome of *Mus musculus*. However, based on observations in NIKI mice, we hypothesize that mice may harbor other NIRVs derived from viruses of the *Mononegavirales* order that could be presented as self-peptides in the thymus, thereby contributing to immune tolerance. Supporting this hypothesis, *in-silico* analysis of the murine immune peptidome identified many peptides with sequence similarities to *Mononegavirales* peptides.

We identified hits within the *Paramyxoviridae*, *Rhabdoviridae*, *Nyamiviridae*, *Pneumoviridae*, and *Lispiviridae* families, as well as additional filovirus-like peptides in the murine dataset. The conservation of viral proteins across *Mononegavirales* suggests potential cross-reactivity of TCRs during infections, which may extend to NP-NIRV. The N-terminal region of EBOV NP, highly conserved among *Mononegavirales*,[4,251,252] aligns with the murine NP-NIRV. In contrast, the human immune peptidome yielded far fewer hits, though a peptide with similarities to Bornavirus was identified. Humans are known to harbor Bornavirus NIRVs,[4,41] with potential cellular functions.[47,48] This suggests that Bornavirus NIRVs might also contribute to immune tolerance, a possibility that warrants further investigation. The observed variation in *Mononegavirales*-like peptide representation between murine and human peptidomes may stem from several factors, including differences in evolutionary exposure to viral pathogens, variations in immune system adaptations and species-specific selective pressures of NIRVs.

It is important to note that the BLASTp search was limited to *Mononegavirales* sequences, focusing on the potential cross-reactivity of peptides from this order with EBOV. This decision was based on paleovirological studies indicating that viruses from the order *Mononegavirales* are commonly integrated into mammalian genomes.[4,7] While only hits with an E-value below one were considered, false positives, such as plant virus hits within the *Rhabdoviridae* family,

likely arose due to the small size of peptide sequences, which increases the chance of matching unrelated sequences. The cut-off (E<=1) was informed by previous analyses of conserved peptides between EBOV NP and NP-NIRV, ensuring a stringent yet inclusive approach. Notably, murine EBOV NP-NIRV-derived peptides were not part of the available immune peptidome database, suggesting its incompleteness. The dataset authors highlighted challenges in isolating MHC-II peptides due to their low abundance, contamination with non-specific peptides, and variability in peptide lengths and binding motifs.[257]

The inherent limitations of mass spectrometry, particularly in distinguishing true MHC-II peptides and accounting for tissue-specific variation, add complexity to the analysis. Despite these challenges, the high number of hits suggests that many NIRV-derived peptides may be presented as self-antigens, reinforcing their potential role in immune tolerance.

Future studies should focus on optimizing MHC-II peptide isolation to improve immune peptidome databases and refine predictions of MHC-II-peptide binding. Further investigation is also needed to identify NIRVs that may contribute to the expression of these peptides. Following this, ELISpot assays could be employed to verify whether these peptides are recognized as self-antigens, by stimulating T cells with identified NIRV-derived peptides and measuring cytokine production to confirm tolerogenic responses.

6.6   Depletion of Tregs Increases Morbidity in Mice During EBOV Infections

Our findings in NIKI mice suggest that the contribution of a single NIRV during EBOV infection is minimal. However, *in-silico* analysis indicates that multiple NIRVs may contribute to immune tolerance in mice. If *Mononegavirales*-like peptides are presented as self-antigens in the thymus, a broader NIRV-specific Treg population could become active during EBOV infection, suggesting that *Mus musculus* may harbor a diverse population of Tregs specific to NP-NIRV and other NIRVs derived from viruses of the order *Mononegavirales*.

When Tregs were depleted in DEREG mice, morbidity increased during EBOV infection, evidenced by marked weight loss. Notably, this effect was not observed in Treg-depleted mice infected with LASV. Our results highlight the critical role of Tregs in regulating immune responses during EBOV infection, compared to their limited role in LASV infection.

Elevated levels of viremia in EBOV-infected DEREG mice, persisting long after the final DT treatment, indicate that Treg depletion disrupts virus clearance, with the highest viral loads observed at the end of the experiment. These findings underscore the essential role of Tregs in modulating early immune responses, preventing excessive inflammation, and facilitating effective adaptive immunity required for viral clearance.[100]

The role of Tregs during viral infection appears to be virus- and context-dependent. For instance, in lymphotropic retrovirus infections such as human immunodeficiency viruses (HIV), Treg depletion enhances antiviral responses and reduces viral load,[285–287] while in respiratory syncytial virus (RSV) and mucosal herpes simplex virus (HSV) infections, Treg depletion exacerbates disease, delaying viral clearance and increasing pathology.[100,288,289] The lung, as the primary replication site for RSV, and the intranasal infection route used in our experiments may explain the observed similarities in DEREG mice across viral infections. These findings align with our results, emphasizing the importance of Tregs in maintaining immune homeostasis and mitigating disease severity during viral infections.

It is important to recognize that depleting all Foxp3-expressing cells significantly impacts murine physiology. Tregs are critical for immune homeostasis and the prevention of autoimmunity, with their depletion leading to fatal T-cell-mediated autoimmune disorders.[290] However, in our study, DT-treated uninfected mice showed no increased morbidity, suggesting that Treg depletion alone does not affect baseline health within the experimental timeframe. Nonetheless, the absence of Tregs activates DCs prior to T cell proliferation, which results from the disruption of DC-Treg interactions. Without Treg-mediated regulation, DCs become more immunogenic, activating self-reactive T cells and breaking self-tolerance. The autoimmune response that follows is primarily directed against self-antigens rather than foreign ones, even in antigen-free conditions.[291] These findings underscore the crucial role of Tregs in preventing autoimmunity to self-peptides. Our findings suggest that *Mononegavirales*-like peptides, if presented as self-antigens, contribute to increased morbidity observed in Treg-depleted mice during EBOV infection.

To our knowledge, this is the first time an EBOV infection in mice was investigated in Treg-depleted mice, revealing that Tregs play a crucial role in modulating immune responses during this infection. However, our study primarily focused on survival and morbidity. Future work should include histological analysis and cytokine profiling to explore inflammation and extend the experimental duration to assess viral clearance or the potential for persistent infections in Treg-depleted mice. Sequencing the TCRs of Tregs during EBOV infection could identify NIRV-specific TCRs, confirming their role in immune regulation. Further studies should also elucidate the mechanisms by which Tregs modulate immune responses during EBOV infection and their influence on disease outcomes.

6.7 Unraveling Filovirus Pathogenicity: Why Humans Suffer While Bats and Rodents Tolerate

The striking differences in filovirus pathogenicity between humans and species such as bats and rodents raise questions about the underlying immune mechanisms. Both bats and rodents are susceptible to filovirus infection without displaying symptoms, whereas humans often suffer severe, fatal outcomes.

6.7.1 The Role of NIRVs in Immune Tolerance

The presence of filovirus NIRVs in bats and rodents has been observed alongside their resistance to filovirus disease.[4,18] In this study, we examined the potential role of the murine NP-NIRV in contributing to this resistance. Our findings suggest that NP-NIRV plays a part in central tolerance mechanisms. Specifically, NP-NIRV expression in mTECs and its AIRE dependency indicate that NP-NIRV-derived peptides are presented as self-antigens during negative selection in T cell development. This self-recognition of NP-NIRV-derived peptides, supported by the low T cell activity induced by NP-NIRV observed in our ELISpot assays, suggests two main consequences during filovirus infections. First, the presentation of NP-NIRV during the negative selection as self probably reduces the pool of potential CD4 Th1 cells, reducing the TCR repertoire against filovirus antigens, and increases the pool of NP-NIRV-specific Tregs. Second, it may lead to the activation of NP-NIRV-specific Tregs during filovirus infections dampening inflammatory immune responses. Thus, we posit that NP-NIRV-derived peptides presentation as self during T cell development likely modulates the immune system, fostering a more tolerogenic response to EBOV and potentially to other filoviruses.

Our *in-silico* analysis revealed a range of virus-like peptides within the murine immune peptidome, suggesting that these peptides, alongside NP-NIRV, might play a role in shaping immune tolerance to EBOV and possibly other viruses of the order *Mononegavirales*.

The idea that other *Mononegavirales*-like peptides could similarly contribute to immune modulation during EBOV infections is further supported by the minor immunological differences observed between NIKI and WT mice in this study, demonstrating that the loss of the NP-NIRV alone is not enough to significantly change EBOV pathogenicity in mice. This finding implies that immune tolerance to filoviruses in mice may be reinforced by a collective effect of virus-like peptides rather than by NP-NIRV alone, possibly leading to a diverse Treg population recognizing *Mononegavirales*-like antigens. This hypothesis aligns with our findings where we observed an increased morbidity in Treg-depleted mice during EBOV infection.

Within the immune system's multi-layered defense network, NIRVs may influence specific components, such as the T cell response, and illustrate how tolerogenic mechanisms might

contribute to a nuanced antiviral response in mice. However, as we will discuss in the following section, other immune components, such as type I IFNs, also play a substantial role in determining disease outcomes.

6.7.2 The Importance of the Type I IFN Response

Studies using IFNAR$^{-/-}$ mice underscore the crucial role of IFN-I responses in EBOV infections.[177,246,264] Research on mouse-adapted EBOV (maEBOV) further highlights that IFN-I evasion is key to EBOV pathogenesis, with virulence correlating to the virus's ability to evade the antiviral response initiated by type I IFNs.[292] While VP24 and NP were identified as primary contributors to WT EBOV adaptation in mice, mutations in other viral proteins and non-coding regions also support the virus's virulence, suggesting a multifactorial basis (e.g., VP35 and GP).[293] Notably, the murine NP-NIRV does not align with maEBOV-specific mutations.

While our findings show that Treg depletion increase morbidity during EBOV infections, it did not result in viremia comparable to that observed in IFNAR$^{-/-}$ mice, indicating that overcoming the IFN-induced antiviral response is a crucial step in EBOV pathogenesis. However, our results suggest that effective adaptive T cell responses are essential for viral clearance. This aligns with studies in severe combined immunodeficiency (SCID) mice, which remain healthy for several weeks post-infection but rapidly succumb to the disease once treated with antibodies targeting IFN α/β.[264]

The robust IFN response in mice may compensate for NP-NIRV loss, as EBOV struggles to replicate in cells with established IFN-α antiviral states in murine models.[264] Similarly, bats exhibit higher constitutive IFN levels, which likely contributes to control viral replication without experiencing disease, along with lower inflammation levels that result in a less exacerbated host immune response.[52,294,295]

6.7.3 Keeping the Balance

Our findings in Treg-depleted mice highlight the complexity of immune responses during EBOV infections. The increased morbidity in the absence of Tregs accentuates their essential role in maintaining a balanced immune response, which may prevent excessive inflammation and immunopathology.

Bats exhibit a muted inflammatory response to filovirus infection, with macrophages and active T cells playing roles in promoting an anti-inflammatory state.[296,297] However, excessive tolerance can lead to pathology even in reservoir hosts. A recent study showed that MARV-infected ERBs mount a controlled pro-inflammatory response at liver infection sites, with mononuclear phagocytes and likely MARV-specific T cells acting to limit viral replication and

pathogenesis. Reduced pro-inflammatory responses can lead to increased viral replication, shedding and severe liver pathology similar to MARV disease in primates, indicating that disease tolerance alone is insufficient for controlling MARV in ERBs.[296] These findings suggest that ERBs rely on a balanced immune strategy that combines localized pro-inflammatory responses with disease tolerance to prevent severe pathology and effectively control MARV infection.

The role of NIRVs in this context remains underexplored. Certain bats in the *Myotis* genus express filovirus VP35 NIRVs that moderately inhibit IFN responses during viral infections, possibly co-opted to regulate innate immune signaling and support a controlled immune response.[244] Our findings suggest that NIRVs may enhance immune tolerance by fine-tuning the immune response to filoviral infection to achieve an optimal balance for effective viral clearance while minimizing immunopathological effects for the host. These findings underscore the possible immunomodulatory functions of NIRVs in mammals.

6.7.4 Molecular Mimicry –A win-win strategy for Virus and Host?

The murine NP-NIRV and other NIRVs may also facilitate immune evasion through molecular mimicry, where pathogens imitate host proteins to evade immune detection.[298] Immune systems typically avoid attacking self-proteins, so pathogens that mimic these structures can reduce the pool of viral epitopes available for targeting.[299,300] While most research on molecular mimicry has focused on full proteins,[301] recent studies indicate that short linear amino acid sequences can also induce cross-reactive antibodies and T cells, influencing immune modulation.[302–304] A study of the human virome identified widespread linear mimicry, particularly in the *Herpesviridae* and *Poxviridae* families, with enrichment in proteins involved in cellular replication, inflammation, and thymic expression.[305] While this mechanism of immune evasion can lead to viral persistence it may also benefit the host by preventing excessive inflammation, enabling controlled immune responses and eventual viral clearance. However, it may render the host infectious, either persistently or at least for an extended period, facilitating viral transmission to other susceptible hosts.

6.8   NIRVs in Evolution

Viruses play a pivotal role in shaping ecosystems,[306] with substantial evidence highlighting the evolutionary influence of retroviruses.[29,30] Emerging data further suggest that many RNA virus families share a long co-evolutionary history with mammals, including the co-option of viral genes into host genomes.[7,41,49] The integration of NIRVs into host genomes represents a rare macromutation, warranting further investigation to elucidate the precise mechanisms underlying this process.[307]

The conservation of these integrations in host genomes suggests a significant evolutionary role in host biology.[7] Although most of these elements are pseudogenes, some produce detectable expression products.[46,49] Certain viral genes appear to have been co-opted for cellular functions, such as a BDV NIRV in humans that interacts with mitochondrial proteins to influence cell viability.[48] Others seem to have adapted for pathogen defense, likely driven by evolutionary pressures from host-virus interactions.[4,49] These integrations may exert antiviral functions by interfering with viral replication or modulating host immune responses. A protein produced by a BDV NIRV in the thirteen-lined ground squirrel effectively inhibits BVD infection and replication, representing a direct mechanism of pathogen defense.[45] Conversely, some NIRVs display more complex functions. For instance, a noncoding RNA product of a BDV-like element in humans reduces the expression of a neighboring gene, thereby enhancing the nuclear factor kappa B (NF-κB) pathway to strengthen pathogen defense.[46]

Besides BVD NIRVs, many filovirus-like NIRVs have been identified in mammals.[4,18] While replication interfering filovirus NIRVs have not been discovered so far, filovirus VP35 NIRVs in mouse-eared bats (*Myotis*) that moderately inhibit IFN responses have been studied in greater depth.[244] A strong suppressor of IFN responses is likely to be selected against, as it could lead to heightened vulnerability to viral infections. Instead, a scenario can be envisioned where moderate inhibitory activity fine-tunes IFN and inflammatory responses, mitigating potential harm to the virus-infected host.[308] Notably, negative regulators of IFN and inflammatory pathways have been identified,[309,310] and it is conceivable that a viral protein could be co-opted to fulfill such a role.[241]

A "fine-tuning"-role might also apply for the murine NP-NIRV. The intact ORF of NP-NIRV in *Mus musculus* suggests its functional relevance through transcription. While functions such as transcriptional regulation and RNA interference have been observed with BDV NIRVs and NIRVs in mosquitos,[31,33,37,46] the expression of the murine NP-NIRV in mTECs, its AIRE dependency, and potential self-recognition all suggest its involvement in immune tolerance mechanisms through the presentation of NP-NIRV-derived peptides to developing T cells during their maturation.

NP-NIRV's amino acid similarity to EBOV-NP indicates that conserved residues may be crucial to NP-NIRV's function. It is reasonable to hypothesize that NP NIRVs primarily function to disrupt viral replication,[4,45] given NP's critical role in the viral life cycle.[143,251,263] In the case of the murine NP-NIRV, it may interfere with the replication of extant viruses, including as-yet-unidentified ones, or potentially with the replication of extinct ancestral filoviruses. Alternatively, the murine NP-NIRV may have lost its ability to disrupt viral replication over the course of evolution while retaining its role in immune tolerance as a self-protein. The conservation of specific amino acids supports the hypothesis that NP-NIRV may contribute to immune tolerance by promoting self-recognition of conserved viral antigens, potentially extending beyond EBOV and other filoviruses.

The question why so many NIRVs seem to originate specifically from the NP of viruses within the *Mononegavirales* order warrants further investigation.[4,7] Aside from the polymerase L, NP is showing particularly high conservation across the order,[4,18,252] which may explain the relatively high prevalence of NP-NIRVs in mammalian genomes. Additionally, the synthesis of mRNAs in *Mononegavirales* is believed to follow a transcription gradient, with NP, positioned as the first gene in the viral genome, being abundantly expressed during infection. This could further increase the likelihood of its integration into host genomes.[311,312]

Furthermore, NP is the most immunodominant protein in T cell responses,[313,314] which may explain the evolutionary pressure to retain NP-NIRVs in host genomes. Intriguingly, Hurwitz *et al.* proposed that, akin to the role of CRISPR in bacteria, mammalian cells might co-opt viral sequences to support immune memory. By expressing viral peptides from these sequences, such a mechanism could enhance B and T cell responses even after viral clearance.[315] A EVE-derived CRISPR-like immunity in eukaryotes has also been proposed by other researchers.[316]

The immunodominance of NP-specific T cell responses supports the hypothesis that the murine NP-NIRV may influence T cell responses through NIRV-specific Tregs, potentially contributing to immune tolerance. Supporting this, other studies have proposed that EVEs may influence T and B cell repertoires by expressing EVE-encoded antigens, potentially inducing central or peripheral immunological tolerance.[51,53] However, substantial immune modulation may require an immune peptidome with a broader array of virus-like peptides, potentially generating a more diverse population of NIRV-specific Tregs.

Given NP's importance in T cell-mediated immunity, incorporating NP into vaccine formulations could enhance cell-mediated responses alongside GP-driven humoral immunity, potentially mimicking natural immune protection more effectively and promoting durable immunity.[317–319] Moreover, NP's conservation across orthoebolaviruses and beyond highlights

its potential for universal vaccine development. Identifying immunodominant conserved peptides within NP could pave the way for a universal *Orthoebolavirus* vaccine, with valuable insights potentially arising from NIRV-derived immune peptidomes in mammals resistant to filovirus disease.

The potential role of NIRVs in immune tolerance might be an elegant strategy of antiviral defense that prioritizes resource efficiency over the continuous production of interfering proteins -a likely product of evolutionary pressures. This subtle mechanism protects the host from severe disease and death but does not prevent infection, thus enabling viral transmission within the population. Such transmission could increase stress within populations but might also facilitate interspecies spread, potentially benefiting NIRV-harboring species.

Notably, NIRV integrations in mammalian genomes have predominantly originated from viruses within the order *Mononegavirales*, possibly reflecting an evolutionary relationship shaped by historical host-virus interactions and the functional impact of these integrations.[4] It may also indicate an increased tendency of these viruses to infect germline cells. In particular, viruses capable of establishing persistent infections (EBOV, immune privileged sites)[165,320] or replicating within the nucleus (BDV)[42] are prominently represented among identified NIRVs.[7]

Given the high mortality rates associated with certain members of this order, such as Bornaviruses and Filoviruses, strong selective pressures likely drive the evolution of resistance mechanisms against them. Although immune responses vary across host taxa, bats and mice display minimal disease symptoms following WT filoviral infections,[246,248] suggesting the presence of evolved immune adaptations tailored to counteract filoviruses. NIRVs may represent one such adaptation, contributing to resistance against specific viruses and/or associated diseases.[49,50]

The presence of EBOV NIRVs suggests a long-standing co-evolutionary relationship between the virus and their hosts, carrying potential implications for the ongoing search for the natural EBOV reservoir host.[4,7,18,52,241] Similar to NIRVs in mosquitoes that may influence vector competence,[38] mammalian NIRVs might enhance a species' capacity to function as a viral reservoir. Since natural filovirus infections are rarely observed, the presence of EBOV NIRVs in certain genomes could highlight species worth monitoring as potential reservoirs. However, much of the research on NIRVs relies on *in-silico* analyses of annotated genomes. Broadening these investigations to include filovirus-like NIRVs in non-annotated mammalian genomes could help identify filovirus reservoirs and improve outbreak prediction models. Considering the extensive distribution of filovirus-like NIRVs across species, we advocate for expanded sampling efforts to better understand filovirus ecology. Additionally, with the rise of artificial intelligence (AI) and advancements in bioinformatics and structural biology, we can anticipate

a transformative acceleration in uncovering biological insights. These technologies hold the potential to elucidate complex interconnections, enabling a deeper understanding of the evolutionary significance and impact of NIRVs on host-virus interactions.

6.9   Concluding Remarks

This thesis highlights the significance of paleoviral sequences in understanding virus-host co-evolution and immunity. Although NIRVs are less common than retroviral integrations, they provide valuable insights into the ancient interactions between RNA viruses and their hosts, illustrating the dynamic and complex role of viral evolution in host adaptation.[4,7,49] Our findings advance the field by exploring the potential role of NIRVs in immune tolerance, wherein virus-like antigens may be tolerated by the host without triggering full-scale immune activation. This may contribute to a sophisticated balance between immune tolerance and antiviral defense mechanisms.

The discovery of NIRVs illustrates the impact of virus-to-host gene flow on mammalian genome evolution, showcasing viruses' role in genetic innovation.[7,18,49] The potential involvement of NIRVs in immune tolerance and other antiviral defense strategies underscore the necessity of understanding how viral remnants within genomes may influence resistance or susceptibility to pathogenic infections. These interactions are particularly relevant for zoonotic RNA viruses, which account for the majority of emerging infectious diseases and pose significant risks to global public health.[220]

The reasons for the disparate pathogenicity of filoviruses, such as EBOV, among humans, bats, and rodents are multifactorial, illustrating the significant impact of the host immune response on disease outcomes. Our findings warrant further research into NIRV-driven immune mechanisms, which could inform innovative strategies for outbreak prevention and therapeutic interventions. Extending these insights across species and other viruses, particularly within the order *Mononegavirales*, could enhance the applications of NIRV research, potentially improving public health responses to zoonotic and emerging viral threats.

7 References

1. Feschotte, C. & Gilbert, C. Endogenous viruses: insights into viral evolution and impact on host biology. *Nat. Rev. Genet.* **13**, 283–296 (2012).

2. Aswad, A. & Katzourakis, A. Paleovirology: The Study of Endogenous Viral Elements. in *Virus Evolution: Current Research and Future Directions* 273–292 (Caister Academic Press, 2016). doi:10.21775/9781910190234.10.

3. Warke, S., Tembhurne, P., Bobade, S. & Ingle, V. C. Paleovirology: Blessing or Curse of Ancient Viruses - A Review. *Agric. Rev.* **40**, (2019).

4. Belyi, V. A., Levine, A. J. & Skalka, A. M. Unexpected Inheritance: Multiple Integrations of Ancient Bornavirus and Ebolavirus/Marburgvirus Sequences in Vertebrate Genomes. *PLoS Pathog.* **6**, e1001030 (2010).

5. Lander, E. S. *et al.* Initial sequencing and analysis of the human genome. *Nature* **409**, 860–921 (2001).

6. International Human Genome Sequencing Consortium. Finishing the euchromatic sequence of the human genome. *Nature* **431**, 931–945 (2004).

7. Katzourakis, A. & Gifford, R. J. Endogenous Viral Elements in Animal Genomes. *PLoS Genet.* **6**, e1001191 (2010).

8. Imakawa, K. *et al.* Endogenous Retroviruses and Placental Evolution, Development, and Diversity. *Cells* **11**, 2458 (2022).

9. Oliver, K. R. & Greene, W. K. Transposable elements and viruses as factors in adaptation and evolution: an expansion and strengthening of the TE-Thrust hypothesis. *Ecol. Evol.* **2**, 2912 (2012).

10. Mi, S. *et al.* Syncytin is a captive retroviral envelope protein involved in human placental morphogenesis. *Nature* **403**, 785–789 (2000).

11.   Dupressoir, A., Lavialle, C. & Heidmann, T. From ancestral infectious retroviruses to bona fide cellular genes: Role of the captured *syncytins* in placentation. *Placenta* **33**, 663–671 (2012).

12.   Chuong, E. B. The placenta goes viral: Retroviruses control gene expression in pregnancy. *PLoS Biol.* **16**, e3000028 (2018).

13.   Imakawa, K., Nakagawa, S. & Miyazawa, T. Baton pass hypothesis: successive incorporation of unconserved endogenous retroviral genes for placentation during mammalian evolution. *Genes Cells* **20**, 771–788 (2015).

14.   Cornelis, G. *et al.* An endogenous retroviral envelope syncytin and its cognate receptor identified in the viviparous placental Mabuya lizard. *Proc. Natl. Acad. Sci.* **114**, E10991–E11000 (2017).

15.   Chameettachal, A., Mustafa, F. & Rizvi, T. A. Understanding Retroviral Life Cycle and its Genomic RNA Packaging. *J. Mol. Biol.* **435**, 167924 (2023).

16.   Tarlinton, R. & Greenwood, A. D. Koala retrovirus and neoplasia: correlation and underlying mechanisms. *Curr. Opin. Virol.* **67**, 101427 (2024).

17.   Stoye, J. P. Endogenous retroviruses: Still active after all these years? *Curr. Biol.* **11**, R914–R916 (2001).

18.   Taylor, D. J., Leach, R. W. & Bruenn, J. Filoviruses are ancient and integrated into mammalian genomes.

19.   Moniruzzaman, M. & Aylward, F. O. Endogenous DNA viruses take center stage in eukaryotic genome evolution. *Proc. Natl. Acad. Sci. U. S. A.* **120**, e2305212120.

20.   Ayarpadikannan, S. & Kim, H.-S. The Impact of Transposable Elements in Genome Evolution and Genetic Instability and Their Implications in Various Diseases. *Genomics Inform.* **12**, 98–104 (2014).

21.   Sotero-Caio, C. G., Platt, R. N., Suh, A. & Ray, D. A. Evolution and Diversity of Transposable Elements in Vertebrate Genomes. *Genome Biol. Evol.* **9**, 161–177 (2017).

22.   Feschotte, C. Transposable elements and the evolution of regulatory networks. *Nat. Rev. Genet.* **9**, 397–405 (2008).

23.   Blair, C. D., Olson, K. E. & Bonizzoni, M. The Widespread Occurrence and Potential Biological Roles of Endogenous Viral Elements in Insect Genomes. *Curr. Issues Mol. Biol.* **34**, 13–30 (2019).

24.   Shafritz, D. A., Shouval, D., Sherman, H. I., Hadziyannis, S. J. & Kew, M. C. Integration of hepatitis B virus DNA into the genome of liver cells in chronic liver disease and hepatocellular carcinoma. Studies in percutaneous liver biopsies and post-mortem tissue specimens. *N. Engl. J. Med.* **305**, 1067–1073 (1981).

25.   Arbuckle, J. H. *et al.* The latent human herpesvirus-6A genome specifically integrates in telomeres of human chromosomes in vivo and in vitro. *Proc. Natl. Acad. Sci. U. S. A.* **107**, 5563–5568 (2010).

26.   Zhdanov, V. M. Integration of viral genomes. *Nature* **256**, 471–473 (1975).

27.   Geuking, M. B. *et al.* Recombination of retrotransposon and exogenous RNA virus results in nonretroviral cDNA integration. *Science* **323**, 393–396 (2009).

28.   Desfarges, S. & Ciuffi, A. Viral Integration and Consequences on Host Gene Expression. *Viruses Essent. Agents Life* 147–175 (2012) doi:10.1007/978-94-007-4899-6_7.

29.   Emerman, M. & Malik, H. S. Paleovirology—Modern Consequences of Ancient Viruses. *PLoS Biol.* **8**, e1000301 (2010).

30.   Frank, J. A. & Feschotte, C. Co-option of endogenous viral sequences for host cell function. *Curr. Opin. Virol.* **25**, 81–89 (2017).

31.   Palatini, U. *et al.* Comparative genomics shows that viral integrations are abundant and express piRNAs in the arboviral vectors Aedes aegypti and Aedes albopictus. *BMC Genomics* **18**, 512 (2017).

32.   Fort, P. *et al.* Fossil Rhabdoviral Sequences Integrated into Arthropod Genomes: Ontogeny, Evolution, and Potential Functionality. *Mol. Biol. Evol.* **29**, 381–390 (2012).

33.   Suzuki, Y. *et al.* Non-retroviral Endogenous Viral Element Limits Cognate Virus Replication in Aedes aegypti Ovaries. *Curr. Biol. CB* **30**, 3495-3506.e6 (2020).

34.   Gammon, D. B. & Mello, C. C. RNA interference-mediated antiviral defense in insects. *Curr. Opin. Insect Sci.* **8**, 111 (2015).

35.   Kolliopoulou, A. *et al.* PIWI pathway against viruses in insects. *WIREs RNA* **10**, e1555 (2019).

36.   Duc, C. *et al.* Trapping a somatic endogenous retrovirus into a germline piRNA cluster immunizes the germline against further invasion. *Genome Biol.* **20**, 127 (2019).

37.   Aguiar, E. R. G. R. *et al.* A single unidirectional piRNA cluster similar to the flamenco locus is the major source of EVE-derived transcription and small RNAs in Aedes aegypti mosquitoes. *RNA* **26**, 581–594 (2020).

38.   Houé, V., Bonizzoni, M. & Failloux, A.-B. Endogenous non-retroviral elements in genomes of Aedes mosquitoes and vector competence. *Emerg. Microbes Infect.* **8**, 542–555 (2019).

39.   Marconcini, M. *et al.* Profile of Small RNAs, vDNA Forms and Viral Integrations in Late Chikungunya Virus Infection of Aedes albopictus Mosquitoes. *Viruses* **13**, 553 (2021).

40.   Huhtamo, E. *et al.* Novel insect-specific flavivirus isolated from northern Europe. *Virology* **433**, 471–478 (2012).

41.   Horie, M. *et al.* Endogenous non-retroviral RNA virus elements in mammalian genomes. *Nature* **463**, 84–87 (2010).

42.   Horie, M., Kobayashi, Y., Suzuki, Y. & Tomonaga, K. Comprehensive analysis of endogenous bornavirus-like elements in eukaryote genomes. *Philos. Trans. R. Soc. B Biol. Sci.* **368**, 20120499 (2013).

43.   Kawasaki, J., Kojima, S., Mukai, Y., Tomonaga, K. & Horie, M. 100-My history of bornavirus infections hidden in vertebrate genomes. *Proc. Natl. Acad. Sci.* **118**, e2026235118 (2021).

44. Tomonaga, K., Kobayashi, T. & Ikuta, K. Molecular and cellular biology of Borna disease virus infection. *Microbes Infect.* **4**, 491–500 (2002).

45. Fujino, K., Horie, M., Honda, T., Merriman, D. K. & Tomonaga, K. Inhibition of Borna disease virus replication by an endogenous bornavirus-like element in the ground squirrel genome. *Proc. Natl. Acad. Sci.* **111**, 13175–13180 (2014).

46. Sofuku, K., Parrish, N. F., Honda, T. & Tomonaga, K. Transcription Profiling Demonstrates Epigenetic Control of Non-retroviral RNA Virus-Derived Elements in the Human Genome. *Cell Rep.* **12**, 1548–1554 (2015).

47. Myers, K. N. *et al.* The bornavirus-derived human protein EBLN1 promotes efficient cell cycle transit, microtubule organisation and genome stability. *Sci. Rep.* **6**, 35548 (2016).

48. Fujino, K. *et al.* A Human Endogenous Bornavirus-Like Nucleoprotein Encodes a Mitochondrial Protein Associated with Cell Viability. *J. Virol.* **95**, 10.1128/jvi.02030-20 (2021).

49. Taylor, D. J. & Barnhart, M. H. Genomic transfers help to decipher the ancient evolution of filoviruses and interactions with vertebrate hosts. *PLOS Pathog.* **20**, e1011864 (2024).

50. Aswad, A. & Katzourakis, A. Paleovirology and virally derived immunity. *Trends Ecol. Evol.* **27**, 627–636 (2012).

51. Young, G. R. *et al.* Negative Selection by an Endogenous Retrovirus Promotes a Higher-Avidity CD4+ T Cell Response to Retroviral Infection. *PLOS Pathog.* **8**, e1002709 (2012).

52. Brook, C. E. & Dobson, A. P. Bats as 'special' reservoirs for emerging zoonotic pathogens. *Trends Microbiol.* **23**, 172–180 (2015).

53. Kassiotis, G. & Stoye, J. P. Immune responses to endogenous retroelements: taking the bad with the good. *Nat. Rev. Immunol.* **16**, 207–219 (2016).

54. Maguire, C. *et al.* Molecular Mimicry as a Mechanism of Viral Immune Evasion and Autoimmunity. Preprint at https://doi.org/10.1101/2024.03.08.583134 (2024).

55. The Nobel Prize in Physiology or Medicine 1960. *NobelPrize.org* https://www.nobelprize.org/prizes/medicine/1960/medawar/lecture/.

56. Shirafkan, F., Hensel, L. & Rattay, K. Immune tolerance and the prevention of autoimmune diseases essentially depend on thymic tissue homeostasis. *Front. Immunol.* **15**, (2024).

57. Murphy, K., Weaver, C., Berg, L. & Janeway, C. *Janeway's Immunobiology*. (W.W. Norton and Company, New York, NY, 2022).

58. Romagnani, S. Immunological tolerance and autoimmunity. *Intern. Emerg. Med.* **1**, 187–196 (2006).

59. Klein, L., Kyewski, B., Allen, P. M. & Hogquist, K. A. Positive and negative selection of the T cell repertoire: what thymocytes see and don't see. *Nat. Rev. Immunol.* **14**, 377 (2014).

60. Kurd, N. & Robey, E. A. T cell selection in the thymus: a spatial and temporal perspective. *Immunol. Rev.* **271**, 114 (2016).

61. Klein, L., Hinterberger, M., Wirnsberger, G. & Kyewski, B. Antigen presentation in the thymus for positive selection and central tolerance induction. *Nat. Rev. Immunol.* **9**, 833–844 (2009).

62. Elsen, P. J. van den. Expression Regulation of Major Histocompatibility Complex Class I and Class II Encoding Genes. *Front. Immunol.* **2**, 48 (2011).

63. Palmer, E. Negative selection — clearing out the bad apples from the T-cell repertoire. *Nat. Rev. Immunol.* **3**, 383–391 (2003).

64. Derbinski, J., Schulte, A., Kyewski, B. & Klein, L. Promiscuous gene expression in medullary thymic epithelial cells mirrors the peripheral self. *Nat. Immunol.* **2**, 1032–1039 (2001).

65. Kyewski, B. & Klein, L. A CENTRAL ROLE FOR CENTRAL TOLERANCE. *Annu. Rev. Immunol.* **24**, 571–606 (2006).

66.   Qi, Y., Zhang, R., Lu, Y., Zou, X. & Yang, W. Aire and Fezf2, two regulators in medullary thymic epithelial cells, control autoimmune diseases by regulating TSAs: Partner or complementer? *Front. Immunol.* **13**, (2022).

67.   Berrih-Aknin, S., Panse, R. L. & Dragin, N. AIRE: a missing link to explain female susceptibility to autoimmune diseases. *Ann. N. Y. Acad. Sci.* **1412**, 21–32 (2018).

68.   Eisenbarth, G. S. & Gottlieb, P. A. Autoimmune Polyendocrine Syndromes. *N. Engl. J. Med.* **350**, 2068–2079 (2004).

69.   Apert, C., Romagnoli, P. & van Meerwijk, J. P. M. IL-2 and IL-15 dependent thymic development of Foxp3-expressing regulatory T lymphocytes. *Protein Cell* **9**, 322–332 (2018).

70.   Xing, Y. & Hogquist, K. A. T-Cell Tolerance: Central and Peripheral. *Cold Spring Harb. Perspect. Biol.* **4**, a006957 (2012).

71.   Malhotra, D. *et al.* Polyclonal CD4+ T cell tolerance is established by distinct mechanisms, according to self-peptide expression patterns. *Nat. Immunol.* **17**, 187 (2016).

72.   Krueger, A., Ziętara, N. & Łyszkiewicz, M. T Cell Development by the Numbers. *Trends Immunol.* **38**, 128–139 (2017).

73.   Chen, L. & Flies, D. B. Molecular mechanisms of T cell co-stimulation and co-inhibition. *Nat. Rev. Immunol.* **13**, 227–242 (2013).

74.   Audiger, C., Rahman, M. J., Yun, T. J., Tarbell, K. V. & Lesage, S. The Importance of Dendritic Cells in Maintaining Immune Tolerance. *J. Immunol.* **198**, 2223–2231 (2017).

75.   Kissler, S., Anderton, S. M. & Wraith, D. C. Antigen-presenting Cell Activation: a Link Between Infection and Autoimmunity? *J. Autoimmun.* **16**, 303–308 (2001).

76.   Fife, B. T. & Pauken, K. E. The role of the PD-1 pathway in autoimmunity and peripheral tolerance. *Ann. N. Y. Acad. Sci.* **1217**, 45–59 (2011).

77.   Keir, M. E., Butte, M. J., Freeman, G. J. & Sharpe, A. H. PD-1 and Its Ligands in Tolerance and Immunity. *Annu. Rev. Immunol.* **26**, 677–704 (2008).

78.   Parish, I. A. *et al.* The molecular signature of CD8+ T cells undergoing deletional tolerance. *Blood* **113**, 4575–4585 (2009).

79.   Krishnamurty, A. T. & Turley, S. J. Lymph node stromal cells: cartographers of the immune system. *Nat. Immunol.* **21**, 369–380 (2020).

80.   Cheru, N., Hafler, D. A. & Sumida, T. S. Regulatory T cells in peripheral tissue tolerance and diseases. *Front. Immunol.* **14**, (2023).

81.   Fontenot, J. D., Gavin, M. A. & Rudensky, A. Y. Foxp3 programs the development and function of CD4+CD25+ regulatory T cells. *Nat. Immunol.* **4**, 330–336 (2003).

82.   Vignali, D. A. A., Collison, L. W. & Workman, C. J. How regulatory T cells work. *Nat. Rev. Immunol.* **8**, 523–532 (2008).

83.   Tang, Q. *et al.* Visualizing regulatory T cell control of autoimmune responses in nonobese diabetic mice. *Nat. Immunol.* **7**, 83–92 (2006).

84.   Tadokoro, C. E. *et al.* Regulatory T cells inhibit stable contacts between CD4+ T cells and dendritic cells in vivo. *J. Exp. Med.* **203**, 505–511 (2006).

85.   Huang, H., Ma, Y., Dawicki, W., Zhang, X. & Gordon, J. R. Comparison of Induced versus Natural Regulatory T Cells of the Same TCR Specificity for Induction of Tolerance to an Environmental Antigen. *J. Immunol.* **191**, 1136–1143 (2013).

86.   Yadav, M. *et al.* Neuropilin-1 distinguishes natural and inducible regulatory T cells among regulatory T cell subsets in vivo. *J. Exp. Med.* **209**, 1713–1722 (2012).

87.   Benoist, C. & Mathis, D. Treg Cells, Life History, and Diversity. *Cold Spring Harb. Perspect. Biol.* **4**, a007021 (2012).

88.   Lathrop, S. K. *et al.* Peripheral education of the immune system by colonic commensal microbiota. *Nature* **478**, 250–254 (2011).

89.   Mishra, S., Srinivasan, S., Ma, C. & Zhang, N. CD8+ Regulatory T Cell – A Mystery to Be Revealed. *Front. Immunol.* **12**, (2021).

90.   Bienvenu, B. *et al.* Peripheral CD8+CD25+ T Lymphocytes from MHC Class II-Deficient Mice Exhibit Regulatory Activity1. *J. Immunol.* **175**, 246–253 (2005).

91.   Zong, Y., Deng, K. & Chong, W. P. Regulation of Treg cells by cytokine signaling and co-stimulatory molecules. *Front. Immunol.* **15**, (2024).

92.   Loebbermann, J. *et al.* Regulatory T cells expressing granzyme B play a critical role in controlling lung inflammation during acute viral infection. *Mucosal Immunol.* **5**, 161 (2012).

93.   Létourneau, S., Krieg, C., Pantaleo, G. & Boyman, O. IL-2– and CD25-dependent immunoregulatory mechanisms in the homeostasis of T-cell subsets. *J. Allergy Clin. Immunol.* **123**, 758–762 (2009).

94.   Chinen, T. *et al.* An essential role for the IL-2 receptor in Treg cell function. *Nat. Immunol.* **17**, 1322–1333 (2016).

95.   Perez, V. L. *et al.* Induction of Peripheral T Cell Tolerance In Vivo Requires CTLA-4 Engagement. *Immunity* **6**, 411–417 (1997).

96.   Chocarro, L. *et al.* Understanding LAG-3 Signaling. *Int. J. Mol. Sci.* **22**, 5282 (2021).

97.   Akkaya, B. *et al.* Regulatory T cells mediate specific suppression by depleting peptide–MHC class II from dendritic cells. *Nat. Immunol.* **20**, 218–231 (2019).

98.   Facciabene, A., Motz, G. T. & Coukos, G. T-Regulatory Cells: Key Players in Tumor Immune Escape and Angiogenesis. *Cancer Res.* **72**, 2162–2171 (2012).

99.   Jung, M. K. & Shin, E.-C. Regulatory T Cells in Hepatitis B and C Virus Infections. *Immune Netw.* **16**, 330–336 (2016).

100.   Lund, J. M., Hsing, L., Pham, T. T. & Rudensky, A. Y. Coordination of Early Protective Immunity to Viral Infection by Regulatory T Cells. *Science* **320**, 1220–1224 (2008).

101.   Okeke, E. B. & Uzonna, J. E. The Pivotal Role of Regulatory T Cells in the Regulation of Innate Immune Cells. *Front. Immunol.* **10**, 680 (2019).

102.   Bacchetta, R., Barzaghi, F. & Roncarolo, M.-G. From IPEX syndrome to FOXP3 mutation: a lesson on immune dysregulation. *Ann. N. Y. Acad. Sci.* **1417**, 5–22 (2018).

103. Andersen, M. H., Schrama, D., thor Straten, P. & Becker, J. C. Cytotoxic T Cells. *J. Invest. Dermatol.* **126**, 32–41 (2006).

104. Luckheeram, R. V., Zhou, R., Verma, A. D. & Xia, B. CD4+T Cells: Differentiation and Functions. *Clin. Dev. Immunol.* **2012**, 925135 (2012).

105. Nakayama, T. *et al.* Th2 Cells in Health and Disease. *Annu. Rev. Immunol.* **35**, 53–84 (2017).

106. Peck, A. & Mellins, E. D. Precarious Balance: Th17 Cells in Host Defense. *Infect. Immun.* **78**, 32–38 (2010).

107. Singh, R. P. *et al.* Th17 cells in inflammation and autoimmunity. *Autoimmun. Rev.* **13**, 1174–1181 (2014).

108. Zhou, L., Chong, M. M. W. & Littman, D. R. Plasticity of CD4+ T Cell Lineage Differentiation. *Immunity* **30**, 646–655 (2009).

109. Sawant, D. V. & Vignali, D. A. A. Once a Treg, always a Treg? *Immunol. Rev.* **259**, 173–191 (2014).

110. Crotty, S. T Follicular Helper Cell Biology: A Decade of Discovery and Diseases. *Immunity* **50**, 1132–1148 (2019).

111. Chandwaskar, R. & Awasthi, A. Emerging Roles of Th9 Cells as an Anti-tumor Helper T Cells. *Int. Rev. Immunol.* **38**, 204–211 (2019).

112. Neurath, M. F. & Kaplan, M. H. Th9 cells in immunity and immunopathological diseases. *Semin. Immunopathol.* **39**, 1–4 (2017).

113. Athie-Morales, V., Smits, H. H., Cantrell, D. A. & Hilkens, C. M. U. Sustained IL-12 Signaling Is Required for Th1 Development 1. *J. Immunol.* **172**, 61–69 (2004).

114. Szabo, S. J. *et al.* A Novel Transcription Factor, T-bet, Directs Th1 Lineage Commitment. *Cell* **100**, 655–669 (2000).

115. Mullen, A. C. *et al.* Role of T-bet in Commitment of TH1 Cells Before IL-12-Dependent Selection. *Science* **292**, 1907–1910 (2001).

116. Peterson, J. D., Waltenbaugh, C. & Miller, S. D. IgG subclass responses to Theiler's murine encephalomyelitis virus infection and immunization suggest a dominant role for Th1 cells in susceptible mouse strains. *Immunology* **75**, 652 (1992).

117. Carli, M. D., D'elios, M. M., Zancuoghi, G., Romagnani, S. & Prete, G. D. Review Human Th1 and Th2 Cells: Functional Properties, Regulation of Development and Role in Autoimmunity. *Autoimmunity* **18**, 301–308 (1994).

118. Ishigame, H. *et al.* Excessive Th1 responses due to the absence of TGF-β signaling cause autoimmune diabetes and dysregulated Treg cell homeostasis. *Proc. Natl. Acad. Sci.* **110**, 6961–6966 (2013).

119. Ma, R., Su, H., Jiao, K. & Liu, J. Role of Th17 cells, Treg cells, and Th17/Treg imbalance in immune homeostasis disorders in patients with chronic obstructive pulmonary disease. *Immun. Inflamm. Dis.* **11**, e784 (2023).

120. Miyauchi, K. Helper T Cell Responses to Respiratory Viruses in the Lung: Development, Virus Suppression, and Pathogenesis. *Viral Immunol.* **30**, 421–430 (2017).

121. Kiley, M. P. *et al.* Filoviridae: a Taxonomic Home for Marburg and Ebola Viruses ? *Intervirology* **18**, 24–32 (2008).

122. Siegert, R., Shu, H.-L., Slenczka, W., Peters, D. & Müller, G. Zur Ätiologie einer unbekannten, von Affen ausgegangenen menschlichen Infektionskrankheit. *DMW - Dtsch. Med. Wochenschr.* **92**, 2341–2343 (2009).

123. Commission, R. of an I. Ebola haemorrhagic fever in Zaire, 1976. *Bull. World Health Organ.* **56**, 271 (1978).

124. Biedenkopf, N. *et al.* Renaming of genera Ebolavirus and Marburgvirus to Orthoebolavirus and Orthomarburgvirus, respectively, and introduction of binomial species names within family Filoviridae. *Arch. Virol.* **168**, 220 (2023).

125. Kuhn, J. H. *et al.* ICTV Virus Taxonomy Profile: Filoviridae. *J. Gen. Virol.* **100**, 911–912 (2019).

126.   Emanuel, J., Marzi, A. & Feldmann, H. Filoviruses: Ecology, Molecular Biology, and Evolution. *Adv. Virus Res.* **100**, 189–221 (2018).

127.   Baseler, L., Chertow, D. S., Johnson, K. M., Feldmann, H. & Morens, D. M. The Pathogenesis of Ebola Virus Disease. *Annu. Rev. Pathol.* **12**, 387–418 (2017).

128.   Hoenen, T., Groseth, A. & Feldmann, H. Therapeutic strategies to target the Ebola virus life cycle. *Nat. Rev. Microbiol.* **17**, 593–606 (2019).

129.   Jeffers, S. A., Sanders, D. A. & Sanchez, A. Covalent Modifications of the Ebola Virus Glycoprotein. *J. Virol.* **76**, 12463–12472 (2002).

130.   Dolnik, O. *et al.* Ectodomain shedding of the glycoprotein GP of Ebola virus. *EMBO J.* **23**, 2175–2184 (2004).

131.   Volchkova, V. A., Klenk, H.-D. & Volchkov, V. E. Delta-Peptide Is the Carboxy-Terminal Cleavage Fragment of the Nonstructural Small Glycoprotein sGP of Ebola Virus. *Virology* **265**, 164–171 (1999).

132.   de La Vega, M.-A., Wong, G., Kobinger, G. P. & Qiu, X. The Multiple Roles of sGP in Ebola Pathogenesis. *Viral Immunol.* **28**, 3–9 (2015).

133.   Volchkov, V. E. *et al.* GP mRNA of Ebola Virus Is Edited by the Ebola Virus Polymerase and by T7 and Vaccinia Virus Polymerases1. *Virology* **214**, 421–430 (1995).

134.   Sanchez, A., Trappier, S. G., Mahy, B. W., Peters, C. J. & Nichol, S. T. The virion glycoproteins of Ebola viruses are encoded in two reading frames and are expressed through transcriptional editing. *Proc. Natl. Acad. Sci.* **93**, 3602–3607 (1996).

135.   Ning, Y.-J., Deng, F., Hu, Z. & Wang, H. The roles of ebolavirus glycoproteins in viralpathogenesis. *Virol. Sin.* **32**, 3–15 (2017).

136.   Moller-Tank, S., Kondratowicz, A. S., Davey, R. A., Rennert, P. D. & Maury, W. Role of the Phosphatidylserine Receptor TIM-1 in Enveloped-Virus Entry. *J. Virol.* **87**, 8327–8341 (2013).

137.   Characterization of Human and Murine T-Cell Immunoglobulin Mucin Domain 4 (TIM-4) IgV Domain Residues Critical for Ebola Virus Entry | Journal of Virology. https://journals.asm.org/doi/10.1128/jvi.00100-16.

138.   Takada, A., Feldmann, H., Ksiazek, T. G. & Kawaoka, Y. Antibody-Dependent Enhancement of Ebola Virus Infection. *J. Virol.* **77**, 7539–7544 (2003).

139.   Takada, A., Ebihara, H., Feldmann, H., Geisbert, T. W. & Kawaoka, Y. Epitopes Required for Antibody-Dependent Enhancement of Ebola Virus Infection. *J. Infect. Dis.* **196**, S347–S356 (2007).

140.   Saeed, M. F., Kolokoltsov, A. A., Albrecht, T. & Davey, R. A. Cellular Entry of Ebola Virus Involves Uptake by a Macropinocytosis-Like Mechanism and Subsequent Trafficking through Early and Late Endosomes. *PLOS Pathog.* **6**, e1001110 (2010).

141.   Wang, H. *et al.* Ebola Viral Glycoprotein Bound to Its Endosomal Receptor Niemann-Pick C1. *Cell* **164**, 258–268 (2016).

142.   Fénéant, L., Wijs, K. M. S., Nelson, E. A. & White, J. M. An exploration of conditions proposed to trigger the Ebola virus glycoprotein for fusion. *PLOS ONE* **14**, e0219312 (2019).

143.   Bodmer, B. S., Hoenen, T. & Wendt, L. Molecular insights into the Ebola virus life cycle. *Nat. Microbiol.* **9**, 1417–1426 (2024).

144.   Hoenen, T. *et al.* Inclusion Bodies Are a Site of Ebolavirus Replication. *J. Virol.* **86**, 11779–11788 (2012).

145.   Bodmer, B. S. *et al.* Ebola virus inclusion bodies are liquid organelles whose formation is facilitated by nucleoprotein oligomerization. *Emerg. Microbes Infect.* **12**, 2223727 (2023).

146.   Wu, C. *et al.* Disruption of Ebola NP0VP35 Inclusion Body-like Structures reduce Viral Infection. *J. Mol. Biol.* **435**, 168241 (2023).

147.   Smith, D. R. *et al.* Inhibition of heat-shock protein 90 reduces Ebola virus replication. *Antiviral Res.* **87**, 187–194 (2010).

148. Biedenkopf, N., Lier, C. & Becker, S. Dynamic Phosphorylation of VP30 Is Essential for Ebola Virus Life Cycle. *J. Virol.* **90**, 4914–4925 (2016).

149. Lier, C., Becker, S. & Biedenkopf, N. Dynamic phosphorylation of Ebola virus VP30 in NP-induced inclusion bodies. *Virology* **512**, 39–47 (2017).

150. Evidence for Viral mRNA Export from Ebola Virus Inclusion Bodies by the Nuclear RNA Export Factor NXF1 | Journal of Virology. https://journals.asm.org/doi/10.1128/jvi.00900-22.

151. Furuyama, W., Shifflett, K., Feldmann, H. & Marzi, A. The Ebola virus soluble glycoprotein contributes to viral pathogenesis by activating the MAP kinase signaling pathway. *PLOS Pathog.* **17**, e1009937 (2021).

152. Falzarano, D. *et al.* Structure-Function Analysis of the Soluble Glycoprotein, sGP, of Ebola Virus. *ChemBioChem* **7**, 1605–1611 (2006).

153. Basler, C. F. & Amarasinghe, G. K. Evasion of Interferon Responses by Ebola and Marburg Viruses. *J. Interferon Cytokine Res.* **29**, 511–520 (2009).

154. Leung, D. W. *et al.* Structure of the Ebola VP35 interferon inhibitory domain. *Proc. Natl. Acad. Sci.* **106**, 411–416 (2009).

155. Wan, W. *et al.* Structure and assembly of the Ebola virus nucleocapsid. *Nature* **551**, 394 (2017).

156. Banadyga, L. *et al.* Ebola virus VP24 interacts with NP to facilitate nucleocapsid assembly and genome packaging. *Sci. Rep.* **7**, 7698 (2017).

157. Schudt, G. *et al.* Transport of Ebolavirus Nucleocapsids Is Dependent on Actin Polymerization: Live-Cell Imaging Analysis of Ebolavirus-Infected Cells. *J. Infect. Dis.* **212**, S160–S166 (2015).

158. Adu-Gyamfi, E., Digman, M. A., Gratton, E. & Stahelin, R. V. Single-Particle Tracking Demonstrates that Actin Coordinates the Movement of the Ebola Virus Matrix Protein. *Biophys. J.* **103**, L41–L43 (2012).

159. Yamayoshi, S. *et al.* Ebola Virus Matrix Protein VP40 Uses the COPII Transport System for Its Intracellular Transport. *Cell Host Microbe* **3**, 168–177 (2008).

160. Olukitibi, T. A., Ao, Z., Mahmoudi, M., Kobinger, G. A. & Yao, X. Dendritic Cells/Macrophages-Targeting Feature of Ebola Glycoprotein and its Potential as Immunological Facilitator for Antiviral Vaccine Approach. *Microorganisms* **7**, 402 (2019).

161. Bray, M. & Geisbert, T. W. Ebola virus: The role of macrophages and dendritic cells in the pathogenesis of Ebola hemorrhagic fever. *Int. J. Biochem. Cell Biol.* **37**, 1560–1566 (2005).

162. Martinez, O. *et al.* Ebola Virus Exploits a Monocyte Differentiation Program To Promote Its Entry. *J. Virol.* **87**, 3801–3814 (2013).

163. Geisbert, T. W. *et al.* Pathogenesis of Ebola Hemorrhagic Fever in Cynomolgus Macaques: Evidence that Dendritic Cells Are Early and Sustained Targets of Infection. *Am. J. Pathol.* **163**, 2347–2370 (2003).

164. Geisbert, T. W. & Hensley, L. E. Ebola virus: new insights into disease aetiopathology and possible therapeutic interventions. *Expert Rev. Mol. Med.* **6**, 1–24 (2004).

165. Caviness, K., Kuhn, J. H. & Palacios, G. Ebola virus persistence as a new focus in clinical research. *Curr. Opin. Virol.* **23**, 43–48 (2017).

166. Muñoz-Fontela, C. & McElroy, A. K. Ebola Virus Disease in Humans: Pathophysiology and Immunity. in *Marburg- and Ebolaviruses: From Ecosystems to Molecules* (eds. Mühlberger, E., Hensley, L. L. & Towner, J. S.) 141–169 (Springer International Publishing, Cham, 2017). doi:10.1007/82_2017_11.

167. McElroy, A. K. *et al.* Human Ebola virus infection results in substantial immune activation. *Proc. Natl. Acad. Sci. U. S. A.* **112**, 4719–4724 (2015).

168. Ruibal, P. *et al.* Unique human immune signature of Ebola virus disease in Guinea. *Nature* **533**, 100–104 (2016).

169.   Escudero-Pérez, B., Lawrence, P. & Castillo-Olivares, J. Immune correlates of protection for SARS-CoV-2, Ebola and Nipah virus infection. *Front. Immunol.* **14**, (2023).

170.   Crouse, J., Kalinke, U. & Oxenius, A. Regulation of antiviral T cell responses by type I interferons. *Nat. Rev. Immunol.* **15**, 231–242 (2015).

171.   Feldmann, H. *et al.* Filovirus-induced endothelial leakage triggered by infected monocytes/macrophages. *J. Virol.* **70**, 2208–2214 (1996).

172.   Huang, Y., Dai, H. & Ke, R. Principles of Effective and Robust Innate Immune Response to Viral Infections: A Multiplex Network Analysis. *Front. Immunol.* **10**, (2019).

173.   Fanunza, E., Frau, A., Corona, A. & Tramontano, E. Insights into Ebola Virus VP35 and VP24 Interferon Inhibitory Functions and their Initial Exploitation as Drug Targets. *Infect. Disord. - Drug TargetsDisorders* **19**, 362–374 (2019).

174.   McNab, F., Mayer-Barber, K., Sher, A., Wack, A. & O'Garra, A. Type I interferons in infectious disease. *Nat. Rev. Immunol.* **15**, 87–103 (2015).

175.   Cabeza-Cabrerizo, M., Cardoso, A., Minutti, C. M., Costa, M. P. da & Sousa, C. R. e. Dendritic Cells Revisited. *Annu. Rev. Immunol.* **39**, 131–166 (2021).

176.   Rottstegge, M. *et al.* Avatar Mice Underscore the Role of the T Cell-Dendritic Cell Crosstalk in Ebola Virus Disease and Reveal Mechanisms of Protection in Survivors. *J. Virol.* **96**, e00574-22 (2022).

177.   Lüdtke, A. *et al.* Ebola virus infection kinetics in chimeric mice reveal a key role of T cells as barriers for virus dissemination. *Sci. Rep.* **7**, 43776 (2017).

178.   Niemetz, L. R. The role of conventional dendritic cell subsets in T-cell activation in Ebola virus infection. (Staats-und Universitätsbibliothek Hamburg Carl von Ossietzky, 2024).

179.   Niemetz, L. *et al.* Ebola Virus Infection of Flt3-Dependent, Conventional Dendritic Cells and Antigen Cross-presentation Leads to High Levels of T-Cell Activation. *J. Infect. Dis.* jiae441 (2024) doi:10.1093/infdis/jiae441.

180. Embgenbroich, M. & Burgdorf, S. Current Concepts of Antigen Cross-Presentation. *Front. Immunol.* **9**, (2018).

181. Miceli, M. C. & Parnes, J. R. Role of CD4 and CD8 in T Cell Activation and Differentiation. in *Advances in Immunology* (ed. Dixon, F. J.) vol. 53 59–122 (Academic Press, 1993).

182. Speranza, E. *et al.* T-Cell Receptor Diversity and the Control of T-Cell Homeostasis Mark Ebola Virus Disease Survival in Humans. *J. Infect. Dis.* **218**, S508–S518 (2018).

183. Younan, P. *et al.* Ebola virus-mediated T-lymphocyte depletion is the result of an abortive infection. *PLOS Pathog.* **15**, e1008068 (2019).

184. Iampietro, M., Amurri, L., Reynard, O. & Bukreyev, A. Interplay of Ebola Virus With Immune Cells Leading to Their Death by Diverse Mechanisms. *J. Infect. Dis.* **228**, S582–S586 (2023).

185. Iampietro, M. *et al.* Ebola virus glycoprotein directly triggers T lymphocyte death despite of the lack of infection. *PLOS Pathog.* **13**, e1006397 (2017).

186. Lu, L. L., Suscovich, T. J., Fortune, S. M. & Alter, G. Beyond binding: antibody effector functions in infectious diseases. *Nat. Rev. Immunol.* **18**, 46–61 (2018).

187. Colavita, F. *et al.* Inflammatory and Humoral Immune Response during Ebola Virus Infection in Survivor and Fatal Cases Occurred in Sierra Leone during the 2014–2016 Outbreak in West Africa. *Viruses* **11**, 373 (2019).

188. Saphire, E. O., Schendel, S. L., Gunn, B. M., Milligan, J. C. & Alter, G. Antibody-mediated protection against Ebola virus. *Nat. Immunol.* **19**, 1169–1178 (2018).

189. Fuentes, S., Ravichandran, S., Coyle, E. M., Klenow, L. & Khurana, S. Human Antibody Repertoire following Ebola Virus Infection and Vaccination. *iScience* **23**, (2020).

190. Davis, C. W. *et al.* Longitudinal Analysis of the Human B Cell Response to Ebola Virus Infection. *Cell* **177**, 1566-1582.e17 (2019).

191. Ebola virus disease. https://www.who.int/health-topics/ebola.

192. Izudi, J. & Bajunirwe, F. Case fatality rate for Ebola disease, 1976–2022: A meta-analysis of global data. *J. Infect. Public Health* **17**, 25–34 (2024).

193. Crowe, S. J. *et al.* Prognostic Indicators for Ebola Patient Survival - Volume 22, Number 2—February 2016 - Emerging Infectious Diseases journal - CDC. doi:10.3201/eid2202.151250.

194. Prescott, J. B. *et al.* Immunobiology of Ebola and Lassa virus infections. *Nat. Rev. Immunol.* **17**, 195–207 (2017).

195. Jacob, S. T. *et al.* Ebola virus disease. *Nat. Rev. Dis. Primer* **6**, 1–31 (2020).

196. Eichner, M., Dowell, S. F. & Firese, N. Incubation Period of Ebola Hemorrhagic Virus Subtype Zaire. *Osong Public Health Res. Perspect.* **2**, 3–7 (2011).

197. Casillas, A. M., Nyamathi, A. M., Sosa, A., Wilder, C. L. & Sands, H. A Current Review of Ebola Virus: Pathogenesis, Clinical Presentation, and Diagnostic Assessment. *Biol. Res. Nurs.* **4**, 268–275 (2003).

198. Feldmann, H. & Geisbert, T. W. Ebola haemorrhagic fever. *The Lancet* **377**, 849–862 (2011).

199. Levi, M., Toh, C. H., Thachil, J. & Watson, H. G. Guidelines for the diagnosis and management of disseminated intravascular coagulation. *Br. J. Haematol.* **145**, 24–33 (2009).

200. Falasca, L. *et al.* Molecular mechanisms of Ebola virus pathogenesis: focus on cell death. *Cell Death Differ.* **22**, 1250–1259 (2015).

201. Rowe, A. K. *et al.* Clinical, virologic, and immunologic follow-up of convalescent Ebola hemorrhagic fever patients and their household contacts, Kikwit, Democratic Republic of the Congo. Commission de Lutte contre les Epidémies à Kikwit. *J. Infect. Dis.* **179 Suppl 1**, S28-35 (1999).

202. Racine, T. & Kobinger, G. P. Viral pathogenesis: Unlocking Ebola persistence. *Nat. Microbiol.* **2**, 1–2 (2017).

203. Keita, A. K. *et al.* Resurgence of Ebola virus in 2021 in Guinea suggests a new paradigm for outbreaks. *Nature* **597**, 539–543 (2021).

204. Boon, S. D. *et al.* Ebola Virus Infection Associated with Transmission from Survivors - Volume 25, Number 2—February 2019 - Emerging Infectious Diseases journal - CDC. doi:10.3201/eid2502.181011.

205. Crozier, I. *et al.* The Evolution of Medical Countermeasures for Ebola Virus Disease: Lessons Learned and Next Steps. *Vaccines* **10**, 1213 (2022).

206. Mulangu, S. *et al.* A Randomized, Controlled Trial of Ebola Virus Disease Therapeutics. *N. Engl. J. Med.* **381**, 2293–2303 (2019).

207. Feldmann, H., Sprecher, A. & Geisbert, T. W. Ebola. *N. Engl. J. Med.* **382**, 1832–1842 (2020).

208. Woolsey, C. & Geisbert, T. W. Current state of Ebola virus vaccines: A snapshot. *PLOS Pathog.* **17**, e1010078 (2021).

209. Henao-Restrepo, A. M. *et al.* Efficacy and effectiveness of an rVSV-vectored vaccine in preventing Ebola virus disease: final results from the Guinea ring vaccination, open-label, cluster-randomised trial (Ebola Ça Suffit!). *Lancet Lond. Engl.* **389**, 505–518 (2017).

210. Callendret, B. *et al.* A prophylactic multivalent vaccine against different filovirus species is immunogenic and provides protection from lethal infections with Ebolavirus and Marburgvirus species in non-human primates. *PloS One* **13**, e0192312 (2018).

211. Xu, D. *et al.* Design of universal Ebola virus vaccine candidates via immunofocusing. *Proc. Natl. Acad. Sci.* **121**, e2316960121 (2024).

212. CDC. Outbreak History. *Ebola* https://www.cdc.gov/ebola/outbreaks/index.html (2024).

213. Ohimain, E. I. & Silas-Olu, D. The 2013–2016 Ebola virus disease outbreak in West Africa. *Curr. Opin. Pharmacol.* **60**, 360–365 (2021).

214. Judson, S., Prescott, J. & Munster, V. Understanding Ebola Virus Transmission. *Viruses* **7**, 511 (2015).

215. Osterholm, M. T. *et al.* Transmission of Ebola Viruses: What We Know and What We Do Not Know. *mBio* **6**, 10.1128/mbio.00137-15 (2015).

216. Judson, S. D. & Munster, V. J. The Multiple Origins of Ebola Disease Outbreaks. *J. Infect. Dis.* **228**, S465–S473 (2023).

217. Mate, S. E. *et al.* Molecular Evidence of Sexual Transmission of Ebola Virus. *N. Engl. J. Med.* **373**, 2448–2454 (2015).

218. Marí Saéz, A. *et al.* Investigating the zoonotic origin of the West African Ebola epidemic. *EMBO Mol. Med.* **7**, 17–23 (2015).

219. Shenge, J. A. & Opayele, A. V. The Impact and Control of Emerging and Re-Emerging Viral Diseases in the Environment: An African Perspective. in *Current Microbiological Research in Africa: Selected Applications for Sustainable Environmental Management* (eds. Abia, A. L. K. & Lanza, G. R.) 185–202 (Springer International Publishing, Cham, 2020). doi:10.1007/978-3-030-35296-7_7.

220. Lawrence, P., Heung, M., Nave, J., Henkel, C. & Escudero-Pérez, B. The natural virome and pandemic potential: Disease X. *Curr. Opin. Virol.* **63**, 101377 (2023).

221. Mandl, J. N. *et al.* Reservoir Host Immune Responses to Emerging Zoonotic Viruses. *Cell* **160**, 20–35 (2015).

222. Groseth, A., Feldmann, H. & Strong, J. E. The ecology of Ebola virus. *Trends Microbiol.* **15**, 408–416 (2007).

223. Weber, N. *et al.* Robust evidence for bats as reservoir hosts is lacking in most African virus studies: a review and call to optimize sampling and conserve bats. *Biol. Lett.* **19**, 20230358 (2023).

224. Arnaout, Y. *et al.* Genetic identification of bat species for pathogen surveillance across France. *PLOS ONE* **17**, e0261344 (2022).

225.   Calisher, C. H., Childs, J. E., Field, H. E., Holmes, K. V. & Schountz, T. Bats: Important Reservoir Hosts of Emerging Viruses. *Clin. Microbiol. Rev.* **19**, 531–545 (2006).

226.   Amman, B. R. *et al.* Isolation of Angola-like Marburg virus from Egyptian rousette bats from West Africa. *Nat. Commun.* **11**, 510 (2020).

227.   Goldstein, T. *et al.* The discovery of Bombali virus adds further support for bats as hosts of ebolaviruses. *Nat. Microbiol.* **3**, 1084–1089 (2018).

228.   Düx, A. *et al.* Detection of Bombali Virus in a Mops condylurus Bat in Kyela, Tanzania. *Viruses* **16**, 1227 (2024).

229.   Leendertz, S. A. J., Gogarten, J. F., Düx, A., Calvignac-Spencer, S. & Leendertz, F. H. Assessing the Evidence Supporting Fruit Bats as the Primary Reservoirs for Ebola Viruses. *EcoHealth* **13**, 18–25 (2016).

230.   Riesle-Sbarbaro, S. A. *et al.* Selective replication and vertical transmission of Ebola virus in experimentally infected Angolan free-tailed bats. *Nat. Commun.* **15**, 925 (2024).

231.   Moreno Santillán, D. D. *et al.* Large-scale genome sampling reveals unique immunity and metabolic adaptations in bats. *Mol. Ecol.* **30**, 6449–6467 (2021).

232.   Irving, A. T., Ahn, M., Goh, G., Anderson, D. E. & Wang, L.-F. Lessons from the host defences of bats, a unique viral reservoir. *Nature* **589**, 363–370 (2021).

233.   Pei, G., Balkema-Buschmann, A. & Dorhoi, A. Disease tolerance as immune defense strategy in bats: One size fits all? *PLOS Pathog.* **20**, e1012471 (2024).

234.   O'Shea, T. J. *et al.* Bat Flight and Zoonotic Viruses - Volume 20, Number 5—May 2014 - Emerging Infectious Diseases journal - CDC. doi:10.3201/eid2005.130539.

235.   Zhang, G. *et al.* Comparative Analysis of Bat Genomes Provides Insight into the Evolution of Flight and Immunity. *Science* **339**, 456–460 (2013).

236.   Clayton, E. & Munir, M. Fundamental Characteristics of Bat Interferon Systems. *Front. Cell. Infect. Microbiol.* **10**, (2020).

237.   Cowled, C. *et al.* Molecular characterisation of Toll-like receptors in the black flying fox Pteropus alecto. *Dev. Comp. Immunol.* **35**, 7 (2010).

238.   Reeder, D. M. & Moore, M. S. White-Nose Syndrome: A Deadly Emerging Infectious Disease of Hibernating Bats. in *Bat Evolution, Ecology, and Conservation* (eds. Adams, R. A. & Pedersen, S. C.) 413–434 (Springer, New York, NY, 2013). doi:10.1007/978-1-4614-7397-8_20.

239.   Hughes, G. J., Orciari, L. A. & Rupprecht, C. E. Evolutionary timescale of rabies virus adaptation to North American bats inferred from the substitution rate of the nucleoprotein gene. *J. Gen. Virol.* **86**, 1467–1474 (2005).

240.   Forero-Muñoz, N. R. *et al.* The coevolutionary mosaic of bat betacoronavirus emergence risk. *Virus Evol.* **10**, vead079 (2024).

241.   Skirmuntt, E. C., Escalera-Zamudio, M., Teeling, E. C., Smith, A. & Katzourakis, A. The Potential Role of Endogenous Viral Elements in the Evolution of Bats as Reservoirs for Zoonotic Viruses. *Annu. Rev. Virol.* **7**, 103–119 (2020).

242.   Taylor, D. J., Dittmar, K., Ballinger, M. J. & Bruenn, J. A. Evolutionary maintenance of filovirus-like genes in bat genomes. *BMC Evol. Biol.* **11**, 336 (2011).

243.   Kondoh, T. *et al.* Putative endogenous filovirus VP35-like protein potentially functions as an IFN antagonist but not a polymerase cofactor. *PLOS ONE* **12**, e0186450 (2017).

244.   Edwards, M. R. *et al.* Conservation of Structure and Immune Antagonist Functions of Filoviral VP35 Homologs Present in Microbat Genomes. *Cell Rep.* **24**, 861-872.e6 (2018).

245.   Ogawa, H. & Honda, T. Viral Sequences Are Repurposed for Controlling Antiviral Responses as Non-Retroviral Endogenous Viral Elements. *Acta Med. Okayama* **76**, 503–510 (2022).

246.   Bradfute, S. B., Warfield, K. L. & Bray, M. Mouse Models for Filovirus Infections. *Viruses* **4**, 1477–1508 (2012).

247. Harding, J. D. Nonhuman Primates and Translational Research: Progress, Opportunities, and Challenges. *ILAR J.* **58**, 141–150 (2017).

248. Bennett, R. S. *et al.* Nonhuman Primate Models of Ebola Virus Disease. in *Marburg- and Ebolaviruses: From Ecosystems to Molecules* (eds. Mühlberger, E., Hensley, L. L. & Towner, J. S.) 171–193 (Springer International Publishing, Cham, 2017). doi:10.1007/82_2017_20.

249. Liu, D. X. *et al.* Ebola Virus Disease Features Hemophagocytic Lymphohistiocytosis/Macrophage Activation Syndrome in the Rhesus Macaque Model. *J. Infect. Dis.* **228**, 371–382 (2023).

250. Widerspick, L., Steffen, J. F., Tappe, D. & Muñoz-Fontela, C. Animal Model Alternatives in Filovirus and Bornavirus Research. *Viruses* **15**, 158 (2023).

251. Watanabe, S., Noda, T. & Kawaoka, Y. Functional mapping of the nucleoprotein of Ebola virus. *J. Virol.* **80**, 3743–3751 (2006).

252. Shi, W. *et al.* A Filovirus-Unique Region of Ebola Virus Nucleoprotein Confers Aberrant Migration and Mediates Its Incorporation into Virions. *J. Virol.* **82**, 6190–6199 (2008).

253. Hoenen, T., Watt, A., Mora, A. & Feldmann, H. Modeling the lifecycle of Ebola virus under biosafety level 2 conditions with virus-like particles containing tetracistronic minigenomes. *J. Vis. Exp. JoVE* 52381 (2014) doi:10.3791/52381.

254. Escudero-Pérez, B. *et al.* Comparative pathogenesis of Ebola virus and Reston virus infection in humanized mice. *JCI Insight* **4**, e126070 (2019).

255. Farr, A. G. & Anderson, S. K. Epithelial heterogeneity in the murine thymus: fucose-specific lectins bind medullary epithelial cells. *J. Immunol. Baltim. Md 1950* **134**, 2971–2977 (1985).

256. Yates, A. D. *et al.* Ensembl 2020. *Nucleic Acids Res.* **48**, D682–D688 (2020).

257. Nanaware, P. P. *et al.* Distinguishing Signal From Noise in Immunopeptidome Studies of Limiting-Abundance Biological Samples: Peptides Presented by I-Ab in C57BL/6 Mouse Thymus. *Front. Immunol.* **12**, 658601 (2021).

258. Kaabinejadian, S. *et al.* Accurate MHC Motif Deconvolution of Immunopeptidomics Data Reveals a Significant Contribution of DRB3, 4 and 5 to the Total DR Immunopeptidome. *Front. Immunol.* **13**, (2022).

259. Collado, J. A. *et al.* Composition of the HLA-DR-associated human thymus peptidome. *Eur. J. Immunol.* **43**, 2273–2282 (2013).

260. Hermida Lorenzo, R. J. *et al.* Metagenomic Snapshots of Viral Components in Guinean Bats. *Microorganisms* **9**, 599 (2021).

261. Kumar, P. G. *et al.* The Autoimmune Regulator (AIRE) Is a DNA-binding Protein *. *J. Biol. Chem.* **276**, 41357–41364 (2001).

262. Purohit, S., Kumar, P. G., Laloraya, M. & She, J.-X. Mapping DNA-binding domains of the autoimmune regulator protein. *Biochem. Biophys. Res. Commun.* **327**, 939–944 (2005).

263. Jain, S., Martynova, E., Rizvanov, A., Khaiboullina, S. & Baranwal, M. Structural and Functional Aspects of Ebola Virus Proteins. *Pathogens* **10**, 1330 (2021).

264. Bray, M. The role of the Type I interferon response in the resistance of mice to filovirus infection. *J. Gen. Virol.* **82**, 1365–1373 (2001).

265. Nakamura, R. *et al.* Availability of a Microglia and Macrophage Marker, Iba-1, for Differential Diagnosis of Spontaneous Malignant Reticuloses from Astrocytomas in Rats. *J. Toxicol. Pathol.* **26**, 55 (2013).

266. Lahl, K. *et al.* Selective depletion of Foxp3+ regulatory T cells induces a scurfy-like disease. *J. Exp. Med.* **204**, 57 (2007).

267. Liu, Z. *et al.* Systematic comparison of 2A peptides for cloning multi-genes in a polycistronic vector. *Sci. Rep.* **7**, 2193 (2017).

268. Donnelly, M. L. L. *et al.* Analysis of the aphthovirus 2A/2B polyprotein 'cleavage' mechanism indicates not a proteolytic reaction, but a novel translational effect: a putative ribosomal 'skip'. *J. Gen. Virol.* **82**, 1013–1025 (2001).

269. Miyake, T. *et al.* Ebola Virus Inclusion Body Formation and RNA Synthesis Are Controlled by a Novel Domain of Nucleoprotein Interacting with VP35. *J. Virol.* **94**, e02100-19 (2020).

270. Kawano, H. *et al.* Aire Expression Is Inherent to Most Medullary Thymic Epithelial Cells during Their Differentiation Program. *J. Immunol.* **195**, 5149–5158 (2015).

271. van Laar, G. G., van Hamburg, J. P. & Tas, S. W. Extrathymic AIRE-expressing cells: Friends or foes in autoimmunity and cancer? *Autoimmun. Rev.* **21**, 103141 (2022).

272. Yamano, T. *et al.* Aire-expressing ILC3-like cells in the lymph node display potent APC features. *J. Exp. Med.* **216**, 1027–1037 (2019).

273. Rammensee, H.-G., Friede, T. & Stevanović, S. MHC ligands and peptide motifs: first listing. *Immunogenetics* **41**, 178–228 (1995).

274. EL-Manzalawy, Y., Dobbs, D. & Honavar, V. On Evaluating MHC-II Binding Peptide Prediction Methods. *PLOS ONE* **3**, e3268 (2008).

275. Faria, S. S. *et al.* The neutrophil-to-lymphocyte ratio: a narrative review. *ecancermedicalscience* **10**, 702 (2016).

276. Yan, X. *et al.* Neutrophil to lymphocyte ratio as prognostic and predictive factor in patients with coronavirus disease 2019: A retrospective cross-sectional study. *J. Med. Virol.* **92**, 2573–2581 (2020).

277. Barchet, W. *et al.* Virus-induced Interferon α Production by a Dendritic Cell Subset in the Absence of Feedback Signaling In Vivo. *J. Exp. Med.* **195**, 507–516 (2002).

278. Kochs, G. *et al.* In Vivo Conditions Enable IFNAR-Independent Type I Interferon Production by Peritoneal CD11b+ Cells upon Thogoto Virus Infection. *J. Virol.* **90**, 9330–9337 (2016).

279. Carlin, A. F. *et al.* An IRF-3-, IRF-5-, and IRF-7-Independent Pathway of Dengue Viral Resistance Utilizes IRF-1 to Stimulate Type I and II Interferon Responses. *Cell Rep.* **21**, 1600–1612 (2017).

280. Anzaghe, M. *et al.* Type I interferon receptor-independent interferon-α induction upon infection with a variety of negative-strand RNA viruses. *J. Gen. Virol.* **102**, (2021).

281. Murray, C. *et al.* Interdependent and independent roles of type I interferons and IL-6 in innate immune, neuroinflammatory and sickness behaviour responses to systemic poly I:C. *Brain. Behav. Immun.* **48**, 274 (2015).

282. Zimmermann, M. *et al.* IFNα enhances the production of IL-6 by human neutrophils activated via TLR8. *Sci. Rep.* **6**, 19674 (2016).

283. Mishra, A. R., Byrareddy, S. N. & Nayak, D. IFN-I Independent Antiviral Immune Response to Vesicular Stomatitis Virus Challenge in Mouse Brain. *Vaccines* **8**, 326 (2020).

284. Meyts, I. & Casanova, J.-L. Viral infections in humans and mice with genetic deficiencies of the type I IFN response pathway. *Eur. J. Immunol.* **51**, 1039–1061 (2021).

285. Eggena, M. P. *et al.* Depletion of Regulatory T Cells in HIV Infection Is Associated with Immune Activation1. *J. Immunol.* **174**, 4407–4414 (2005).

286. Zelinskyy, G. *et al.* The regulatory T-cell response during acute retroviral infection is locally defined and controls the magnitude and duration of the virus-specific cytotoxic T-cell response. *Blood* **114**, 3199–3207 (2009).

287. Zelinskyy, G., Dietze, K., Sparwasser, T. & Dittmer, U. Regulatory T Cells Suppress Antiviral Immune Responses and Increase Viral Loads during Acute Infection with a Lymphotropic Retrovirus. *PLOS Pathog.* **5**, e1000406 (2009).

288. Fulton, R. B., Meyerholz, D. K. & Varga, S. M. Foxp3+ CD4 Regulatory T Cells Limit Pulmonary Immunopathology by Modulating the CD8 T Cell Response during Respiratory Syncytial Virus Infection. *J. Immunol.* **185**, 2382–2392 (2010).

289.   Durant, L. R. *et al.* Regulatory T Cells Prevent Th2 Immune Responses and Pulmonary Eosinophilia during Respiratory Syncytial Virus Infection in Mice. *J. Virol.* **87**, 10946–10954 (2013).

290.   Kim, J. *et al.* Cutting Edge: Depletion of Foxp3+ Cells Leads to Induction of Autoimmunity by Specific Ablation of Regulatory T Cells in Genetically Targeted Mice1. *J. Immunol.* **183**, 7631–7634 (2009).

291.   Yi, J. *et al.* Unregulated antigen-presenting cell activation by T cells breaks self tolerance. *Proc. Natl. Acad. Sci.* **116**, 1007–1016 (2019).

292.   Bradfute, S. B. History and impact of the mouse-adapted Ebola virus model. *Antiviral Res.* **210**, 105493 (2023).

293.   Ebihara, H. *et al.* Molecular Determinants of Ebola Virus Virulence in Mice. *PLOS Pathog.* **2**, e73 (2006).

294.   Zhou, P. *et al.* Contraction of the type I IFN locus and unusual constitutive expression of IFN-α in bats. *Proc. Natl. Acad. Sci.* **113**, 2696–2701 (2016).

295.   Bondet, V. *et al.* Constitutive IFNα Protein Production in Bats. *Front. Immunol.* **12**, (2021).

296.   Guito, J. C. *et al.* Coordinated inflammatory responses dictate Marburg virus control by reservoir bats. *Nat. Commun.* **15**, 1826 (2024).

297.   Jayaprakash, A. D. *et al.* Marburg and Ebola Virus Infections Elicit a Complex, Muted Inflammatory State in Bats. *Viruses* **15**, 350 (2023).

298.   Cusick, M. F., Libbey, J. E. & Fujinami, R. S. Molecular Mimicry as a Mechanism of Autoimmune Disease. *Clin. Rev. Allergy Immunol.* **42**, 102–111 (2012).

299.   Hurford, A. & Day, T. IMMUNE EVASION AND THE EVOLUTION OF MOLECULAR MIMICRY IN PARASITES. *Evolution* **67**, 2889–2904 (2013).

300.   Gowthaman, U. & Eswarakumar, V. P. Molecular mimicry: Good artists copy, great artists steal. *Virulence* **4**, 433–434 (2013).

301.   Lasso, G., Honig, B. & Shapira, S. D. A Sweep of Earth's Virome Reveals Host-Guided Viral Protein Structural Mimicry and Points to Determinants of Human Disease. *Cell Syst.* **12**, 82-91.e3 (2021).

302.   Doxey, A. C. & McConkey, B. J. Prediction of molecular mimicry candidates in human pathogenic bacteria. *Virulence* **4**, 453–466 (2013).

303.   Adiguzel, Y. Molecular mimicry between SARS-CoV-2 and human proteins. *Autoimmun. Rev.* **20**, 102791 (2021).

304.   Lebeau, G. *et al.* Zika E Glycan Loop Region and Guillain–Barré Syndrome-Related Proteins: A Possible Molecular Mimicry to Be Taken in Account for Vaccine Development. *Vaccines* **9**, 283 (2021).

305.   Maguire, C. *et al.* Molecular Mimicry as a Mechanism of Viral Immune Evasion and Autoimmunity. *bioRxiv* 2024.03.08.583134 (2024) doi:10.1101/2024.03.08.583134.

306.   French, R. K. & Holmes, E. C. An Ecosystems Perspective on Virus Evolution and Emergence. *Trends Microbiol.* **28**, 165–175 (2020).

307.   Iida, A. *et al.* Heritable endogenization of an RNA virus in a mammalian species. 2020.01.19.911933 Preprint at https://doi.org/10.1101/2020.01.19.911933 (2020).

308.   Graham, A. L., Allen, J. E. & Read, A. F. Evolutionary Causes and Consequences of Immunopathology. *Annu. Rev. Ecol. Evol. Syst.* **36**, 373–397 (2005).

309.   Hayden, M. S. & Ghosh, S. NF-κB, the first quarter-century: remarkable progress and outstanding questions. *Genes Dev.* **26**, 203–234 (2012).

310.   Ivashkiv, L. B. & Donlin, L. T. Regulation of type I interferon responses. *Nat. Rev. Immunol.* **14**, 36–49 (2014).

311.   Shabman, R. S. *et al.* An Upstream Open Reading Frame Modulates Ebola Virus Polymerase Translation and Virus Replication. *PLOS Pathog.* **9**, e1003147 (2013).

312. Brauburger, K. *et al.* Analysis of the Highly Diverse Gene Borders in Ebola Virus Reveals a Distinct Mechanism of Transcriptional Regulation. *J. Virol.* **88**, 12558–12571 (2014).

313. Sullivan, B. M. *et al.* Memory T cell responses in survivors of the 2013–2016 West African Ebola outbreak. *J. Immunol.* **200**, 126.10 (2018).

314. Sakabe, S. *et al.* Analysis of CD8+ T cell response during the 2013–2016 Ebola epidemic in West Africa. *Proc. Natl. Acad. Sci. U. S. A.* **115**, E7578 (2018).

315. Hurwitz, J. L., Jones, B. G., Charpentier, E. & Woodland, D. L. Hypothesis: RNA and DNA Viral Sequence Integration into the Mammalian Host Genome Supports Long-Term B Cell and T Cell Adaptive Immunity. *Viral Immunol.* **30**, 628–632 (2017).

316. Ophinni, Y., Palatini, U., Hayashi, Y. & Parrish, N. F. piRNA-Guided CRISPR-like Immunity in Eukaryotes. *Trends Immunol.* **40**, 998–1010 (2019).

317. Herst, C. V. *et al.* An effective CTL peptide vaccine for Ebola Zaire Based on Survivors' CD8+ targeting of a particular nucleocapsid protein epitope with potential implications for COVID-19 vaccine design. *Vaccine* **38**, 4464–4475 (2020).

318. Tipton, T. R. W. *et al.* Characterisation of the T-cell response to Ebola virus glycoprotein amongst survivors of the 2013–16 West Africa epidemic. *Nat. Commun.* **12**, 1153 (2021).

319. Wiedemann, A. *et al.* Long-term cellular immunity of vaccines for Zaire Ebola Virus Diseases. *Nat. Commun.* **15**, 7666 (2024).

320. Liu, J. *et al.* Ebola virus persistence and disease recrudescence in the brains of antibody-treated nonhuman primate survivors. *Sci. Transl. Med.* **14**, eabi5229 (2022).

321. Madeira, F. *et al.* The EMBL-EBI Job Dispatcher sequence analysis tools framework in 2024. *Nucleic Acids Res.* **52**, W521–W525 (2024).

8 Appendix

The following section includes supplementary figures.

8.1 BLAT Search of NP-NIRV in Mouse Genome

Supplementary Figure 1: BLAT Search of NP-NIRV in Mouse Genome

Red arrows and vertical markers denote the position of the filovirus-like sequence. **A:** Results table shows its orientation is reversed in the mouse genome. **B:** HSP distribution on the genome highlights the sequence's location on chromosome 9 (indicated by a square). **C:** Assembly exceptions pinpoint the sequence's position. Source: https://www.ensembl.org/Mus_musculus/Tools/Blast;"Ensembl Mus musculus", version 102.38; accessed on 16.01.2021.

8.2 BLAT search of NP-NIRV with flanking transposons

Supplementary Figure 2: BLAT of Mouse NIRV with Flanking Transposons

Red arrows represent Type I Transposons/LINEs, while the blue arrow marks the mouse NIRV. Data source: https://www.ensembl.org/Mus_musculus/Tools/Blast; "Ensembl Mus musculus", version 103.39; accessed on 08.04.2021.

8.3 NP-NIRV Nucleotide and Ammino acid Sequence

A Sequence in 3'-5' Orientation:

B Putative Protein Product:

```
MGLGLFLIYCSFFLPKLVKGGGACLESLHSGYKSQRTRKGLIYFHKVGLL
RGPLGIFSFLIHGSFTFRSILIHQSIHQPSGCDTTEMITNI
```

Supplementary Figure 3: NP-NIRV Nucleotide and Ammino Acid Sequence

A: The filovirus-like sequence is oriented in the 3′-5′ orientation. The yellow-highlighted region represents a potential protein-coding segment, with the start codon (*gta*) and stop codon (*gat*) marked in red. The black underline indicates a predicted AIRE binding site. **B:** The corresponding amino acid sequence of the translated putative protein is shown.

8.4   Pairwise Alignment of EBOV NP and Mouse NP-NIRV

The following figure shows the pairwise alignment of EBOV NP and mouse NP-NIRV protein sequences. The analysis was conducted using EBI Search with the EMBOSS Needle program (version 6.6.0).[321]

```
Mouse_NIRV     1 GLFLIYCSFFLPKLVKGGGACLESLHSGYKSQR-----TRKGLIYFHKVG      45
                 |.||.:.|.|||||||.|..||||        |.||      ..:|||.:....
EBOV_NP        1 GQFLSFASLFLPKLVVGEKACLE------KVQRQIQVHAEQGLIQYPTAW      44


Mouse_NIRV    46 LLRGPLGIFSFLIHGSFTFRSILIHQSIHQPSGCDTTEMI      85
                 ...|.:.:...|:..:|..:.:|||||.:|..:|.|..:.:
EBOV_NP       45 QSVGHMMVIFRLMRTNFLIKFLLIHQGMHMVAGHDANDAV      84
```

Supplementary Figure 4: Pairwise Sequence Alignment of EBOV NP and Mouse NP-NIRV

Alignment of EBOV NP and mouse NP-NIRV protein sequences shows 31/90 (34.4%) identical residues, 44/90 (48.9%) similar residues, and 11/90 (12.2%) gaps, with a score of 118.5. (I) denotes identical residues, (.) indicates conserved changes, and (:) represents partial similarity with lower conservation. The analysis was conducted using EBI Search with the EMBOSS Needle program (version 6.6.0).
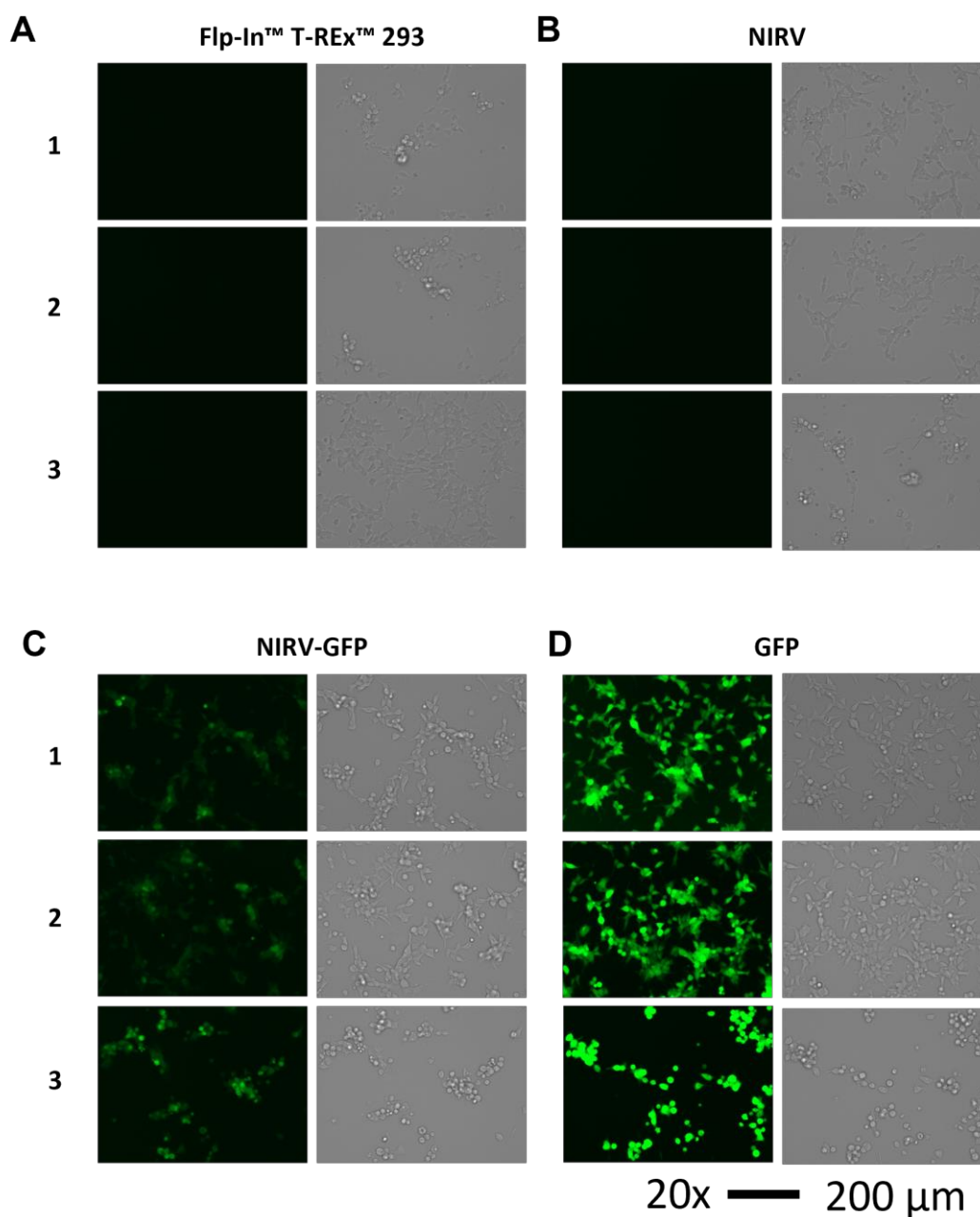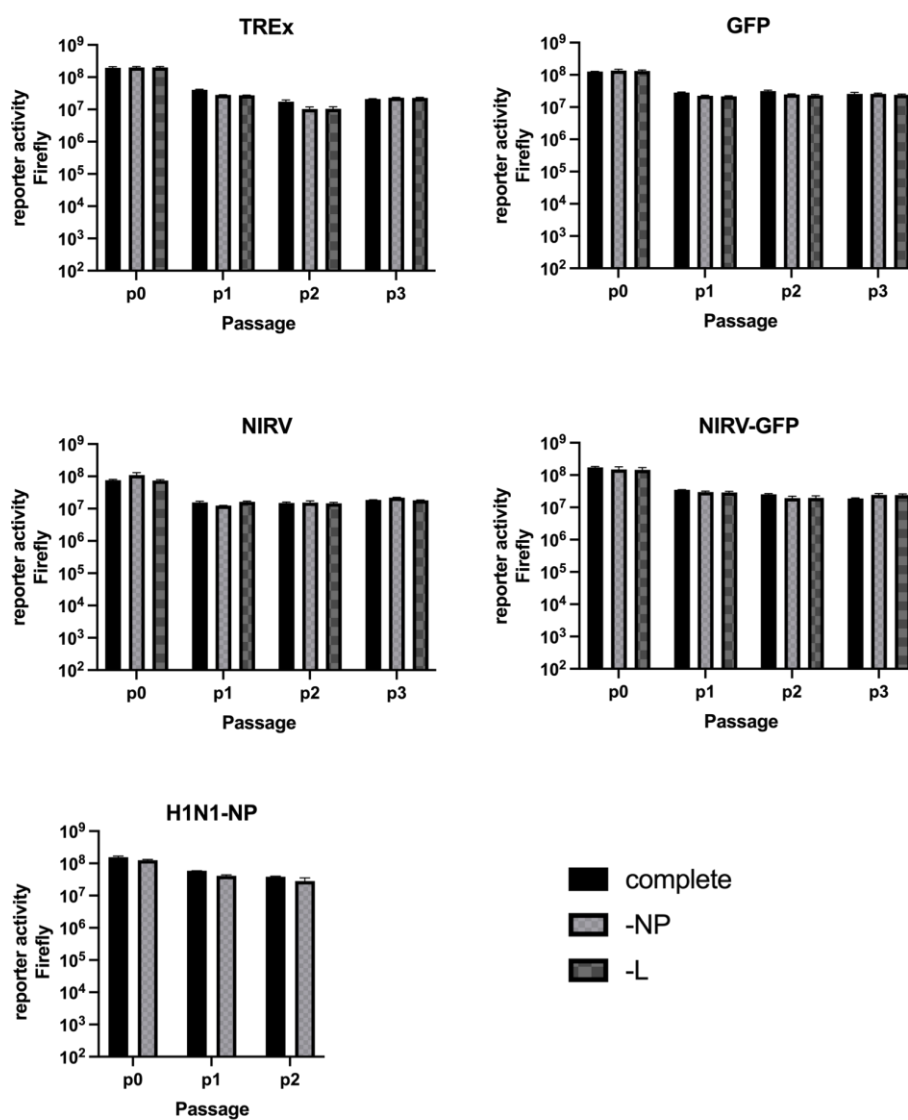
Supplementary Figure 5: Flp-In T-REx 293 Cell Lines Cultured Under Different Conditions

Representative images of Flp-In T-REx host cell line (TREx) (**A**), Flp-In T-REx cell lines stably expressing NP-NIRV (**B**), NP-NIRV-GFP construct (**C**), and GFP (**D**) under various culture conditions: (**1**) Hygromycin B and Blasticidin; (**2**) Tetracycline, Hygromycin B, and Blasticidin; (**3**) Zeocin, Hygromycin B, and Blasticidin. Channels: brightfield and UV. Images were captured at 20x magnification using the EVOS FL Auto Imaging System.
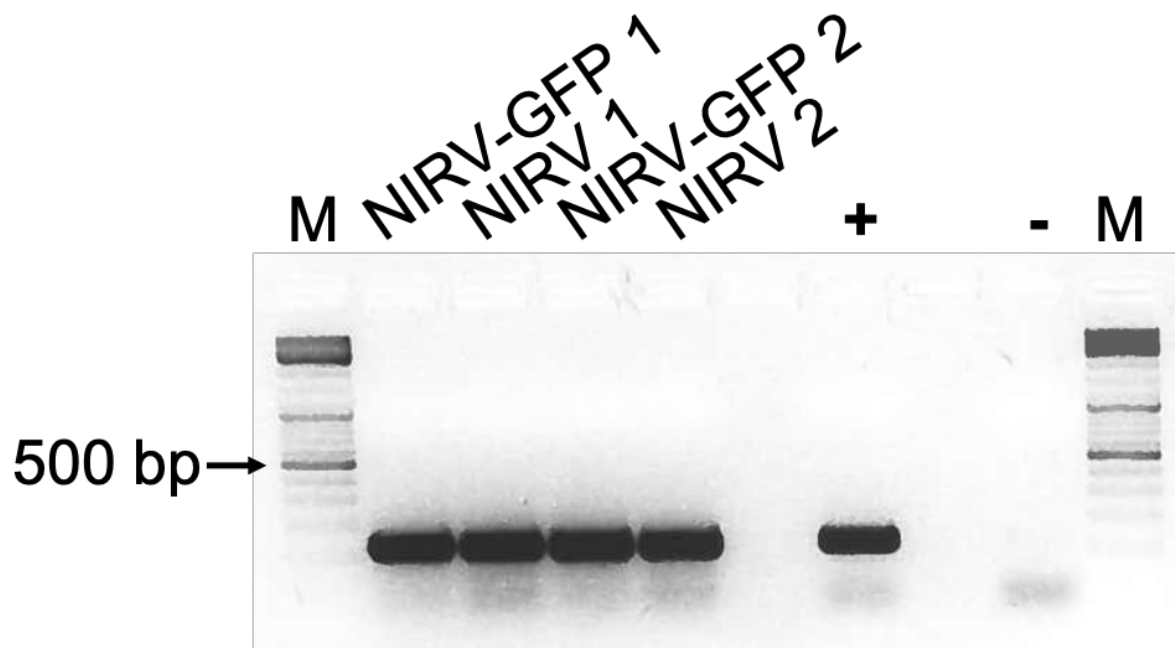
Supplementary Figure 6: Detection of NP-NIRV in Flp-In T-REx 293 Cell Lines

PCR targeting NP-NIRV using qRT-PCR primers shows strong expression in both samples for each cell line. "+" and "–" denote the lanes containing the positive and negative controls, respectively. "M" represents the lane with the GeneRuler DNA Ladder Mix (Supplementary Figure 11).

Supplementary Figure 7: Firefly Luciferase Reporter Activity

Transfection control: Reporter activity of Firefly luciferase was measured in Flp-In T-REx host cells (TREx) and Flp-In T-REx cell lines stably expressing GFP, NP-NIRV, the NP-NIRV-GFP construct, or H1N1-NP across passages p0 to p2 (p3). Differences between reporter activity was non-significant (Kruskal-Wallis test). Bars indicate the mean ± SEM from two independent experiments performed in triplicate.
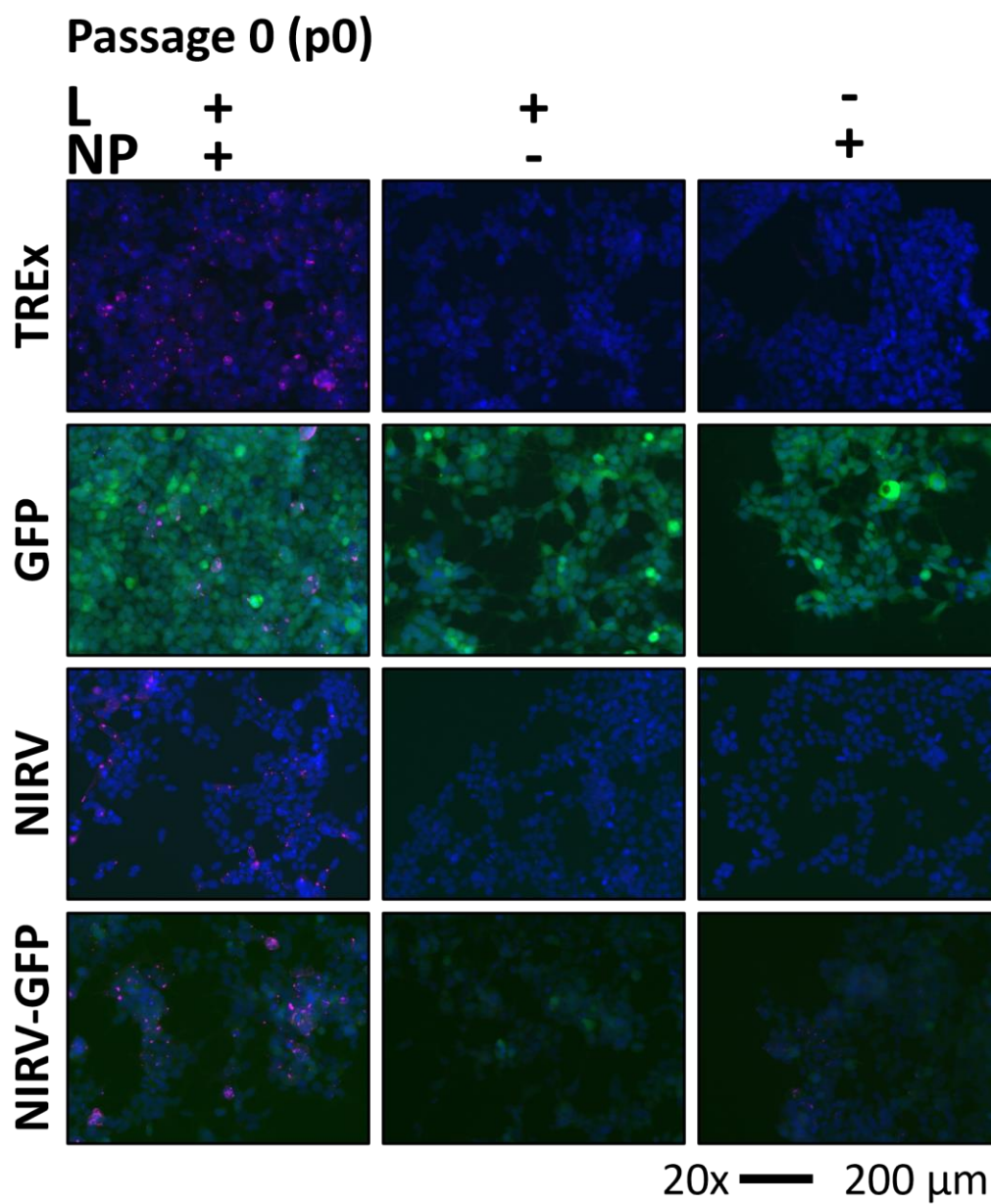
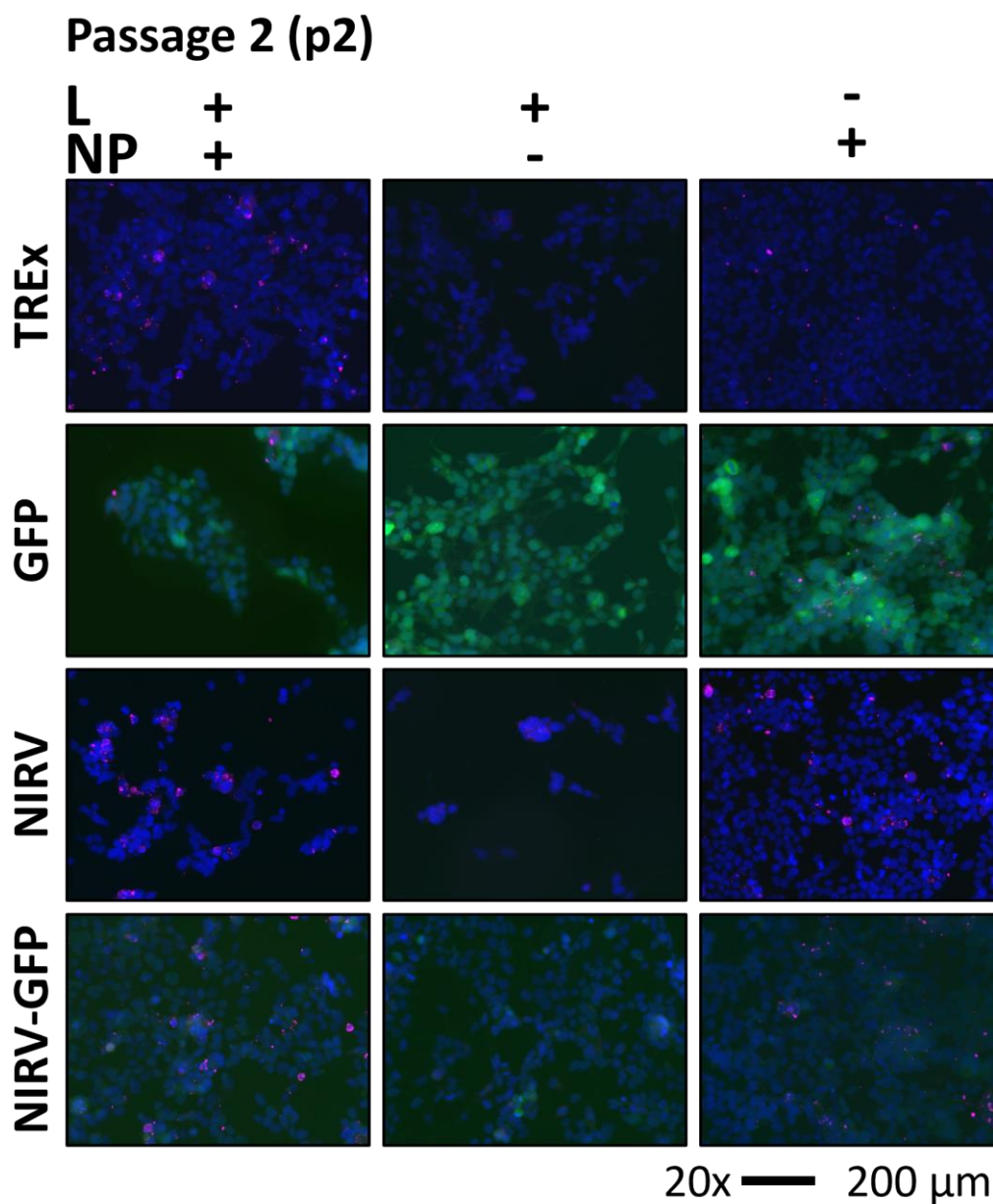**Supplementary Figure 8: Inclusion Body Formation in 293 Cell Lines (p0)**

Immunofluorescent staining of Flp-In T-REx host cell line (TREx) and Flp-In T-REx cell lines stably expressing GFP, NP-NIRV, NP-NIRV-GFP construct transfected with trVLP system. DAPI staining (Blue) and EBOV NP staining (Magenta). L = Plasmid expressing EBOV polymerase, NP = Plasmid expressing EBOV-NP, "+" = transfected, "-" not transfected. Representative pictures of passage 0.
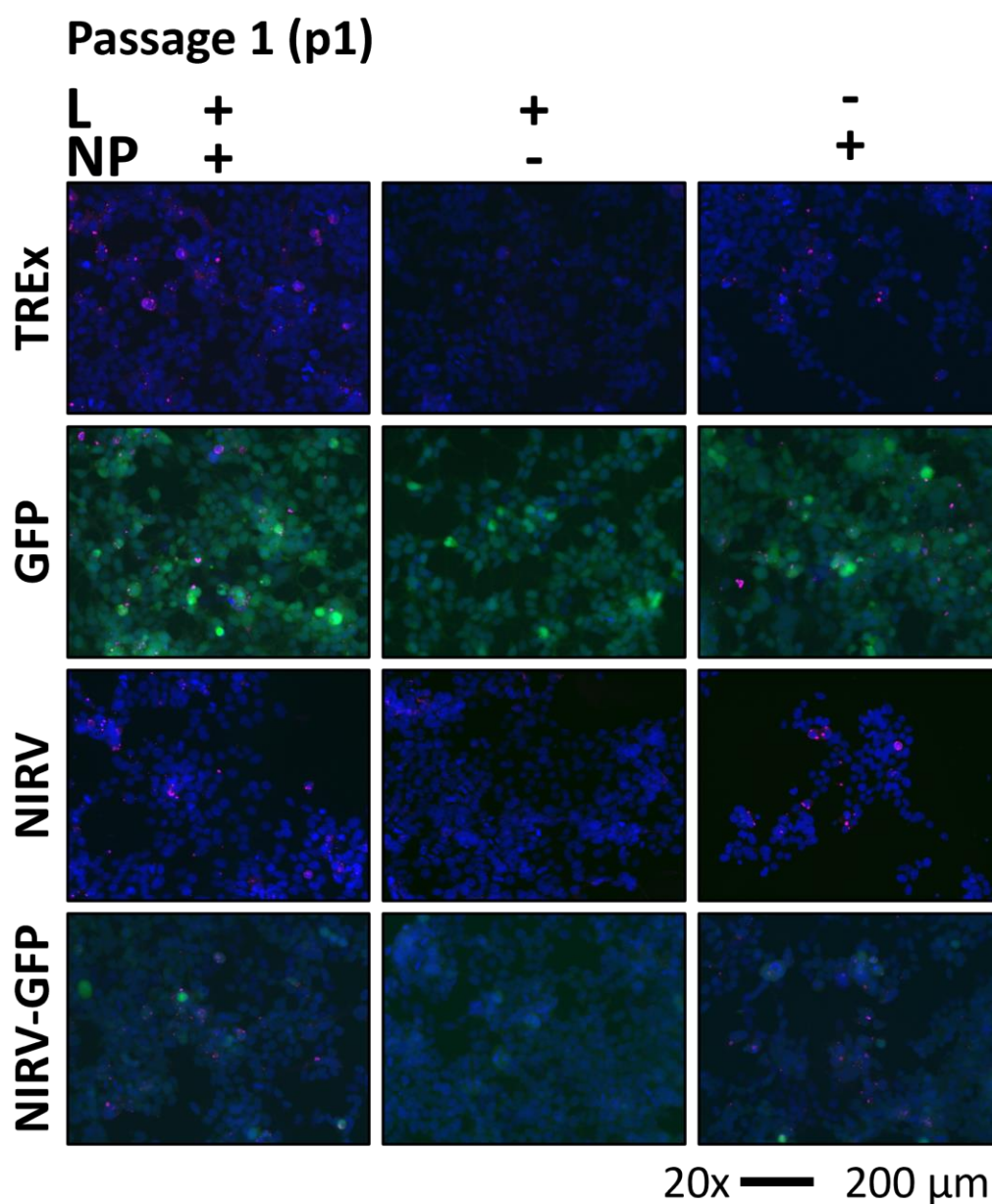
Supplementary Figure 9: Inclusion Body Formation in 293 Cell Lines (p1)

Immunofluorescent staining of Flp-In T-REx host cell line (TREx) and Flp-In T-REx cell lines stably expressing GFP, NP-NIRV, NP-NIRV-GFP construct transfected with trVLP system. DAPI staining (Blue) and EBOV NP staining (Magenta). L = Plasmid expressing EBOV polymerase, NP = Plasmid expressing EBOV-NP, "+" = transfected, "-" not transfected. Representative pictures of passage 1.

Supplementary Figure 10: Inclusion Body Formation in 293 Cell Lines (p2)

Immunofluorescent staining of Flp-In T-REx host cell line (TREx) and Flp-In T-REx cell lines stably expressing GFP, NP-NIRV, NP-NIRV-GFP construct transfected with trVLP system. DAPI staining (Blue) and EBOV NP staining (Magenta). L = Plasmid expressing EBOV polymerase, NP = Plasmid expressing EBOV-NP, "+" = transfected, "-" not transfected. Representative pictures of passage 2.

8.5   DNA-Marker
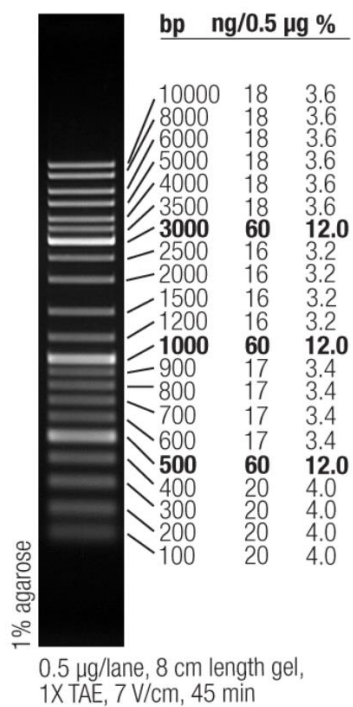
Supplementary Figure 11: Marker

Thermo Scientific GeneRuler DNA Ladder Mix, ready-to-use, Thermo Fisher Scientific Inc., Cat. # SM0331.

Ich versichere, dass dieses gebundene Exemplar der Dissertation und das in elektronischer Form eingereichte Dissertationsexemplar (über den Docata-Upload) und das bei der Fakultät zur Archivierung eingereichte gedruckte gebundene Exemplar der Dissertationsschrift identisch sind.

I, the undersigned, declare that this bound copy of the dissertation and the dissertation submitted in electronic form (via the Docata upload) and the printed bound copy of the dissertation submitted to the faculty for archiving are identical.

Hamburg, 22.11.2024

Ort, Datum

Christoph Heukel,

Vorname und Nachname, Unterschrift